UNIVERSITÀ
DEGLI STUDI
DI TRIESTE

UNIVERSITÀ DEGLI STUDI DI TRIESTE

XXXV CICLO DEL DOTTORATO DI RICERCA IN

SCIENZE DELLA TERRA, FLUIDODINAMICA E
MATEMATICA. INTERAZIONI E METODICHE

NUMERICAL METHODS FOR ELECTROMAGNETIC INVERSION

Settore scientifico-disciplinare: **MAT/08**

DOTTORANDO/A
ELEONORA DENICH

COORDINATORE
PROF. STEFANO MASET

SUPERVISORE DI TESI
PROF. PAOLO NOVATI

CO-SUPERVISORE DI TESI
STEFANO PICOTTI

ANNO ACCADEMICO 2021-2022

Contents

Acknowledgements

The research reported in this work was supported by OGS and CINECA under HPC-TRES program award number 2019-04.

Abstract

In this work we are interested in the reconstruction of the subsurface composition of the earth, by recorded measurements taken at the surface. Among the available electromagnetic (EM) sounding methods in geophysics, we focus on one technique, that consists of placing a magnetic dipole above the surface, composed of a transmitter coil and different couples of adjacent receiver coils, placed at different distances. In this setting, the electromagnetic induction effect, modelled by first-order linear Maxwell's differential equations, produce eddy alternating currents in the soil which induce response electromagnetic fields, that can be used to determine the conductivity profile of the ground by meaning of an inversion procedure. By assuming that the local subsurface structures are composed by horizontal and homogeneous layers, general integral solutions of Maxwell equations can be derived and represented as Hankel transforms, that, in general, are difficult to expressed in closed form. Moreover, the slow decay of the oscillations determined by the Bessel function makes the problem very difficult to handle, because traditional quadrature rules typically fail to converge. We consider two approaches to numerically evaluate these integrals. The first one is based on the decomposition of the integrand function in a first one for which the corresponding Hankel transform is known exactly, and a second oscillating function that decays exponentially. For realistic sets of parameters, the oscillations are quite rapidly damped, and the corresponding integral can be accurately computed by a classical quadrature rule. The second approach consists in the development and application of a Gaussian quadrature rule for weight functions involving fractional powers, exponentials and Bessel functions of the first kind. Moreover, we derive an analytical approximation of these integrals that has a general validity. Finally, by assuming as forward model a homogeneous layered earth, we consider the inverse problem of computing the model parameters from a set of measured field values at different distances. We employ two optimization algorithms. The first one is based on the BFGS line-search method and, to reduce the number of integral evaluations, the analytic approximation of these integrals is used in the initial iterations to have a first estimate of the solution. For the second approach, based on the reformulation of the minimization problem in the nonlinear least-squares sense, we employ the damped Gauss-Newton method. To avoid the dependence on the initial guess of the iterative procedure, we consider a set of different initial models and use each one to solve the optimization problem. The numerical experiments, carried out for the study of river-levees integrity, allow to estimate the errors associated to these kinds of investigations, and confirm the reliability of the techniques.

Introduction

The aim of electromagnetic (EM) sounding methods in geophysics is to obtain information about the subsurface of the earth by recorded measurements taken at the surface. In particular, the goal is to determine variations in the electrical conductivity of the earth with depth by employing an inversion procedure. Any sounding method involves receivers for measurements of one or more components of electric or magnetic fields produced by some natural or artificial source of electromagnetic energy, i.e., the transmitter. Most EM techniques consist of measurements at a number of frequencies or times using a fixed source and receiver. Alternatively, soundings can be made by measuring the response at several source-receiver separations at a single frequency or time.

In this work we focus on a particular technique of the latter type, that consists of placing a magnetic dipole above the surface, composed of a transmitter coil and various couples of adjacent receiver coils. The receiver couples are placed at different distances (offsets) from the transmitter coil. The most common dipole geometry consists of transmitter and receiver loops that can be horizontal co-planar (HCP configuration) and perpendicular (PRP configuration). Other two settings consist in vertical co-planar loops (VCP configuration) and in vertical coaxial loops (VCX configuration). In this setting, the electromagnetic induction effect, modelled by first-order linear Maxwell's differential equations, produce eddy alternating currents in the soil which induce response electromagnetic fields, that can be used to determine the conductivity profile of the ground by means of an inversion algorithm. A typical inversion strategy consists in an iterative procedure involving the computation of the EM response of a layered model (forward modelling) and the solution of the inverse problem. Then, the algorithm attempts to minimize the mismatch between the measured data and the predicted data, by updating the model parameters at each iteration.

By assuming that the local subsurface structures are composed by horizontal and homogeneous layers, general integral solutions of Maxwell's equations (i.e., the EM fields) for vertical and horizontal magnetic dipoles, can be

derived (see [64]) and represented as Hankel transforms of order l, as follows,

$$I_f(r,p) = \int_0^\infty f(\lambda,p) J_l(\lambda r) d\lambda, \tag{1}$$

where r is the offset and J_l is the Bessel function of the first kind of order l (we refer to [65] for an overview of Bessel functions). The function $f(\lambda,p)$ depends on the vector p characterizing the subsurface model parameters, i.e., the conductivity and the thickness of each layer.

In the case of conductivities of geological materials, only the imaginary part of the complex function $I_f(r,p)$ is considered. Indeed, while the instruments used for experimental surveys collect both in-phase and quadrature measurements of the magnetic field components, the former become important only over highly conductive materials, and are particularly effective for locating confined conductors, such as metal bodies, or boulders of graphite or sulfide.

From a mathematical point of view, in general, the function $I_f(r,p)$ is difficult to express in closed form and therefore it is necessary to use a numerical scheme. Anyway, the slow decay of the oscillations determined by the Bessel function makes the problem very difficult to handle, because traditional quadrature rules typically fail to converge. The technique commonly employed to evaluate numerically this kind of integrals is the digital filtering. This method is essentially a standard quadrature rule, but the main difference is that the weights are computed by solving a linear equation obtained by imposing the rule to be correct on a set of training functions that are not polynomials and for which the corresponding integral (1) is known (see e.g. [31]).

In this work we consider two different approaches (see [13] and [11]) to evaluate integrals of type (1). The first one is based on the decomposition of the function $f(\lambda,p)$ as

$$f(\lambda,p) = f_1(\lambda,p) + f_2(\lambda,p),$$

where $f_1(\lambda,p)$ is such that $I_{f_1}(r,p)$ is known exactly, and the oscillating function $f_2(\lambda,p)$ decays exponentially. For realistic sets of parameters, the oscillations are quite rapidly damped and the corresponding integral $I_{f_2}(r,p)$ can be accurately computed by a classical quadrature rule on finite intervals. We remark that the frequency of the oscillations increases with r, so that the evaluation of $I_f(r,p)$ becomes more difficult. In this view the decomposition of $f(\lambda,p)$ allows to reduce the sensitivity with respect to r. The idea of splitting the integral in two parts was introduced in [33] where, however, the second integral is still approximated by digital filtering, without exploiting the fast decay of the oscillations.

The second approach we employ for the computation of the electromagnetic fields is the application of a Gaussian quadrature formula. In particular, we develop a Gaussian rule for weight functions involving fractional powers, exponentials and Bessel functions of the first kind that can be used to evaluate integrals of type (1).

Moreover, we derive an analytical approximation of these integrals that has a general validity and allows to overcome the limitations of common methods based on the modelling of apparent conductivity in the low induction number (LIN) approximation.

Having at our disposal a reliable method for evaluating (1), by assuming as forward model a homogeneously layered earth, we also consider the inverse problem of computing the model parameters (i.e., conductivity and thickness of the layers) from a set of measured field values at different offsets. In particular, we focus on the specific case of the DUALEM (DUAL-geometry Electro-Magnetic; http://www.dualem.com) system, in which the receiver couples are placed at $2, 4, 6$ and 8 m from the transmitter coil, and typical source-receiver geometries are the HCP and PRP configurations. Anyway, the results can be generalized for applications at any scale. We employ two optimization algorithms. The first one is based on the BFGS line-search method ([6, 16, 26, 53]) and, in order to reduce as much as possible the number of integral evaluations, the general analytic approximation of these integrals is used in the initial iterations of the tomographic procedure, to have a first estimate of the solution.

For the second approach we employ the damped Gauss-Newton method [14]. To avoid the dependence on the initial guess of the iterative procedure, we consider a grid of values of initial models and we use each one to solve the optimization problem. After analyzing of the set of solutions, we describe a strategy to obtain the approximate solution of the inverse problem. Anyway, this inversion algorithm can be very expensive in terms of computational costs. The numerical experiments, carried out for the study of river-levees integrity, an important environmental problem in Italy due to the high hydrological risks, allow to estimate the errors associated to these kind of investigations and confirm the reliability of the techniques.

The numerical methods and the associated simulations are implemented in Matlab. Moreover, in order to accelerate the minimization procedure, we run in parallel the simulations on a virtual machine equipped with the NVIDIA A100 Tensor Core GPU.

This work, divided in four chapters, is organized as follows. In the first chapter we introduce some notions of electromagnetic theory, state Maxwell's equations and describe how to derive their general solutions. In particular, following [64], in the presence of a layered earth we write the integral solutions

for vertical and horizontal magnetic dipoles and the exact solutions in the case of a homogeneous earth model.

The second chapter deals with the forward problem, i.e., the computation of the EM fields. After a brief review of the numerical techniques usually employed, we propose and analyze a novel approach, based on the splitting of the integrand function. Moreover, we develop the Gaussian quadrature rule that can be used to evaluate integrals of type (1).

In Chapter 3, under the low induction number approximation, we present the commonly used LIN approximation. Moreover, we also derive new analytical approximations of the integral representations of the fields.

Finally, in Chapter 4 we consider the inverse problem, consisting in the computation of the unknown underground conductivity distribution from a set of modeled magnetic fields components. In particular, we apply two optimization algorithms based on line-search methods and provide numerical experiments, carried out for the study of the internal composition of river levees.

We remark that, for what concerns the notation, in the first chapter we have used bold characters for 3D vectors, in line with the standards in physics. In the remaining part of the work we have adopted the mathematical standard (normal character) for all the vector quantities.

Chapter 1

Basic electromagnetic theory

In this chapter we treat the basic of electromagnetic theory necessary to derive integral formulations of the fields. Moreover, for sake of clarity, all the main results are collected in the form of propositions with relative proofs. We refer to [64, 57] for a complete and exhaustive discussion of the covered topics.

1.1 Maxwell's equations

All electromagnetic phenomena are governed by Maxwell's equations, which are first-order linear differential equations. The first equation, which represents the physical law that electric fields result from time-varying magnetic induction fields, is

$$\nabla \times \mathbf{e}(\mathbf{x}, t) = -\frac{\partial \mathbf{b}(\mathbf{x}, t)}{\partial t}, \tag{1.1}$$

where $\mathbf{x} = (x, y, z)$ is the position vector in Cartesian coordinates, t is the time, $\mathbf{e}$ is the electric field vector in (V/m), $\mathbf{b}$ is the magnetic induction vector in (Wb/m^2) and $\nabla \times (\cdot)$ is the curl operator (see Appendix A). The second equation is used to represent the fact that the magnetic fields are caused by electric current flow, and it is given by

$$\nabla \times \mathbf{h}(\mathbf{x}, t) = \mathbf{j}(\mathbf{x}, t) + \frac{\partial \mathbf{d}(\mathbf{x}, t)}{\partial t}, \tag{1.2}$$

where $\mathbf{h}$ is the magnetic field in (A/m), $\mathbf{j}$ is the current density in (A/m^2) and $\mathbf{d}$ is the electric displacement in (C/m^2). This equation represents two kinds of current flow: one, $\mathbf{j}$, in which charge carries flow through a medium without hindrance, and another, $\partial \mathbf{d}/\partial t$, in which charge separation, and hence an impeding electric field, arises. The first type of current is called

ohmic or galvanic, while the second type is known by the name displacement current. The four vectors **e**, **b**, **d** and **h**, which define an electromagnetic field, are assumed to be continuous functions of position and time, with first and second order continuous derivatives.

Two conditions satisfied by the vectors **b** and **d** may be deduced directly from Maxwell's equations. In fact, by taking the divergence $\nabla \cdot (\cdot)$ (see Appendix A) of equation (1.1), we obtain

$$\nabla \cdot (\nabla \times \mathbf{e}(\mathbf{x}, t)) + \nabla \cdot \frac{\partial \mathbf{b}(\mathbf{x}, t)}{\partial t} = 0,$$

and hence, by (A.5) and due to the commutation of the operators $\nabla \cdot (\cdot)$ and $\partial/\partial t$, we have

$$\nabla \cdot \frac{\partial \mathbf{b}(\mathbf{x}, t)}{\partial t} = \frac{\partial}{\partial t} \nabla \cdot \mathbf{b}(\mathbf{x}, t) = 0.$$

It follows that at every point in the field the divergence of **b** is constant. If ever in its past history the field has vanished, this constant must be zero and, since we may reasonably suppose that the initial generation of the field was at a time not infinitely remote, we conclude that

$$\nabla \cdot \mathbf{b}(\mathbf{x}, t) = 0, \tag{1.3}$$

and the field **b** is called solenoidal. Likewise, the divergence of equation (1.2) leads to

$$\nabla \cdot \mathbf{j}(\mathbf{x}, t) + \frac{\partial}{\partial t} \nabla \cdot \mathbf{d}(\mathbf{x}, t) = 0.$$

Using the relation

$$\nabla \cdot \mathbf{j}(\mathbf{x}, t) + \frac{\partial \rho(\mathbf{x}, t)}{\partial t} = 0, \tag{1.4}$$

which expresses the conservation of charges in the neighborhood of a point, we have

$$\frac{\partial}{\partial t} \left(\nabla \cdot \mathbf{d}(\mathbf{x}, t) - \rho(\mathbf{x}, t) \right) = 0.$$

If again we admit that at some time in its past or future history the field may vanish, it is necessary that

$$\nabla \cdot \mathbf{d}(\mathbf{x}, t) = \rho(\mathbf{x}, t). \tag{1.5}$$

Therefore, the charges distributed with a density ρ constitute the sources of the vector **d**. The divergence equations (1.3) and (1.5) are frequently included as part of Maxwell's system.

1.2 The constitutive equations

At this point, the only assumptions that we made are that an electromagnetic field is characterized by the four vectors **e**, **b**, **d** and **h**, which at ordinary points satisfy Maxwell's equations, and that the distribution of current that gives rise to the field is such as to ensure the conservation of charge. In order to make the system determinate, we are now forced to impose further relationships, called constitutive equations.

Let us begin with the assumptions that at any point within the medium

$$\mathbf{j}(\mathbf{x},t) = \mathbf{j}(\mathbf{e}(\mathbf{x},t)),$$

and that at any given point in the field, whether in free space or within matter,

$$\mathbf{d}(\mathbf{x},t) = \mathbf{d}(\mathbf{e}(\mathbf{x},t)) \quad \text{and} \quad \mathbf{h}(\mathbf{x},t) = \mathbf{h}(\mathbf{b}(\mathbf{x},t)).$$

If the medium is isotropic, i.e., the physical properties are uniform in all directions of the medium, **j** and **d** are parallel to **e**, and **h** is parallel to **b**. Moreover, the relations between the vectors are linear in almost the soluble problems of electromagnetic theory. Therefore, for the isotropic linear case, we have the following conditions, called constitutive equations,

$$\mathbf{j}(\mathbf{x},t) = \sigma\mathbf{e}(\mathbf{x},t), \tag{1.6}$$

$$\mathbf{d}(\mathbf{x},t) = \epsilon\mathbf{e}(\mathbf{x},t), \tag{1.7}$$

$$\mathbf{h}(\mathbf{x},t) = \frac{1}{\mu}\mathbf{b}(\mathbf{x},t), \tag{1.8}$$

where σ is the electrical conductivity in (S/m), ϵ is the dielectric permittivity in (F/m) and μ is the magnetic permeability in (H/m). The relation (1.6) is known as Ohm's law. By definition, the electrical conductivity represents the ability of the material to conduct electric current, while the electric permittivity and the magnetic permeability are a measure of polarizability and magnetization, respectively, of the medium. Moreover, the dielectric permittivity and the magnetic permeability have well defined values even in the absence of matter, that is,

$$\epsilon_0 = 8.854 \cdot 10^{-12}\ F/m, \tag{1.9}$$

$$\mu_0 = 4\pi \cdot 10^{-7}\ H/m. \tag{1.10}$$

By using the time domain Fourier transform (B.1) (see Appendix B for the definitions of the Fourier transform and some useful properties), equations

(1.6), (1.7) and (1.8) can be written in the frequency domain as

$$\mathbf{J}(\mathbf{x},\omega) = \sigma\mathbf{E}(\mathbf{x},\omega),$$
$$\mathbf{D}(\mathbf{x},\omega) = \epsilon\mathbf{E}(\mathbf{x},\omega), \tag{1.11}$$
$$\mathbf{H}(\mathbf{x},\omega) = \frac{1}{\mu}\mathbf{B}(\mathbf{x},\omega). \tag{1.12}$$

Also the Maxwell's equations can be stated in the frequency domain as shown in the following proposition.

Proposition 1 *By assuming for the fields* $\mathbf{e}$*,* $\mathbf{b}$*,* $\mathbf{d}$ *and* $\mathbf{h}$ *the boundary conditions*

$$\lim_{t\to\pm\infty}\mathbf{e}(\mathbf{x},t) = \lim_{t\to\pm\infty}\mathbf{b}(\mathbf{x},t) = \lim_{t\to\pm\infty}\mathbf{d}(\mathbf{x},t) = \lim_{t\to\pm\infty}\mathbf{h}(\mathbf{x},t) = 0, \tag{1.13}$$

the Maxwell's equations in the frequency domain are given by

$$\nabla\times\mathbf{E}(\mathbf{x},\omega) + i\mu\omega\mathbf{H}(\mathbf{x},\omega) = 0, \tag{1.14}$$

and

$$\nabla\times\mathbf{H}(\mathbf{x},\omega) - (\sigma + i\epsilon\omega)\mathbf{E}(\mathbf{x},\omega) = 0. \tag{1.15}$$

Proof. Applying the Fourier transformation (B.1) to equation (1.1) leads to

$$\nabla\times\mathbf{E}(\mathbf{x},\omega) + \int_{-\infty}^{\infty}\frac{\partial\mathbf{b}(\mathbf{x},t)}{\partial t}e^{-i\omega t}dt = 0,$$

where, since $\mathbf{b}$ is assumed to be continuous with regard to position and time, we have also used the commutation of the curl and integral operators. Then, integrating by part and using boundary condition (1.13), we have

$$\nabla\times\mathbf{E}(\mathbf{x},\omega) + i\omega\mathbf{B}(\mathbf{x},\omega) = 0.$$

Finally, by relation (1.12) we obtain equation (1.14). The derivation of equation (1.15) is analogous. ■

1.3 The wave equations

In this section, by assuming that the earth subsoil is composed by several juxtaposed homogeneous isotropic linear regions, we derive the wave equations used for each region directly from Maxwell's equations.

Proposition 2 *The wave equations for the electric and magnetic fields in the time domain are given by*

$$\nabla^2\mathbf{e}(\mathbf{x},t) - \mu\epsilon\frac{\partial^2\mathbf{e}(\mathbf{x},t)}{\partial t^2} - \mu\sigma\frac{\partial\mathbf{e}(\mathbf{x},t)}{\partial t} = 0 \tag{1.16}$$

and

$$\nabla^2\mathbf{h}(\mathbf{x},t) - \mu\epsilon\frac{\partial^2\mathbf{h}(\mathbf{x},t)}{\partial t^2} - \mu\sigma\frac{\partial\mathbf{h}(\mathbf{x},t)}{\partial t} = 0. \tag{1.17}$$

Proof. Taking the curl of (1.1) and (1.2), we obtain

$$\nabla\times(\nabla\times\mathbf{e}(\mathbf{x},t)) + \nabla\times\left(\frac{\partial\mathbf{b}(\mathbf{x},t)}{\partial t}\right) = 0,$$

$$\nabla\times(\nabla\times\mathbf{h}(\mathbf{x},t)) - \nabla\times\left(\frac{\partial\mathbf{d}(\mathbf{x},t)}{\partial t}\right) = \nabla\times\mathbf{j}(\mathbf{x},t),$$

and using relations (1.6), (1.7), (1.8) yields to

$$\nabla\times\nabla\times\mathbf{e}(\mathbf{x},t) + \nabla\times\left[\frac{\partial}{\partial t}(\mu\mathbf{h}(\mathbf{x},t))\right] = 0,$$

$$\nabla\times\nabla\times\mathbf{h}(\mathbf{x},t) - \nabla\times\left[\frac{\partial}{\partial t}(\epsilon\mathbf{e}(\mathbf{x},t))\right] = \sigma\nabla\times\mathbf{e}(\mathbf{x},t).$$

Since $\mathbf{h}$ and $\mathbf{e}$ are piecewise continuous with continuous first and second order derivatives, we can write

$$\nabla\times\nabla\times\mathbf{e}(\mathbf{x},t) + \mu\frac{\partial}{\partial t}(\nabla\times\mathbf{h}(\mathbf{x},t)) = 0, \tag{1.18}$$

$$\nabla\times\nabla\times\mathbf{h}(\mathbf{x},t) - \epsilon\frac{\partial}{\partial t}(\nabla\times\mathbf{e}(\mathbf{x},t)) = \sigma\nabla\times\mathbf{e}(\mathbf{x},t). \tag{1.19}$$

Now, we observe that by (1.2), (1.6), (1.7),

$$\nabla\times\mathbf{h}(\mathbf{x},t) = \mathbf{j}(\mathbf{x},t) + \frac{\partial\mathbf{d}(\mathbf{x},t)}{\partial t} = \sigma\mathbf{e}(\mathbf{x},t) + \epsilon\frac{\mathbf{e}(\mathbf{x},t)}{\partial t},$$

and, from (1.1), (1.8),

$$\nabla\times\mathbf{e}(\mathbf{x},t) = -\frac{\partial\mathbf{b}(\mathbf{x},t)}{\partial t} = -\mu\frac{\partial\mathbf{h}(\mathbf{x},t)}{\partial t}.$$

Hence, equations (1.18)-(1.19) becomes

$$\nabla\times\nabla\times\mathbf{e}(\mathbf{x},t) + \mu\epsilon\frac{\partial^2\mathbf{e}(\mathbf{x},t)}{\partial^2 t} + \mu\sigma\frac{\partial\mathbf{e}(\mathbf{x},t)}{\partial t} = 0,$$

$$\nabla\times\nabla\times\mathbf{h}(\mathbf{x},t) + \mu\epsilon\frac{\partial^2\mathbf{h}(\mathbf{x},t)}{\partial^2 t} + \mu\sigma\frac{\partial\mathbf{h}(\mathbf{x},t)}{\partial t} = 0.$$

Finally, using the vector identity (A.6) and since for homogeneous regions it holds $\nabla\cdot\mathbf{e}(\mathbf{x},t) = 0$ and $\nabla\cdot\mathbf{h}(\mathbf{x},t) = 0$, we obtain the result. ■

Corollary 1 *In the frequency domain, the wave equations for the electric and magnetic fields, called Helmholtz equations, are*

$$\nabla^2\mathbf{E}(\mathbf{x},\omega) + (\mu\epsilon\omega^2 - i\mu\sigma\omega)\mathbf{E}(\mathbf{x},\omega) = 0 \tag{1.20}$$

and

$$\nabla^2\mathbf{H}(\mathbf{x},\omega) + (\mu\epsilon\omega^2 - i\mu\sigma\omega)\mathbf{H}(\mathbf{x},\omega) = 0. \tag{1.21}$$

Proof. The result follow straightfully by applying the Fourier transform (B.1) to equations (1.16) and (1.17). ■

Remark 1 *The quantity $\sqrt{\mu\epsilon\omega^2 - i\mu\sigma\omega}$ (cf. (1.20)-1.21)) is known as the wave number and it is a function of three physical properties of the earth and of the frequency. For all the following analysis we assume to work with frequency less than 10^5 Hz. In this situation displacement currents are much smaller than conductive currents, e.g. $\mu\epsilon\omega^2 \ll \mu\sigma\omega$. Therefore, without loss of generality, we define the wave number as*

$$k := \sqrt{-i\mu\sigma\omega}.$$

1.4 The polarization vectors

To describe the electromagnetic state of a matter, it is convenient to introduce two auxiliar fields $\mathbf{P}$ and $\mathbf{M}$, known respectively as the electric and magnetic polarization. These fields are defined by

$$\mathbf{P}(\mathbf{x},\omega) := \mathbf{D}(\mathbf{x},\omega) - \epsilon_0\mathbf{E}(\mathbf{x},\omega)$$

and

$$\mathbf{M}(\mathbf{x},\omega) := \frac{1}{\mu_0}\mathbf{B}(\mathbf{x},\omega) - \mathbf{H}(\mathbf{x},\omega).$$

We notice that these vectors vanish in free space (cf. (1.11), (1.12)). Moreover, $\mathbf{P}$ has the dimensions of $\mathbf{D}$, while $\mathbf{M}$ and $\mathbf{H}$ are dimensionally alike. The total observed polarization vectors are composed of source and induced parts, that is,

$$\mathbf{P}(\mathbf{x},\omega) = \mathbf{P}^I(\mathbf{x},\omega) + \mathbf{P}^S(\mathbf{x},\omega)$$

and

$$\mathbf{M}(\mathbf{x},\omega) = \mathbf{M}^I(\mathbf{x},\omega) + \mathbf{M}^S(\mathbf{x},\omega).$$

For isotropic and linear earth media $\mathbf{P}^I$ is parallel to and proportional to $\mathbf{E}$, while $\mathbf{M}^I$ is parallel to and proportional to $\mathbf{H}$. In particular, they are defined by

$$\mathbf{P}^I(\mathbf{x},\omega) := \chi_e\epsilon_0\mathbf{E}(\mathbf{x},\omega)$$

and

$$\mathbf{M}^I(\mathbf{x},\omega) := \chi_m \mathbf{H}(\mathbf{x},\omega),$$

where

$$\chi_e = \frac{\epsilon}{\epsilon_0} - 1 \quad \text{and} \quad \chi_m = \frac{\mu}{\mu_0} - 1$$

are the electric and magnetic susceptibility of the medium, respectively, and ϵ_0 is the dielectric permittivity of vacuum (see (1.9)). Moreover, the electric source current density and the magnetic source current density are respectively described by

$$\mathbf{J}_e^S(\mathbf{x},\omega) = i\omega \mathbf{P}^S(\mathbf{x},\omega) \tag{1.22}$$

and

$$\mathbf{J}_m^S(\mathbf{x},\omega) = i\mu_0\omega \mathbf{M}^S(\mathbf{x},\omega). \tag{1.23}$$

1.5 Schelkunoff potentials

Maxwell's equations (1.14) and (1.15) in the frequency domain are homogeneous equations that apply in source-free regions. In regions containing sources they must be replaced by the inhomogeneous equations

$$\nabla \times \mathbf{E}(\mathbf{x},\omega) + i\mu\omega \mathbf{H}(\mathbf{x},\omega) = -\mathbf{J}_m^S(\mathbf{x},\omega), \tag{1.24}$$

and

$$\nabla \times \mathbf{H}(\mathbf{x},\omega) - (\sigma + i\epsilon\omega)\mathbf{E}(\mathbf{x},\omega) = \mathbf{J}_e^S(\mathbf{x},\omega), \tag{1.25}$$

with $\mathbf{J}_m^S$ and $\mathbf{J}_e^S$ as in (1.22) and (1.23). A technique used to obtain the solutions of equations (1.24) and (1.25) is that of expressing $\mathbf{E}$ and $\mathbf{H}$ in terms of auxiliary functions known as potentials. The reason is that equations in potentials sometimes are easier to solve than equations in fields. In the following we introduce a set of potentials due to Schelkunoff [50], which are very convenient in solving wave equations in a space composed of homogeneous regions. First of all, we assume that in each region the electric and magnetic field are given by a superposition of sources of electric type and magnetic type. Thus, let

$$\mathbf{E}(\mathbf{x},\omega) = \mathbf{E}_m(\mathbf{x},\omega) + \mathbf{E}_e(\mathbf{x},\omega), \tag{1.26}$$

and

$$\mathbf{H}(\mathbf{x},\omega) = \mathbf{H}_m(\mathbf{x},\omega) + \mathbf{H}_e(\mathbf{x},\omega), \tag{1.27}$$

where $\mathbf{E}_m$, $\mathbf{H}_m$ and $\mathbf{E}_e$, $\mathbf{H}_e$ refer to electromagnetic fields produced by magnetic and electric sources, respectively. By substituting (1.26) and (1.27) in

(1.24) and (1.25), we obtain

$$\nabla \times \mathbf{E}_m(\mathbf{x},\omega) + i\mu\omega\mathbf{H}_m(\mathbf{x},\omega) = -\mathbf{J}_m^S(\mathbf{x},\omega),$$
$$\nabla \times \mathbf{E}_e(\mathbf{x},\omega) + i\mu\omega\mathbf{H}_e(\mathbf{x},\omega) = -\mathbf{J}_m^S(\mathbf{x},\omega), \tag{1.28}$$
$$\nabla \times \mathbf{H}_m(\mathbf{x},\omega) - (\sigma + i\epsilon\omega)\mathbf{E}_m(\mathbf{x},\omega) = \mathbf{J}_e^S(\mathbf{x},\omega), \tag{1.29}$$
$$\nabla \times \mathbf{H}_e(\mathbf{x},\omega) - (\sigma + i\epsilon\omega)\mathbf{E}_e(\mathbf{x},\omega) = \mathbf{J}_e^S(\mathbf{x},\omega).$$

Assuming moreover that in equations (1.28) and (1.29), the current densities $\mathbf{J}_m^S$ and $\mathbf{J}_e^S$ are zero, we have that $\mathbf{E}_m$, $\mathbf{E}_e$, $\mathbf{H}_m$ and $\mathbf{H}_e$ are solutions of

$$\nabla \times \mathbf{E}_m(\mathbf{x},\omega) = -\mathbf{J}_m^S(\mathbf{x},\omega) - i\mu\omega\mathbf{H}_m(\mathbf{x},\omega), \tag{1.30}$$
$$\nabla \times \mathbf{H}_m(\mathbf{x},\omega) = (\sigma + i\epsilon\omega)\mathbf{E}_m(\mathbf{x},\omega), \tag{1.31}$$
$$\nabla \times \mathbf{E}_e(\mathbf{x},\omega) = -i\mu\omega\mathbf{H}_e(\mathbf{x},\omega), \tag{1.32}$$
$$\nabla \times \mathbf{H}_e(\mathbf{x},\omega) = \mathbf{J}_e^S(\mathbf{x},\omega) + (\sigma + i\epsilon\omega)\mathbf{E}_e(\mathbf{x},\omega). \tag{1.33}$$

Taking the divergence of equations (1.30), (1.31), (1.32), (1.33) and using again relation (A.5) yields to

$$\nabla \cdot \mathbf{H}_m(\mathbf{x},\omega) = -\frac{1}{i\mu\omega}\nabla \cdot \mathbf{J}_m^S(\mathbf{x},\omega),$$
$$\nabla \cdot \mathbf{E}_m(\mathbf{x},\omega) = 0, \tag{1.34}$$
$$\nabla \cdot \mathbf{H}_e(\mathbf{x},\omega) = 0, \tag{1.35}$$
$$\nabla \cdot \mathbf{E}_e(\mathbf{x},\omega) = -\frac{1}{\sigma + i\epsilon\omega}\nabla \cdot \mathbf{J}_e^S(\mathbf{x},\omega).$$

From equations (1.34) and (1.35), we have that $\mathbf{E}_m$ and $\mathbf{H}_e$ are solenoidal fields and hence may be represented as the curls of two vector functions $\mathbf{F}$ and $\mathbf{A}$ (see (A.5)), that is,

$$\mathbf{E}_m(\mathbf{x},\omega) = -\nabla \times \mathbf{F}(\mathbf{x},\omega), \tag{1.36}$$

and

$$\mathbf{H}_e(\mathbf{x},\omega) = \nabla \times \mathbf{A}(\mathbf{x},\omega), \tag{1.37}$$

where the signs of the equalities are arbitrary.

Remark 2 *We notice that* $\mathbf{F}$ *and* $\mathbf{A}$ *are not uniquely defined by (1.36) and (1.37), because the equality of the curls of two vectors does not demand that the vectors be identical. In fact,* $\mathbf{E}_m$ *and* $\mathbf{H}_e$ *can be also written as*

$$\mathbf{E}_m(\mathbf{x},\omega) = -\nabla \times (\mathbf{F}(\mathbf{x},\omega) + \nabla\psi_F(\mathbf{x},\omega))$$

and

$$\mathbf{H}_e(\mathbf{x},\omega) = \nabla \times (\mathbf{A}(\mathbf{x},\omega) + \nabla\psi_A(\mathbf{x},\omega)),$$

where ψ_F *and* ψ_A *are arbitrary scalar functions of position and frequency.*

For homogeneous regions containing sources $\mathbf{J}_m^S$ and $\mathbf{J}_e^S$, the following proposition holds.

Proposition 3 *The vector potentials* $\mathbf{F}$ *and* $\mathbf{A}$ *satisfy the inhomogeneous Helmholtz equations*

$$\nabla^2\mathbf{F}(\mathbf{x},\omega) + k^2\mathbf{F}(\mathbf{x},\omega) = -\mathbf{J}_m^S(\mathbf{x},\omega) \tag{1.38}$$

and

$$\nabla^2\mathbf{A}(\mathbf{x},\omega) + k^2\mathbf{A}(\mathbf{x},\omega) = -\mathbf{J}_e^S(\mathbf{x},\omega). \tag{1.39}$$

Proof. If we substitute (1.36)-(1.37) into (1.31)-(1.33), we obtain

$$\mathbf{H}_m(\mathbf{x},\omega) = -(\sigma + i\epsilon\omega)\mathbf{F}(\mathbf{x},\omega) - \nabla U(\mathbf{x},\omega), \tag{1.40}$$
$$\mathbf{E}_e(\mathbf{x},\omega) = -i\mu\omega\mathbf{A}(\mathbf{x},\omega) - \nabla V(\mathbf{x},\omega), \tag{1.41}$$

where we have introduced the arbitrary functions $U(\mathbf{x},\omega)$ and $V(\mathbf{x},\omega)$ (c.f. Remark 2). Moreover, equation (1.30), with the aid of equations (1.36) and (1.40), becomes

$$\nabla\times\nabla\times\mathbf{F}(\mathbf{x},\omega) = \mathbf{J}_m^S(\mathbf{x},\omega) - i\mu\omega(\sigma + i\epsilon\omega)\mathbf{F}(\mathbf{x},\omega) - i\mu\omega\nabla U(\mathbf{x},\omega),$$

while, with (1.37) and (1.41), equation (1.33) becomes

$$\nabla\times\nabla\times\mathbf{A}(\mathbf{x},\omega) = \mathbf{J}_e^S(\mathbf{x},\omega) - i\mu\omega(\sigma + i\epsilon\omega)\mathbf{A}(\mathbf{x},\omega) - i\mu\omega\nabla V(\mathbf{x},\omega).$$

Using identity (A.6), from the above expressions we obtain

$$\nabla\nabla\cdot\mathbf{F}(\mathbf{x},\omega) - \nabla^2\mathbf{F}(\mathbf{x},\omega) = \mathbf{J}_m^S(\mathbf{x},\omega) - i\mu\omega(\sigma + i\epsilon\omega)\mathbf{F}(\mathbf{x},\omega) - i\mu\omega\nabla U(\mathbf{x},\omega) \tag{1.42}$$

and

$$\nabla\nabla\cdot\mathbf{A}(\mathbf{x},\omega) - \nabla^2\mathbf{A}(\mathbf{x},\omega) = \mathbf{J}_e^S(\mathbf{x},\omega) - i\mu\omega(\sigma + i\epsilon\omega)\mathbf{F}(\mathbf{x},\omega) - i\mu\omega\nabla V(\mathbf{x},\omega). \tag{1.43}$$

Since U and V are arbitrary, we may impose the relations

$$\nabla\cdot\mathbf{F}(\mathbf{x},\omega) = -i\mu\omega U(\mathbf{x},\omega), \tag{1.44}$$

and

$$\nabla\cdot\mathbf{A}(\mathbf{x},\omega) = -(\sigma + i\epsilon\omega V(\mathbf{x},\omega), \tag{1.45}$$

which are called Lorentz conditions. Finally, by substituting (1.44) and (1.45) in (1.42) and (1.43) we obtain the result. ■

At this point, we can derive the expressions for the total electromagnetic fields due both to $\mathbf{J}_m^S$ and $\mathbf{J}_e^S$.

Proposition 4 *If only one source is present at a time, the electromagnetic fields satisfy the set of equations*

$$\mathbf{E}_e(\mathbf{x},\omega) = -i\mu\omega\mathbf{A}(\mathbf{x},\omega) + \frac{1}{\sigma + i\epsilon\omega}\nabla(\nabla\cdot\mathbf{A}(\mathbf{x},\omega)), \tag{1.46}$$

$$\mathbf{H}_e(\mathbf{x},\omega) = \nabla\times\mathbf{A}(\mathbf{x},\omega), \tag{1.47}$$

for electric sources, and

$$\mathbf{E}_m(\mathbf{x},\omega) = -\nabla\times\mathbf{F}(\mathbf{x},\omega), \tag{1.48}$$

$$\mathbf{H}_m(\mathbf{x},\omega) = -\frac{1}{\sigma + i\epsilon\omega}\mathbf{F}(\mathbf{x},\omega) + \frac{1}{i\mu\omega}\nabla(\nabla\cdot\mathbf{F}(\mathbf{x},\omega)), \tag{1.49}$$

for magnetic sources.

Proof. We only need to prove equations (1.46) and (1.49), since relations (1.48) and (1.47) were previously stated in (1.36)-(1.37). From equations (1.41), (1.40) and by using conditions (1.44), (1.45), we have that

$$\begin{aligned}\mathbf{E}_e(\mathbf{x},\omega) &= -i\mu\omega\mathbf{A}(\mathbf{x},\omega) - \nabla V(\mathbf{x},\omega)\\ &= -i\mu\omega\mathbf{A}(\mathbf{x},\omega) - \frac{1}{\sigma + i\epsilon\omega}\nabla(\nabla\cdot\mathbf{A}(\mathbf{x},\omega)),\end{aligned}$$

and

$$\begin{aligned}\mathbf{H}_m(\mathbf{x},\omega) &= -\frac{1}{\sigma + i\epsilon\omega}\mathbf{F}(\mathbf{x},\omega) - \nabla U(\mathbf{x},\omega)\\ &= -\frac{1}{\sigma + i\epsilon\omega}\mathbf{F}(\mathbf{x},\omega) - \frac{1}{i\mu\omega}\nabla(\nabla\cdot\mathbf{F}(\mathbf{x},\omega)).\end{aligned}$$

■

In many problems in electromagnetic theory the vectors $\mathbf{A}$ and $\mathbf{F}$ have a single component. Therefore, without loss of generality, for the following we define

$$\mathbf{A}(\mathbf{x},\omega) := A(\mathbf{x},\omega)\mathbf{u}_z \tag{1.50}$$

and

$$\mathbf{F}(\mathbf{x},\omega) := F(\mathbf{x},\omega)\mathbf{u}_z, \tag{1.51}$$

where $\mathbf{u}_z = (0,0,1)$ is the unit vector in the z-direction and A, F are scalar functions. When relations (1.50), (1.51) are substituted into equations (1.46), (1.48), (1.47) and (1.49), the electric and magnetic field components may be

expressed as the sets

$$\begin{aligned}\mathbf{E}_e(\mathbf{x},\omega) &= (E_{e,x}(\mathbf{x},\omega), E_{e,y}(\mathbf{x},\omega), E_{e,z}(\mathbf{x},\omega)) \\ &= \left(\frac{1}{\sigma+i\epsilon\omega}\frac{\partial^2 A(\mathbf{x},\omega)}{\partial x\partial z}, \frac{1}{\sigma+i\epsilon\omega}\frac{\partial^2 A(\mathbf{x},\omega)}{\partial y\partial z}, \frac{1}{\sigma+i\epsilon\omega}\left(\frac{\partial^2}{\partial z^2}+k^2\right)A(\mathbf{x},\omega)\right), \end{aligned} \tag{1.52}$$

$$\begin{aligned}\mathbf{H}_e(\mathbf{x},\omega) &= (H_{e,x}(\mathbf{x},\omega), H_{e,y}(\mathbf{x},\omega), H_{e,z}(\mathbf{x},\omega)) \\ &= \left(\frac{\partial A(\mathbf{x},\omega)}{\partial y}, -\frac{\partial A(\mathbf{x},\omega)}{\partial x}, 0\right), \end{aligned} \tag{1.53}$$

$$\begin{aligned}\mathbf{E}_m(\mathbf{x},\omega) &= (E_{m,x}(\mathbf{x},\omega), E_{m,y}(\mathbf{x},\omega), E_{m,z}(\mathbf{x},\omega)) \\ &= \left(-\frac{\partial F(\mathbf{x},\omega)}{\partial y}, \frac{\partial F(\mathbf{x},\omega)}{\partial x}, 0\right), \end{aligned} \tag{1.54}$$

$$\begin{aligned}\mathbf{H}_m(\mathbf{x},\omega) &= (H_{m,x}(\mathbf{x},\omega), H_{m,y}(\mathbf{x},\omega), H_{m,z}(\mathbf{x},\omega)) \\ &= \left(\frac{1}{i\mu\omega}\frac{\partial^2 F(\mathbf{x},\omega)}{\partial x\partial z}, \frac{1}{i\mu\omega}\frac{\partial^2 F(\mathbf{x},\omega)}{\partial y\partial z}, \frac{1}{i\mu\omega}\left(\frac{\partial^2}{\partial z^2}+k^2\right)F(\mathbf{x},\omega)\right). \end{aligned} \tag{1.55}$$

We notice that, the electromagnetic field $[\mathbf{E}_e, \mathbf{H}_e]$ is a field for which $H_z(\mathbf{x},\omega) = 0$, which means that it is transverse magnetic to z (TM_z mode). Similarly, the field $[\mathbf{E}_m, \mathbf{H}_m]$ is transverse electric to z (TE_z mode). Thus, an arbitrary field in a homogeneous source-free region can be expressed as the sum of TM_z and TE_z modes. Moreover, all the components of the electromagnetic fields $\mathbf{E}$ and $\mathbf{H}$ can be derived from the scalar potentials A and F (cf. (1.52), (1.53), (1.54), (1.55)).

Remark 3 *Since we are interesting in the study of the electromagnetic field in the presence of a magnetic dipole, we focus on the computation of* $\mathbf{E}_m$ *and* $\mathbf{H}_m$*. Hence, in the following, the analysis will involve only the scalar potential* F*.*

1.6 Boundary conditions

Each electromagnetic field must satisfy Maxwell's equations with appropriate conditions applied at the interfaces separating the homogeneous regions involved in the problem. In this section we state these conditions, although they can be derived from the integral forms of Maxwell's equations (see [64, Appendix A.1.2] for the details).

Consider two horizontally homogeneous layers that for simplicity we call medium 1 and medium 2. At the interface separating medium 1 from medium

2 the normal components B_n of $\mathbf{B}$, J_n of $\mathbf{J}$ and the tangential components E_t of $\mathbf{E}$, H_t of $\mathbf{H}$ are continuous, that is,

$$\begin{aligned} B_{n_1} &= B_{n_2}, \\ J_{n_1} &= J_{n_2}, \\ E_{t_1} &= E_{t_2}, \\ B_{n_1} &= B_{n_2}. \end{aligned}$$

Moreover, the normal component D_n of $\mathbf{D}$ is continuous at the interface due to the accumulation of a surface-charge density ρ_s, i.e.,

$$D_{n_2} - D_{n_1} = \rho_s.$$

For the Schelkunoff potential $\mathbf{F}$, in the case of a magnetic dipole, the boundary conditions are given by

$$F_1 = F_2, \tag{1.56}$$

$$\frac{1}{\mu_1}\frac{\partial F_1}{\partial z} = \frac{1}{\mu_2}\frac{\partial F_2}{\partial z}. \tag{1.57}$$

1.7 Integral general solutions

In this section we derive the EM fields $\mathbf{E}_m$ and $\mathbf{H}_m$ for a vertical and horizontal magnetic dipole in the presence of a homogeneous or layered earth. As already said, in order to simplify the problem, we develop the analysis in terms of the vector potential $\mathbf{F}$, and then, by using relations (1.54), (1.55), we compute the electric and magnetic fields components. Therefore, in this setting the goal is to find $\mathbf{F}$ that satisfies equation (1.38), with boundary conditions (1.56) and (1.57).

In general, the solution of a boundary-value problem is the sum of the particular solution of the inhomogeneous differential equation and the complementary solution of the homogeneous equation. We first derive the complementary solution and then add the particular solution (accordingly to the type of dipole).

By considering the case of a source-free region and from equation (1.38), the potential F satisfies the partial differential equation

$$\nabla^2 F(\mathbf{x}, \omega) + k^2 F(\mathbf{x}, \omega) = 0.$$

Then, by using the spatial double Fourier transform (see (B.3))

$$\tilde{F}(k_x, k_y, z) = \int_{-\infty}^{+\infty} \int_{-\infty}^{+\infty} F(x, y, z) e^{-i(k_x x + k_y y)} dx dy,$$

we can convert the above equation into the ordinary differential equation

$$\frac{d^2\tilde{F}(z)}{dz^2} - u^2\tilde{F}(z) = 0, \tag{1.58}$$

where $u^2 := k_x^2 + k_y^2 - k^2$. At this point, we have the following result.

Proposition 5 *The solution of (1.58) is*

$$\tilde{F}(k_x, k_y, z) = F^+(k_x, k_y)e^{-uz} + F^-(k_x, k_y)e^{uz}.$$

Proof. The characteristic equation of (1.58) is

$$\gamma^2 - u^2 = 0.$$

Hence, we have that $\gamma = \pm u$ and the solution of (1.58) can be written as the linear combination of a function $c_1(k_x, k_y)e^{-uz}$, that decays downward, and a function $c_2(k_x, k_y)e^{uz}$, that decays upward. Finally, by defining

$$c_1(k_x, k_y) := F^+(k_x, k_y) \quad \text{and} \quad c_2(k_x, k_y) := F^-(k_x, k_y),$$

we obtain the result. ■

In a layer containing the source we must add the particular solution of the inhomogeneous differential equations to the complementary solution.

In this setting, we first consider the scalar Green's function $G(x, y, z)$, which is the response of a unit point source at the origin. In particular, G is the solution of the scalar differential equation

$$\nabla^2 G(x, y, z) + k^2 G(x, y, z) = -\delta(x)\delta(y)\delta(z), \tag{1.59}$$

where δ is the Dirac delta function. Again, by using (B.3) we define $\tilde{G}$ and $\tilde{\tilde{G}}$ as the double and triple Fourier spatial transform, respectively, that is,

$$\tilde{G}(k_x, k_y, z) = \int_{-\infty}^{+\infty}\int_{-\infty}^{+\infty} G(x, y, z)e^{-i(k_x x + k_y y)}dxdy,$$
$$\tilde{\tilde{G}}(k_x, k_y, k_z) = \int_{-\infty}^{+\infty}\int_{-\infty}^{+\infty}\int_{-\infty}^{+\infty} G(x, y, z)e^{-i(k_x x + k_y y + k_z z)}dxdydz.$$

Now, for the transform $\tilde{G}$ the following result holds.

Proposition 6 *The Fourier transform $\tilde{G}$ of the scalar Green's function G can be written as*

$$\tilde{G}(k_x, k_y, z) = \frac{e^{-u|z|}}{2u}. \tag{1.60}$$

Proof. Taking the triple Fourier transform (see (B.3)) of equation (1.59) and using the derivative property of the Fourier transform (cf. Appendix B), leads to

$$\tilde{\tilde{G}}(k_x, k_y, k_z) = \frac{1}{k_x^2 + k_y^2 + k_z^2 - k^2}.$$

Now, we evaluate the inverse transform (see (B.4)) of the above expression of $\tilde{\tilde{G}}$ by considering first integration with respect to k_z, that is,

$$\tilde{G}(k_x, k_y, z) = \frac{1}{2\pi} \int_{-\infty}^{+\infty} \frac{e^{ik_z z}}{k_z^2 + k_x^2 + k_y^2 - k^2} dk_z.$$

Finally, from [15, Vol.1, p.118, n.6] and by remembering that

$$u^2 = k_x^2 + k_y^2 - k^2,$$

we obtain the result. ■

By Proposition 6, in the case of a point source placed at $z = -H$ above the earth, the particular solution in the air of the inhomogeneous equation

$$\nabla^2 F(\mathbf{x}, \omega) + k^2 F(\mathbf{x}, \omega) = S_p(\mathbf{x}, \omega)$$

can be written as

$$\tilde{F}_p(k_x, k_y, z) = F_p(k_x, k_y) e^{-u_0|z+H|}, \tag{1.61}$$

where F_p is the amplitude of the incident field and depends on the source, i.e. on the forcing term S_p.

Consider now a layered underground model as in Figure 1.1, where σ_n and h_n, $n = 1, \ldots, N$, represent conductivity and thickness of the n-th layer, respectively. The deeper layer is assumed to have infinite thickness.

In order to derive the mathematical formulation of the fields, it is convenient to introduce a cylindrical polar coordinate system (ρ, ϕ, z), with the longitudinal axis downward directed, such that the ground plane coincides with the plane $z = 0$. In this case, the solution in the n-th layer, $n = 1, \ldots, N-1$, is given by

$$\tilde{F}_n(k_x, k_y, z) = F_n^+(k_x, k_y) e^{-uz} + F_n^-(k_x, k_y) e^{uz},$$

where $u_n^2 = k_x^2 + k_y^2 - k_n^2$ and k_n is the wave number of the n-th layer. We observe that above the surface of the earth we can use only solutions that decay upward, and in the N layer only solutions that decay downward (see Figure 1.2).

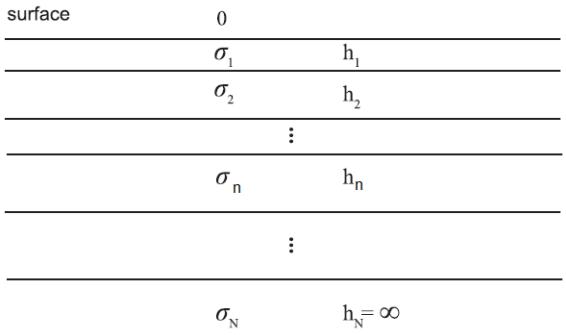

Figure 1.1: Layered underground conductivity model.

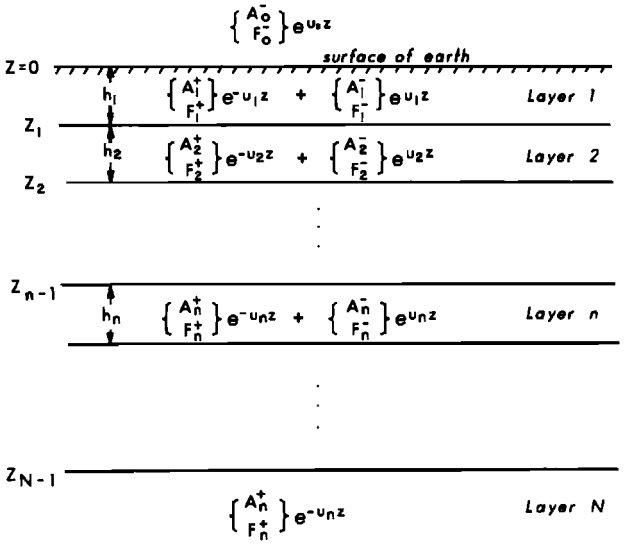

Figure 1.2: Solutions for the vector potentials $\tilde{A}$ and $\tilde{F}$ in a N-layered earth. Image taken from [64].

Since we want to derive the EM field at the surface of the earth, we only consider solutions that decay upward. Therefore, for the homogeneous equation we are interested in solutions of the form

$$\tilde{F}_0(k_x, k_y, z) = F_0^-(k_x, k_y)e^{u_0 z}.$$

Moreover, since the coefficient F_0^- can be written as

$$F_0^-(k_x, k_y) = R_0 F_p(k_x, k_y)e^{-u_0 H},$$

where $R_0 = R_0(k_x, k_y)$ is the reflection coefficient, derived in the following proposition, we have that

$$\tilde{F}_0(k_x, k_y, z) = R_0 F_p(k_x, k_y)e^{-u_0 H}e^{u_0 z}. \tag{1.62}$$

Proposition 7 *For a N-layered earth, the reflection coefficient R_0 is given by*

$$R_0 = \frac{Y_0 - \hat{Y}_1}{Y_0 + \hat{Y}_1},$$

with

$$\begin{aligned}
Y_n &= \frac{u_n}{i\omega\mu_n}, \quad n = 1, \dots N, \\
\hat{Y}_n &= Y_n \frac{\hat{Y}_{n+1} + Y_n \tanh(u_n h_n)}{Y_n + \hat{Y}_{n+1}\tanh(u_n h_n)}, \quad n = 1, \dots N-1, \\
\hat{Y}_N &= Y_N,
\end{aligned}$$

where $u_n = (k_x^2 + k_y^2 - k_n^2)^{\frac{1}{2}}$ and $k_n^2 = -i\omega\mu_n\sigma_n$.

Proof. Since the electric vector is perpendicular to the plane of incidence, choosing this plane to be the xz plane, the electric field has only a y component and, for the n-th layer, it is a solution of the equation

$$(\nabla^2 + k_n^2)E_{y,n} = 0.$$

The general solution is of the form

$$E_{y,n} = [a_n e^{-u_n(z-z_n)} + b_n e^{u_n(z-z_n)}]e^{-i\lambda x},$$

where $u_n^2 = k_n^2 - \lambda^2$, b_0 is the amplitude of the reflected wave and $b_N = 0$. From Maxwell's equations and since $H_z = 0$, we have that

$$\begin{aligned}
H_{x,n} &= \frac{1}{i\mu_n\omega}\frac{\partial E_{ny}}{\partial z} \\
&= -\frac{u_n}{i\mu_n\omega}[a_n e^{-u_n(z-z_n)} + b_n e^{u_n(z-z_n)}]e^{-i\lambda x}.
\end{aligned}$$

As far as reflections are concerned, we may ignore the factor $e^{-i\lambda x}$, since it can only represents propagation parallel to interfaces.

Over the plane $z = z_n$, we have that

$$E_{y,n} = a_n + b_n \quad \text{and} \quad H_{x,n} = -Y_n(a_n - b_n),$$

where

$$Y_n := \frac{u_n}{i\mu_n\omega}.$$

Therefore, we can write

$$a_n = \frac{1}{2}\left(E_{y,n} - \frac{1}{Y_n}H_{x,n}\right) \quad \text{and} \quad b_n = \frac{1}{2}\left(E_{y,n} + \frac{1}{Y_n}H_{x,n}\right). \tag{1.63}$$

At $z = z_{n-1}$, the boundary conditions of continuity of electric and magnetic fields demand that

$$E_{y,n} = E_{y,(n-1)} \quad \text{and} \quad H_{x,n} = H_{x,(n-1)}.$$

Thus,

$$\begin{aligned} E_{y,(n-1)} &= a_n e^{-u_n(z_{n-1}-z_n)} + b_n e^{u_n(z_{n-1}-z_n)}, \\ H_{x,(n-1)} &= -Y_n[a_n e^{-u_n(z_{n-1}-z_n)} - b_n e^{u_n(z_{n-1}-z_n)}]. \end{aligned}$$

Now, if we let $z_n - z_{n-1} = h_n$ and substituting the expressions (1.63) for a_n and b_n, we obtain

$$\begin{aligned} E_{y,(n-1)} &= E_{y,n}\cosh(u_n h_n) - \frac{1}{Y_n}H_{x,n}\sinh(u_n h_n), \\ H_{x,(n-1)} &= -Y_n E_{y,n}\sinh(u_n h_n) + H_{x,n}\cosh(u_n h_n). \end{aligned}$$

The impedance $\hat{Y}_{n-1}$ is defined as

$$\hat{Y}_{n-1} = -\frac{H_{x,(n-1)}}{E_{y,(n-1)}},$$

and, for an N-layered earth, we have that

$$\begin{aligned} \hat{Y}_n &= Y_n\frac{\hat{Y}_{n+1} + Y_n\tanh(u_n h_n)}{Y_n + \hat{Y}_{n+1}\tanh(u_n h_n)}, \quad n = 1, \ldots N-1, \\ \hat{Y}_N &= Y_N. \end{aligned}$$

Finally, the reflection coefficient R_0 is defined as

$$R_0 = -\frac{H_{x,0}}{E_{y,0}} = \frac{Y_0 - \hat{Y}_1}{Y_0 + \hat{Y}_1}.$$

■

By combining the particular and complementary solutions (see (1.61), (1.62)) between the source and the earth, we obtain

$$\begin{aligned}\tilde{F}(k_x, k_y, z) &= F_p(k_x, k_y)e^{-u_0 H}e^{-u_0 z} + F_p(k_x, k_y)R_0 e^{-u_0 H}e^{u_0 z} \\ &= F_p(k_x, k_y)e^{-u_0 H}(e^{-u_0 z} + R_0 e^{u_0 z}).\end{aligned} \tag{1.64}$$

Finally, by using the inverse Fourier transform (cf. (B.4))

$$F(x, y, z) = \frac{1}{4\pi^2}\int_{-\infty}^{+\infty}\int_{-\infty}^{+\infty}\tilde{F}(k_x, k_y, z)e^{i(k_x x + k_y y)}dk_x dk_y,$$

the potential F is given by

$$F(x, y, x) = \frac{1}{4\pi^2}\int_{-\infty}^{+\infty}\int_{-\infty}^{+\infty}F_p(k_x, k_y, z)e^{-u_0 h}(e^{-u_0 z} + R_0 e^{u_0 z})e^{i(k_x x + k_y y)}dk_x dk_y. \tag{1.65}$$

At this point, in order to compute integral expressions of the EM field components, it remains to derive the amplitude of the incident field F_p, accordingly to the particular source.

1.7.1 Vertical Magnetic Dipole

In the case of a vertical magnetic dipole, the magnetization vector (see (1.23)) is given by

$$\mathbf{M}^S(\mathbf{x}, \omega) = \mathbf{m}(\mathbf{x}, \omega)\delta(x)\delta(y)\delta(z),$$

where $\mathbf{m}$ is the magnetic moment of the dipole in (Am^2). Hence, from equations (1.38), (1.23) and the above expression, we have that

$$\begin{aligned}\nabla^2\mathbf{F}(\mathbf{x}, \omega) + k^2\mathbf{F}(\mathbf{x}, \omega) &= -\mathbf{J}_m^S(\mathbf{x}, \omega) \\ &= -i\mu_0\omega\mathbf{M}^S(\mathbf{x}, \omega) \\ &= -i\mu_0\omega\mathbf{m}(\mathbf{x}, \omega)\delta(x)\delta(y)\delta(z),\end{aligned}$$

where μ_0 is the magnetic permeability of vacuum (see (1.10)). By (1.51) and since the dipole is z-directed, the particular solution for a vertical magnetic dipole of moment $m\mathbf{u}_z$ placed at $z = -H$ above the surface of the earth satisfies the differential equation

$$\nabla^2 F(\mathbf{x}, \omega) + k_0^2 F(\mathbf{x}, \omega) = -i\mu_0\omega m(\mathbf{x}, \omega)\delta(x)\delta(y)\delta(z + H).$$

The following proposition holds.

Proposition 8 *In the transform domain, the solution between the dipole and the earth is given by*

$$\tilde{F}(k_x, k_y, z) = F_p(k_x, k_y, z)e^{-u_0 H}e^{-u_0 z}, \tag{1.66}$$

where

$$F_p(k_x, k_y, z) = \frac{i\mu_0\omega m}{2u_0} \tag{1.67}$$

is the amplitude of the incident field.

Proof. The result is obtained from equation (1.60) for the Green's function and from relation (1.64). ■

We observe that, due to the symmetry of the problem, currents flow only horizontally. Therefore, there is no vertical component of electric field and the EM field of a vertical magnetic dipole above a horizontally layered earth is a TE field. Before going on, we need a preliminary lemma.

Lemma 1 *It holds*

$$\int_{-\infty}^{+\infty}\int_{-\infty}^{+\infty} F(k_x^2 + k_y^2)e^{i(k_x x + k_y y)}dk_x dk_y = 2\pi\int_0^{\infty} F(\lambda)\lambda J_0(\lambda\rho)d\lambda, \tag{1.68}$$

with $\lambda^2 = k_x^2 + k_y^2$ *and* $\rho^2 = x^2 + y^2$.

Proof. By making the substitutions $k_x = \lambda\cos\psi$, $k_y = \lambda\sin\psi$, $x = \rho\cos\phi$, $y = \rho\sin\phi$ and then using the cylindrical coordinates (see Appendix A), we have that

$$\int_{-\infty}^{+\infty}\int_{-\infty}^{+\infty} F(k_x^2 + k_y^2)e^{i(k_x x + k_y y)}dk_x dk_y = \int_0^{\infty} F(\lambda)\int_0^{2\pi} e^{i\lambda\rho\cos(\psi-\phi)}d\psi\lambda d\lambda.$$

By considering the integral representation (see [29, p.952, 8.411, n.1])

$$\int_0^{2\pi} e^{i\lambda\rho\cos(\psi-\phi)}d\psi = 2\pi J_0(\lambda\rho),$$

where J_0 is the Bessel function of the first type of order 0, we obtain the result. ■

At this point, by substituting equation (1.67) into (1.65), we have the following expression for the potential between the dipole and the earth:

$$\begin{aligned} F(x, y, z) &= \frac{1}{4\pi^2}\int_{-\infty}^{+\infty}\int_{-\infty}^{+\infty}\frac{i\mu_0\omega m}{2u_0}e^{-u_0 H}(e^{-u_0 z} + R_0 e^{u_0 z})e^{i(k_x x + k_y y)}dk_x dk_y \\ &= \frac{i\mu_0\omega m}{8\pi^2}\int_{-\infty}^{+\infty}\int_{-\infty}^{+\infty}[e^{-u_0(z+H)} + R_0 e^{u_0(z-H)}]\frac{1}{u_0}e^{i(k_x x + k_y y)}dk_x dk_y. \end{aligned}$$

Then, by using equation (1.68) we obtain

$$F(\rho,z)=\frac{i\mu_0\omega m}{4\pi}\int_0^\infty [e^{-u_0(z+H)}+R_0(\lambda)e^{u_0(z-H)}]\frac{\lambda}{u_0}J_0(\lambda\rho)d\lambda, \tag{1.69}$$

where $\lambda^2=k_x^2+k_y^2$ and $\rho^2=x^2+y^2$. Finally, we can derive by differentiation (see (1.54), (1.55)) the electromagnetic fields for a vertical magnetic dipole, in the case of a N-layered earth. We denote them by $\mathbf{E}^{(N)}$ and $\mathbf{H}^{(N)}$,

In particular, due to symmetry, there will be only a ϕ component of electric field. To evaluate it we use the fact that

$$E_\phi^{(N)}=-\frac{y}{\rho}E_x^{(N)}+\frac{x}{\rho}E_y^{(N)}=\frac{y}{\rho}\frac{\partial F}{\partial y}+\frac{x}{\rho}\frac{\partial F}{\partial x},$$

where the last equality comes from (1.54) and the relations (see [1, p.361, p.358])

$$\frac{\partial J_0(\lambda\rho)}{\partial x}=-\lambda\frac{x}{\rho}J_1(\lambda\rho), \tag{1.70}$$

$$\frac{\partial J_0(\lambda\rho)}{\partial y}=-\lambda\frac{y}{\rho}J_1(\lambda\rho), \tag{1.71}$$

where J_1 is the Bessel function of the first type of order 1. Therefore, the ϕ component of the electric field is given by

$$E_\phi^{(N)}=-\frac{i\mu_0\omega m}{4\pi}\int_0^\infty [e^{-u_0(z+H)}+R_0(\lambda)e^{u_0(z-H)}]\frac{\lambda^2}{u_0}J_1(\lambda\rho)d\lambda. \tag{1.72}$$

The horizontal magnetic field has only a radial component, that is,

$$H_\rho^{(N)}=\frac{x}{\rho}H_x^{(N)}+\frac{y}{\rho}H_y^{(N)}=\frac{x}{\rho}\frac{1}{i\mu_0\omega}\frac{\partial^2 F}{\partial x\partial z}+\frac{y}{\rho}\frac{1}{i\mu_0\omega}\frac{\partial^2 F}{\partial y\partial z},$$

where the last equality comes from (1.55). Hence, using relations (1.70) and (1.71), we obtain

$$H_\rho^{(N)}=\frac{m}{4\pi}\int_0^\infty [e^{-u_0(z+H)}-R_0(\lambda)e^{u_0(z-H)}]\lambda^2 J_1(\lambda\rho)d\lambda. \tag{1.73}$$

Finally, using equation (1.55) and applying the relation

$$\frac{\partial^2}{\partial z^2}+k_0^2=u_0^2+k_0^2=\lambda^2,$$

the vertical magnetic field component is given by

$$H_z^{(N)}=\frac{m}{4\pi}\int_0^\infty [e^{-u_0(z+H)}+R_0(\lambda)e^{u_0(z-H)}]\frac{\lambda^3}{u_0}J_0(\lambda\rho)d\lambda. \tag{1.74}$$

Equations (1.72), (1.73) and (1.74), which are Hankel transforms of order 1 and 0, in general, can be evaluated only by numerical integration. If the source and the receiver are on the surface of the earth, simply set H and z to zero.

Remark 4 *For the following we assume the magnetic permeability of the earth to be that of the free space, i.e.* $\mu_n = \mu_0$. *In this setting, the reflection coefficient can be simplified as*

$$R_0 = \frac{\lambda - \hat{u}_1}{\lambda + \hat{u}_1},$$

with

$$\hat{u}_n = u_n \frac{\hat{u}_{n+1} + u_n \tanh(u_n h_n)}{u_n + \hat{u}_{n+1} \tanh(u_n h_n)}, \quad n = 1, \ldots, N-1,$$
$$\hat{u}_N = u_N.$$

Only for the case of the source and receiver on the surface of a homogeneous earth ($N = 1$, $z = H = 0$) under the quasi-static approximation (i.e. $k_0 \approx 0$), we can derive analytic expressions for the fields $H_z^{(1)}$ and $H_\rho^{(1)}$. In this setting, first of all we have

$$R_0 = \frac{\lambda - u_1}{\lambda + u_1},$$

and, after some computations, equations (1.72), (1.73) become

$$E_\phi^{(1)} = -\frac{i\omega\mu_0 m}{2\pi} \int_0^{+\infty} \frac{\lambda^2}{\lambda + u_1} J_1(\lambda\rho) d\lambda, \tag{1.75}$$

$$H_\rho^{(1)} = \frac{m}{2\pi} \int_0^{+\infty} \frac{\lambda^2 u_1}{\lambda + u_1} J_1(\lambda\rho) d\lambda. \tag{1.76}$$

Since $\lambda^2 - u_1^2 = k_1^2$, multiplying the numerator and denominator of the integrand function in (1.75) by the factor $(\lambda - u_1)$, leads to

$$E_\phi^{(1)} = -\frac{i\omega\mu_0 m}{2\pi k_1^2} \int_0^{+\infty} \lambda^2 (\lambda - u_1) J_1(\lambda\rho) d\lambda \tag{1.77}$$

$$= -\frac{m}{2\pi\sigma} \left[\int_0^{+\infty} \lambda^3 J_1(\lambda\rho) d\lambda - \int_0^{+\infty} \lambda^2 u_1 J_1(\lambda\rho) d\lambda \right], \tag{1.78}$$

where σ is the conductivity of the homogeneous earth. Then, using relations (1.70)-(1.71) for the Bessel functions, we have that

$$E_\phi^{(1)} = -\frac{m}{2\pi\sigma} \frac{\partial}{\partial\rho} \left[\int_0^{+\infty} \lambda^2 J_0(\lambda\rho) d\lambda - \int_0^{+\infty} \lambda u_1 J_0(\lambda\rho) d\lambda \right]. \tag{1.79}$$

At this point, we can rewrite the first integral in the above expression as

$$\begin{aligned}\int_0^{+\infty} \lambda^2 J_0(\lambda\rho)d\lambda &= \left[\int_0^{+\infty} e^{-\lambda z}\lambda^2 J_0(\lambda\rho)d\lambda\right]_{z=0} \\ &= \left[\frac{\partial^2}{\partial z^2}\int_0^{+\infty} e^{-\lambda z} J_0(\lambda\rho)d\lambda\right]_{z=0} \\ &= \left[\frac{\partial^2}{\partial z^2}\left(\frac{1}{r}\right)\right]_{z=0},\end{aligned}$$

where the last equality comes from [29, p.707, 6.611, n.1] with $r = \sqrt{\rho^2 + z^2}$, and the second integral as

$$\begin{aligned}\int_0^{+\infty} \lambda u_1 J_0(\lambda\rho)d\lambda &= \left[\int_0^{\infty} e^{-u_1 z}\lambda u_1 J_0(\lambda\rho)d\lambda\right]_{z=0} \\ &= \left[\frac{\partial^2}{\partial z^2}\int_0^{+\infty} e^{-u_1 z}\lambda u_1 J_0(\lambda\rho)d\lambda\right]_{z=0} \\ &= \left[\frac{\partial^2}{\partial z^2}\frac{e^{-ik_1 r}}{r}\right]_{z=0},\end{aligned}$$

where we have also used the Sommerfeld identity (see [55])

$$\int_0^{+\infty} \frac{\lambda}{u_1} e^{-u_1 z} J_0(\lambda\rho)d\lambda = \frac{e^{-ik_1 r}}{r}. \tag{1.80}$$

Therefore, equation (1.79) becomes

$$\begin{aligned}E_\phi^{(1)} &= -\frac{m}{2\pi\sigma}\frac{\partial}{\partial\rho}\left[\frac{\partial^2}{\partial z^2}\left(\frac{1}{r}\right) - \frac{\partial^2}{\partial z^2}\left(\frac{e^{-ik_1 r}}{r}\right)\right]_{z=0} \\ &= -\frac{m}{2\pi\sigma\rho^4}\left[3 - \left(3 + 3ik_1\rho - k_1^2\rho^2\right)e^{-ik_1\rho}\right].\end{aligned} \tag{1.81}$$

By using the above expression of $E_\phi^{(1)}$ and relation (1.14) in cylindrical coordinates, that is,

$$H_z^{(1)} = -\frac{1}{i\omega\mu_0}\frac{1}{\rho}\frac{\partial}{\partial\rho}(\rho E_\phi),$$

we obtain

$$H_z^{(1)} = \frac{m}{2\pi k_1^2\rho^5}[9 - (9 + ik_1\rho - 4k_1^2\rho^2 - ik_1^3\rho^3)e^{-ik_1\rho}]. \tag{1.82}$$

Now, let us consider the radial component $H_\rho^{(1)}$. From equation (1.76) and by using again relations (1.70)-(1.71), we have

$$H_\rho^{(1)} = \frac{m}{4\pi}\frac{\partial}{\partial\rho}\int_0^{+\infty}\frac{\lambda - u_1}{\lambda + u_1}\lambda J_0(\lambda\rho)d\lambda.$$

Then, by multiplying the numerator and denominator of the above integrand by the factor $(\lambda + u_1)$, we obtain

$$H_\rho^{(1)} = \frac{mk_1^2}{4\pi}\frac{\partial}{\partial\rho}\int_0^{+\infty}\frac{\lambda}{(\lambda+u_1)^2}\lambda J_0(\lambda\rho)d\lambda, \tag{1.83}$$

where we have also used the fact that $\lambda^2 - u_1^2 = k_1^2$. At this point, we rewrite equation (1.83) as

$$\begin{aligned} H_\rho^{(1)} &= \frac{m}{4\pi}\frac{\partial}{\partial\rho}\left[\frac{1}{4}\int_0^{+\infty}\frac{4\lambda u_1}{(\lambda+u_1)^2}J_0(\lambda\rho)d\lambda\right] \\ &= \frac{m}{16\pi}\frac{\partial}{\partial\rho}\left\{\int_0^{+\infty}\left[1-\left(\frac{u_1-\lambda}{u_1+\lambda}\right)^2\right]\frac{1}{u_1}J_0(\lambda\rho)d\lambda\right\} \\ &= \frac{m}{16\pi}\frac{\partial}{\partial\rho}\left[\int_0^{+\infty}\frac{1}{u_1}J_0(\lambda\rho)d\lambda - \int_0^{+\infty}\left(\frac{u_1-\lambda}{u_1+\lambda}\right)^2\frac{1}{u_1}J_0(\lambda\rho)d\lambda\right]. \end{aligned} \tag{1.84}$$

For the first integral in (1.84), from [29, p.681, 6.552, n.1] we have

$$\int_0^{+\infty}\frac{1}{u_1}J_0(\lambda\rho)d\lambda = \int_0^{+\infty}\frac{1}{\sqrt{\lambda^2+(ik_1)^2}}J_0(\lambda\rho)d\lambda = I_0\left(\frac{ik_1\rho}{2}\right)K_0\left(\frac{ik_1\rho}{2}\right),$$

where I_0 and K_0 are the modified Bessel functions of order 0 of the first and second kind, respectively. Now, since $k_1^4 = (\lambda^2 - u_1^2)^2 = (u_1 - \lambda)^2(u_1 + \lambda^2)$ and hence

$$(u_1 - \lambda^2) = \frac{k_1^4}{(u_1+\lambda)^2},$$

the second integral in (1.84) becomes

$$\begin{aligned} \int_0^{+\infty}\left(\frac{u_1-\lambda}{u_1+\lambda}\right)^2\frac{1}{u_1}J_0(\lambda\rho)d\lambda &= \int_0^{+\infty}\frac{k_1^4}{(u_1+\lambda)^4}\frac{1}{u_1}J_0(\lambda\rho)d\lambda \\ &= I_2\left(\frac{ik_1\rho}{2}\right)K_2\left(\frac{ik_1\rho}{2}\right), \end{aligned}$$

where the last equality comes from [15, Vol.II, p.8, n.16] and I_2, K_2 are the modified Bessel functions of order 2 of the first and second kind, respectively. Therefore, from (1.84) we obtain

$$H_\rho^{(1)} = \frac{mk_1^2}{16\pi}\frac{\partial}{\partial\rho}\left[I_0\left(\frac{ik_1\rho}{2}\right)K_0\left(\frac{ik_1\rho}{2}\right) - I_2\left(\frac{ik_1\rho}{2}\right)K_2\left(\frac{ik_1\rho}{2}\right)\right].$$

Finally, after differentiation, we can consider a simplified form of the above expression given in [60], that is,

$$H_\rho^{(1)} = -\frac{mk_1^2}{4\pi\rho}\left[I_1\left(\frac{ik_1\rho}{2}\right)K_1\left(\frac{ik_1\rho}{2}\right) - I_2\left(\frac{ik_1\rho}{2}\right)K_2\left(\frac{ik_1\rho}{2}\right)\right], \quad (1.85)$$

where I_1 and K_1 are the modified Bessel functions of order 1 of the first and second kind, respectively.

1.7.2 Horizontal Magnetic Dipole

Similar integral representations of the EM field can be formulated also for a horizontal magnetic dipole in the case of a layered earth. In this section we derive the Cartesian components of the magnetic fields for a horizontal, x-directed magnetic dipole above or on the surface of the earth.

Remark 5 *The fields for a y-directed dipole can be obtained by a simple permutation of coordinates.*

Following the same arguments of the previous section, the vector potential for the particular solution between the dipole and the earth is given by (cf. Proposition 8)

$$\tilde{F}(x, k_y, k_z) = F_p(x, k_y, k_z)e^{-u_0(z+H)},$$

with

$$F_p(x, k_y, k_z) = \frac{i\mu_0\omega m}{2u_0}.$$

Moreover, from (1.49) and since the dipole is x-directed, we obtain that the vertical magnetic field is

$$\tilde{H}_z = \frac{1}{i\mu_0\omega}\frac{\partial^2\tilde{F}_x}{\partial x\partial z} = -ik_x\frac{m}{2}e^{-u_0(z+H)}, \quad (1.86)$$

where we have also used the differentiation property of the Fourier transform (see Appendix B). Now, in order to find the coefficient F_p for the particular solution at $z = -H$, we impose (see (1.86) and (1.55))

$$ik_x\frac{m}{2} = \frac{1}{i\mu_0\omega}\left(\frac{\partial^2}{\partial z^2} + k_0^2\right)F_p.$$

Remembering that

$$\frac{\partial^2}{\partial z^2} + k_0^2 = u_0^2 + k_0^2 = k_x^2 + k_y^2,$$

we obtain

$$F_p = -\frac{i\mu_0\omega m}{2}\frac{ik_x}{k_x^2+k_y^2}.$$

Substituting the above expression in (1.65) leads to

$$F(x,y,z) = -\frac{i\mu_0\omega m}{8\pi^2}\int_{-\infty}^{+\infty}\int_{-\infty}^{+\infty}\left[e^{-u_0(z+H)} + R_0 e^{u_0(z-H)}\right]\frac{ik_x}{k_x^2+k_y^2}e^{i(k_x x+k_y y)}dk_x dk_y.$$

Then, by using (1.68) we have that

$$F(\rho,z) = -\frac{i\mu_0\omega m}{4\pi}\frac{\partial}{\partial x}\int_0^{\infty}\left[e^{-u_0(z+H)} + R_0 e^{u_0(z-H)}\right]\frac{1}{\lambda}J_0(\lambda\rho)d\lambda.$$

At this point, the magnetic fields can be derived from the above equation by using formula (1.55) as follows:

$$\begin{aligned}
H_x^{(N)} &= \frac{1}{i\mu_0\omega}\frac{\partial^2 F}{\partial x\partial z}\\
&= -\frac{m}{4\pi}\frac{\partial^2}{\partial x^2}\int_0^{\infty}\frac{\partial}{\partial z}\left[e^{-u_0(z+H)} + R_0 e^{u_0(z-H)}\right]\frac{1}{\lambda}J_0(\lambda\rho)d\lambda\\
&= \frac{m}{4\pi}\frac{\partial^2}{\partial x^2}\int_0^{\infty}\left[e^{-u_0(z+H)} + R_0 e^{u_0(z-H)}\right]J_0(\lambda\rho)d\lambda,\\
H_y^{(N)} &= \frac{1}{i\mu_0\omega}\frac{\partial^2 F}{\partial y\partial z}\\
&= \frac{m}{4\pi}\frac{\partial^2}{\partial x\partial y}\int_0^{+\infty}\left[e^{-u_0(z+H)} + R_0 e^{u_0(z-H)}\right]J_0(\lambda\rho)d\lambda,\\
H_z^{(N)} &= \frac{1}{i\mu_0\omega}\frac{\partial^2}{\partial z^2}F\\
&= \frac{m}{4\pi}\frac{\partial}{\partial x}\int_0^{\infty}\left[e^{-u_0(z+H)} + R_0 e^{u_0(z-H)}\right]\lambda J_0(\lambda\rho)d\lambda.
\end{aligned}$$

Interchanging the order of differentiation and integration and noting that

$$\begin{aligned}
\frac{\partial}{\partial x} &= \frac{x}{\rho}\frac{\partial}{\partial\rho},\\
\frac{\partial^2}{\partial x^2} &= \left(\frac{1}{\rho}-\frac{x^2}{\rho^3}\right)\frac{\partial}{\partial\rho} + \frac{x^2}{\rho^2}\frac{\partial^2}{\partial\rho^2},\\
\frac{\partial^2}{\partial x\partial y} &= -\frac{xy}{\rho^3}\frac{\partial}{\partial\rho} + \frac{xy}{\rho^2}\frac{\partial^2}{\partial\rho^2},\\
\frac{\partial J_0(\lambda\rho)}{\partial\rho} &= -\lambda J_1(\lambda\rho),\\
\frac{\partial^2 J_0(\lambda\rho)}{\partial\rho} &= \frac{\lambda}{\rho}J_1(\lambda\rho) - \lambda^2 J_0(\lambda\rho),
\end{aligned}$$

we finally obtain

$$H_x^{(N)} = -\frac{m}{4\pi}\left(\frac{1}{\rho} - \frac{2x^2}{\rho^3}\right)\int_0^\infty \left[e^{-u_0(z+H)} + R_0 e^{u_0(z-H)}\right]\lambda J_1(\lambda\rho)d\lambda$$
$$- \frac{m}{4\pi}\frac{x^2}{\rho^2}\int_0^\infty \left[e^{-u_0(z+H)} + R_0 e^{u_0(z-H)}\right]\lambda^2 J_0(\lambda\rho)d\lambda, \quad (1.87)$$

$$H_y^{(N)} = \frac{m}{2\pi}\frac{xy}{\rho^3}\int_0^\infty \left[e^{-u_0(z+H)} + R_0 e^{u_0(z-H)}\right]\lambda J_1(\lambda\rho)d\lambda$$
$$- \frac{m}{4\pi}\frac{xy}{\rho^2}\int_0^\infty \left[e^{-u_0(z+H)} + R_0 e^{u_0(z-H)}\right]\lambda^2 J_0(\lambda\rho)d\lambda, \quad (1.88)$$

$$H_z^{(N)} = \frac{m}{4\pi}\frac{x}{\rho}\int_0^\infty \left[e^{-u_0(z+H)} + R_0 e^{u_0(z-H)}\right]\lambda^2 J_1(\lambda\rho)d\lambda. \quad (1.89)$$

As before, we can derive analytic expressions for the fields only when the transmitter and receiver are on the surface of a homogeneous earth (i.e. $N = 1$ and $z = H = 0$) and by assuming $k_0 \approx 0$. In this setting we can write the horizontal fields (1.87) and (1.88) as

$$H_x^{(1)} = -\frac{m}{4\pi}\frac{\partial}{\partial x}\left(\frac{x}{\rho}\Phi\right) \quad (1.90)$$

and

$$H_y^{(1)} = -\frac{m}{4\pi}\frac{\partial}{\partial y}\left(\frac{x}{\rho}\Phi\right), \quad (1.91)$$

with

$$\Phi = \Phi(\rho) = 2\int_0^\infty \frac{\lambda u_1}{\lambda + u_1} J_1(\lambda\rho)d\lambda.$$

By multiplying the numerator and denominator of the integrand in the above equation by the factor $(\lambda - u_1)$, we obtain

$$\Phi = 2\int_0^\infty \frac{\lambda u_1(\lambda - u_1)}{\lambda^2 - u_1^2} J_1(\lambda\rho)d\lambda = \frac{2}{k_1^2}\int_0^\infty (\lambda - u_1)\lambda u_1 J_1(\lambda\rho)d\lambda$$
$$= \frac{2}{k_1^2}\int_0^\infty (\lambda^2 u_1 - \lambda u_1^2) J_1(\lambda\rho)d\lambda = \Phi_1 + \Phi_2 + \Phi_3, \quad (1.92)$$

where

$$\Phi_1 = \frac{2}{k_1^2}\int_0^\infty \lambda^2 u_1 J_1(\lambda\rho)d\lambda,$$
$$\Phi_2 = -\frac{2}{k_1^2}\int_0^\infty \lambda^3 J_1(\lambda\rho)d\lambda,$$
$$\Phi_3 = 2\int_0^\infty \lambda J_1(\lambda\rho)d\lambda.$$

Now, differentiating the Sommerfeld identity (1.80) once with respect to ρ and twice with respect to z, and setting $z = 0$, yields to

$$\Phi_1 = \frac{2}{k^2\rho^4}\left(k^2\rho^2 - 3ik\rho - 3\right)e^{-ik\rho}.$$

Then, differentiating the integral (see [29, p.707, 6.611, n.1])

$$\int_0^\infty e^{-\lambda z} J_0(\lambda\rho)d\lambda = \frac{1}{\rho},$$

once with respect to ρ and setting $z = 0$ yields to an expression for Φ_3, while further differentiating twice with respect to z before setting $z = 0$, provide a simple expression for Φ_2, that is,

$$\Phi_2 = \frac{6}{k_1^2\rho^4} \quad \text{and} \quad \Phi_3 = \frac{2}{\rho^2}.$$

Using these results in (1.92), leads to

$$\Phi = \frac{2}{k^2\rho^4}\left[3 + k^2\rho^2 - (3 + 3ik\rho - k^2\rho^2)e^{-ik\rho}\right].$$

By substituting the above expression in equations (1.90) and (1.91), we can write the horizontal magnetic fields in the following forms,

$$\begin{aligned} H_x^{(1)} &= -\frac{m}{4\pi}\frac{\partial}{\partial x}\left(\frac{x}{\rho}\Phi\right) = -\frac{m}{4\pi}\left(\frac{\partial}{\partial x}\frac{x}{\rho}\Phi + \frac{x}{\rho}\frac{\partial\Phi}{\partial x}\right) \\ &= -\frac{m}{4\pi}\left(\frac{y^2}{\rho^3}\Phi + \frac{x^2}{\rho^2}\frac{\partial\Phi}{\partial\rho}\right) = -\frac{m}{4\pi\rho^3}\left(y^2\Phi + x^2\rho^2\frac{\partial\Phi}{\partial\rho}\right), \end{aligned} \tag{1.93}$$

and

$$\begin{aligned} H_y^{(1)} &= -\frac{m}{4\pi}\frac{\partial}{\partial y}\left(\frac{x}{\rho}\Phi\right) = -\frac{m}{4\pi}\frac{y}{\rho}\left[-\frac{x}{\rho^2}\Phi + \frac{x}{\rho}\frac{\partial\Phi}{\partial\rho}\right] \\ &= -\frac{m}{4\pi}\left(-\frac{xy}{\rho^3}\Phi + \frac{xy}{\rho^2}\frac{\partial\Phi}{\partial\rho}\right) = \frac{m}{4\pi\rho^3}\left(xy\Phi - xy\rho\frac{\partial\Phi}{\partial\rho}\right), \end{aligned}$$

with

$$\frac{\partial\Phi}{\partial\rho} = \frac{2}{k_1^2 r^5}\left[-2k_1^2\rho^2 - 12 + (-ik_1^3\rho^3 - 5k_1^2\rho^2 + 12ik_1\rho + 12)e^{-ik_1\rho}\right].$$

From expression (1.89), the vertical magnetic field is given by

$$H_z^{(1)} = -\frac{m}{4\pi}\frac{x}{\rho}\frac{\partial}{\partial\rho}\int_0^\infty \frac{\lambda - u_1}{\lambda + u_1}\lambda J_0(\lambda\rho)d\lambda.$$

Except for the sign, this expression is the same as the one for the radial component of the magnetic filed due to a vertical magnetic dipole. In the present case, however, we are evaluating the vertical magnetic field at a distance x from a horizontal magnetic dipole. Hence, from (1.85),

$$H_z^{(1)} = \frac{mk^2x}{4\pi\rho^2}\left[I_1\left(\frac{ik\rho}{2}\right)K_1\left(\frac{ik\rho}{2}\right) - I_2\left(\frac{ik\rho}{e}\right)K_2\left(\frac{ik\rho}{2}\right)\right].$$

Chapter 2

The forward problem

In this chapter we present the commonly used techniques, together with some novel approaches, to numerically evaluate the previously derived integral representations of the fields.

2.1 Digital filtering algorithms

In Chapter 1 we have seen that the evaluation of EM fields involves the computation of Hankel transforms of the type

$$I_f(\rho) = \int_0^\infty f(\lambda) J_l(\lambda\rho) d\lambda, \tag{2.1}$$

where J_l is the Bessel function of order $l = 0, 1$ and f is a function that decays exponentially. In this section we present the standard techniques, commonly named digital filtering algorithms, for the numerical evaluation of this kind of integrals (see e.g. [66] for a recent survey).

The first digital filtering algorithm, for the direct interpretation of geoelectrical resistivity sounding measurements, was introduced in 1971 by Ghosh [25]. One year later, the same method was used by Koefoed, Ghosh and Polman [38] for the computation of the integrals that characterized the magnetic field generated by a vertical oscillating magnetic dipole located at the surface of a horizontally stratified earth. Later, in 1979 Anderson [2] presented a linear digital filtering algorithm for rapid and accurate numerical evaluation of Hankel transform integrals. Below we summarize the steps that characterize the methods. By using the change of variables

$$x = \ln(\rho) \quad \text{and} \quad y = \ln\left(\frac{1}{\lambda}\right), \tag{2.2}$$

integral (2.1) becomes the convolution

$$I_f(x) = \int_{-\infty}^{+\infty} f(y)g(x-y)dy = (f * g)(x), \tag{2.3}$$

where $g(x-y) = e^{x-y}J_l(e^{x-y})$. At this point, it is known that the function f can be written as (see e.g. [43])

$$f(y) = \sum_{n=-\infty}^{+\infty} f(nh)\text{sinc}\left(\frac{y-nh}{h}\right), \tag{2.4}$$

where

$$\text{sinc}\left(\frac{y-nh}{h}\right) = \begin{cases} \frac{\sin\left(\frac{\pi(y-nh)}{h}\right)}{\frac{\pi(y-nh)}{h}} & y \neq nh \\ 1 & y = nh \end{cases} \tag{2.5}$$

is the sinc function. Therefore, by substituting (2.4) in (2.3), one obtains

$$I_f(x) = \sum_{n=-\infty}^{+\infty} f(nh)I_n(x), \tag{2.6}$$

where the integrals

$$I_n(x) = \int_{-\infty}^{+\infty} \text{sinc}\left(\frac{y-nh}{h}\right) g(x-y)dy \tag{2.7}$$

are called the filter coefficients. In order to evaluate $I_n(x)$, the idea is to first consider a function F such that

$$I_F(x) = \int_{-\infty}^{+\infty} F(y)g(x-y)dy \tag{2.8}$$

is known. For example in [38] the integrals considered are

$$\int_{-\infty}^{+\infty} \left(e^{-e^{-y}} - e^{-2e^{-y}}\right)[e^{x-y}J_0(e^{x-y})]dy = \frac{e^x}{\sqrt{1+e^{2x}}} - \frac{e^x}{\sqrt{4+e^{2x}}}$$

and

$$\int_{-\infty}^{+\infty} e^{-y}e^{-e^{-y}}[e^{x-y}J_1(e^{x-y})]dy = \frac{e^{2x}}{(1+e^{2x})^{\frac{3}{2}}},$$

(see [29, p.707, 6.611, n.1] and [29, p.711, 6.621, n.1]), while in [2] the following two Hankel transforms

$$\int_0^{+\infty} \lambda e^{-a\lambda^2}J_0(b\lambda)d\lambda = \frac{e^{-\frac{b^2}{4a}}}{2a}$$

and

$$\int_0^{+\infty} \lambda^2 e^{-a\lambda^2} J_1(b\lambda) d\lambda = \frac{b e^{-\frac{b^2}{4a}}}{(2a)^2}, \tag{2.9}$$

with $a > 0$, $b > 0$, (see also [29, p.716, 6.631, n.4]), are selected and then rewritten in convolutional form.

By considering the Fourier transform of equation (2.8) and by using the convolution theorem (see Appendix B), one obtains

$$\hat{I}_F(\xi) = \hat{F}(\xi)\hat{g}(\xi) \tag{2.10}$$

and hence

$$\hat{g}(\xi) = \frac{\hat{I}_F(\xi)}{\hat{F}(\xi)}. \tag{2.11}$$

Then, the Fourier transform of (2.7), given by

$$\hat{I}_n(\xi) = \mathrm{rect}(\xi - nh)\hat{g}(\xi), \tag{2.12}$$

where $\mathrm{rect}(\xi - nh)$ is the rectangular function, is considered. At this point, $I_n(x)$ is evaluated by substituting expression (2.11) in (2.12) and by taking the inverse Fourier transform. Finally, the practical algorithm that implements the digital filter is obtained by following the above procedure in which the functions $F(y)$ and $I_F(x)$ are sampled by using a constant sampling interval, and hence the Fourier transform is replaced by the discrete Fourier transform (B.5).

As a further development of the above linear filter methods, in 1979 Johansen and Sorensen [34] presented a general theory for the numerical evaluation of Hankel type integrals, by replacing the usual sinc interpolating function with

$$\frac{a\sin(\pi x)}{\sinh(a\pi x)},$$

where $a > 0$ is a smoothness parameter. Moreover, they provided an upper bound for the absolute error on the output function $I_f(x)$. In particular, they considered the Hankel integral (2.1) with $f(\lambda) = k(\lambda)\lambda$, in which $k(\lambda)$ is a generic function and $l > -1$. By the change of variables (2.2) and by defining $K(y) = e^{-y}k(e^{-y})$, $G(x) = e^x I_f(e^x)$ and $H_l(y) = e^y J_l(e^y)$, equation (2.1) can be written as the convolution

$$G(x) = \int_{-\infty}^{+\infty} K(y)H_l(x - y)dy. \tag{2.13}$$

By applying the convolution theorem, the above equation becomes

$$\hat{G}(s) = \hat{K}(s)\hat{H}_l(s), \tag{2.14}$$

where

$$\hat{H}_l(s) = \int_{-\infty}^{+\infty} H_l(x) e^{-i2\pi xs} dx \tag{2.15}$$

is the Fourier transform of $H_l(x)$ and the same for $\hat{K}$ and $\hat{G}$. The integral in (2.15) can be evaluated explicitly. In fact, by using the change of variable $x = \ln t$, equation (2.15) becomes (see [1, p.486, eq.11.4.16])

$$\hat{H}_l(s) = \int_0^{+\infty} J_l(t) t^{-i2\pi s} dt = 2^{-i2\pi s} \frac{\Gamma\left(\frac{l+1}{2} - i\pi s\right)}{\Gamma\left(\frac{l+1}{2} + i\pi s\right)}. \tag{2.16}$$

At this point, the sampled and interpolated version of K is defined as

$$K^\star(y) = \sum_{n=-\infty}^{+\infty} K(nh) P\left(\frac{y - nh}{h}\right), \tag{2.17}$$

with

$$P(y) = a \frac{\sin(\pi y)}{\sinh(\pi a y)}. \tag{2.18}$$

The parameter a is such that

$$\frac{h}{a} = M\pi, \tag{2.19}$$

where M is a fixed positive integer. We notice that, for small values of a it holds

$$P(y) \sim \frac{\sin(\pi y)}{\pi y} = \mathrm{sinc}(\pi y).$$

By substituting (2.17) in (2.13), an approximation $G^\star$ of G is obtained as

$$G^\star(x) = \int_{-\infty}^{+\infty} K^\star(y) H_l(x - y) dy = \sum_{n=-\infty}^{+\infty} K(nh) H_l^\star(x - nh), \tag{2.20}$$

where

$$H_l^\star(x) = \int_{-\infty}^{+\infty} P\left(\frac{y}{h}\right) H_l(x - y) dy. \tag{2.21}$$

Considering only values of $x = mh$, m integer, the function

$$G^\star(mh) = \sum_{n=-\infty}^{+\infty} K(nh) H_l^\star[(m - n)h] \tag{2.22}$$

represents the discrete convolution between sampled values of K and the filter coefficients $H_l^\star$. Then, an approximation $G^{\star\star}(x)$ of $G(x)$ can be construct by the interpolation scheme

$$G^{\star\star}(x) = \sum_{n=-\infty}^{+\infty} G^\star(mh) P\left(\frac{x-mh}{h}\right). \tag{2.23}$$

At this point, the goal is to derive the filter coefficients. The idea is to express $H_l^\star(x)$ as a Fourier integral and evaluate it as a contour integral in the complex plane. In fact, by using the convolution theorem in (2.16) we have that

$$H_l^\star(x) = \int_{-\infty}^{+\infty} h\hat{P}(hs)\hat{H}_l(s)e^{i2\pi xs}ds, \tag{2.24}$$

where

$$\hat{P}(s) = \frac{1}{2}\tanh\left(\frac{\pi}{a}\left(s+\frac{1}{2}\right)\right) - \frac{1}{2}\tanh\left(\frac{\pi}{a}\left(s-\frac{1}{2}\right)\right). \tag{2.25}$$

In this setting, the choice of the function defined in (2.18) instead of the sinc function allows to apply Cauchy residues theorem and hence to express $H_l^\star(x)$ as sums of residues. Moreover, it can be shown that the absolute error in the calculation of $G^\star$ is given by

$$|G(x) - G^\star(x)| \leq 4E(\omega_0, a, s_c)\max\int_0^{+\infty} |k(\lambda e^{\pm i\omega_0})|d\lambda,$$

in which ω_0 is such that $k(\lambda e^{i\omega})$ is analytic within the area $|\omega| < \omega_0$, and

$$E(\omega_0, a, s_c) = \frac{as_c}{\sin(2\pi as_c\omega_0)}e^{-2\pi\omega_0 s_c} + \frac{(2as_c\omega_0)^2}{\pi\omega_0}\sum_{p=1}^{\infty}(-1)^p\frac{e^{-\frac{p\pi}{a}}}{p^2-(2as_c\omega_0)^2},$$

with $s_c = \frac{1}{2h}$.

In 1990 Christensen [9] further developed the method of Johansen and Sorensen for the calculation of the filter coefficients $H_l^\star(x)$ without the restriction (2.19) on the smoothness parameter a.

A total different approach for the evaluation of Hankel type integrals was considered by Koefoed and Dirks [37], Guptasarma [30], Guptasarma and Singh [31], Singh and Mogi [54]. This method is essentially a standard N-points quadrature rule, but the main difference is that the weights are computed by solving a linear equation obtained by imposing the rule to be correct on a set of training functions (not polynomials) for which the corresponding integral is known. In particular, in [30] filters with 7, 11 and

19 points are considered, while in [31] two filters for the Hankel J_0 transform (61 points and 120 points) and two filters for the Hankel J_1 transform (47 points and 140 points) are designed.

In general, given a set of abscissas

$$\lambda_i = \frac{1}{\rho} 10^{u+(i-1)v}, \quad i = 1, \ldots, N,$$

where the parameters u and v are called the shift and the spacing, respectively, Hankel integral transforms of type (2.1), with $l = 0, 1$, are approximated as

$$I_f(\rho) \cong \frac{1}{\rho} \sum_{i=1}^{N} f(\lambda_i) w_i, \tag{2.26}$$

where $w_i, i = 1, \ldots, N$, are the filter weights. In order to determine the weights for a given value of N, the idea is to consider a known Hankel transform and to construct from (2.26) a set of equations for different values of ρ. For example, in [31] the following transforms are employed (see [29, p.711, 6.621, n.1] and [29, p.717, 6.631, n.4]):

$$\int_0^\infty \lambda e^{-c\lambda} J_0(\lambda\rho) d\lambda = \frac{\rho}{(c^2+\rho^2)^{\frac{3}{2}}},$$

$$\int_0^\infty \lambda^e e^{-c\lambda^2} J_1(\lambda\rho) d\lambda = \frac{\rho e^{-\rho^2/4c}}{4c^2},$$

$$\int_0^\infty \left[\lambda e^{-c\lambda} + \alpha\lambda^2 e^{-c\lambda^2}\right] J_1(\lambda\rho) d\lambda = \frac{\rho}{(c^2+\rho^2)^{\frac{3}{2}}} + \alpha\frac{\rho e^{-\rho^2/4c}}{4c^2},$$

with $c, \alpha > 0$.

In particular, given a set of values $\{\rho_j\}_{j=1,\ldots,M}$, with $M > N$, and a function $\tilde{f}(\lambda)$ for which the corresponding integral $I_{\tilde{f}}(\rho)$ (see (2.1)) is known, a set of training functions $\{I_{\tilde{f},j}\}_{j=1,\ldots,M}$ is defined such that $I_{\tilde{f},j} = I_{\tilde{f}}(\rho_j)$. Then, for assumed values of u and v, the method prescribes to solve in the least-squares sense with respect to the filter coefficients w_j, $j = 1, \ldots, N$, the overdetermined linear system

$$I_{\tilde{f},j} = \frac{1}{\rho} \sum_{i=1}^{N} \tilde{f}(\lambda_i) w_i, \quad j = 1, \ldots, M. \tag{2.27}$$

We remark that, by taking $M = N$, the above system can be solved by using for example the GMRES method (see e.g. [39]). Finally, the choice of the parameters u and v was made empirically by considering a grid tabulation and then by searching for the minimum of the root-mean-square relative error computed over a certain range of ρ.

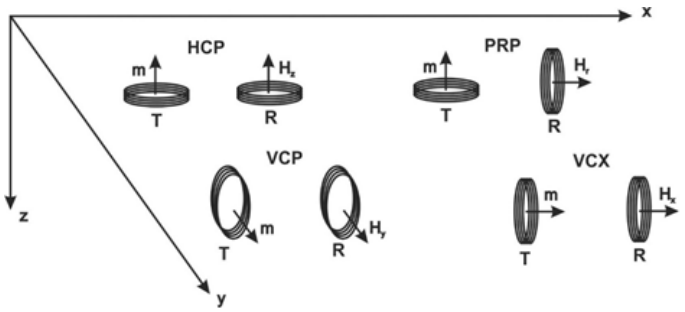

Figure 2.1: Transmitter and receiver coil configurations: horizontal coplanar loops (HCP), perpendicular loops (PRP), vertical coplanar loops (VCP) and vertical coaxial loops (VCX).

2.2 A Gauss-Kronrod approach

In the previous section we have seen the standard technique commonly used to evaluate the Hankel transform of a generic function f. Now, we focus on the computation of the EM fields, for which the function f depends on the reflection coefficient R_0 (see Proposition 7). In this setting, we describe a novel approach, developed in [13], for the evaluation of these fields.

Let us consider a layered underground model where σ_j and h_j, $j = 1, ..., N$, represent conductivity and thickness of the j-th layer, respectively. The deeper layer is assumed to have infinite thickness. Let ν and m be the frequency of the transmitter and the magnetic moment, μ the magnetic permeability of vacuum and r the offset. The angular frequency is $\omega = 2\pi\nu$ and the cylindrical polar coordinate system (ρ, ϕ, z) has the longitudinal axis downward directed, such that the ground plane coincides with the plane $z = 0$, the transmitter is located at $z = -H$ and the receiver is placed along the polar axis.

Referring to Figure 2.1, the most common loop configurations consist in a horizontal transmitter loop (vertical dipole) and a receiver loop that can be horizontal (both axes are vertical) or vertical (perpendicular axes). These two configurations are called HCP (horizontal coplanar) and PRP (perpendicular).

In this setting, the theoretical components of the magnetic field at the receiver, that are the vertical $H_z^{(N)}$ and radial $H_\rho^{(N)}$ in the HCP and PRP geometry, respectively, are obtained from equations (1.73), (1.74) by setting $\rho = r$. Moreover, for the reflection term R_0 we consider the following recursion, obtained by Knight and Raich [36] under the quasi-static approximation

$k_0 \approx 0$ (cf. Proposition 7 and Remark 4):

$$\begin{aligned} R_0(\lambda) &= \frac{R_1(\lambda) + \psi_1(\lambda)}{R_1(\lambda)\psi_1(\lambda) + 1} \\ R_j(\lambda) &= \frac{R_{j+1}(\lambda) + \psi_{j+1}(\lambda)}{R_{j+1}(\lambda)\psi_{j+1}(\lambda) + 1} e^{-2u_j(\lambda)h_j}, \quad j = 1, \ldots, N-1 \\ R_N(\lambda) &= 0, \end{aligned} \tag{2.28}$$

where

$$\psi_j(\lambda) = \frac{u_{j-1}(\lambda) - u_j(\lambda)}{u_{j-1}(\lambda) + u_j(\lambda)}, \quad j = 1, \ldots, N$$

in which $u_0(\lambda) = \lambda$ and $u_j(\lambda) = \sqrt{\lambda^2 - k_j^2}$, $k_j = \sqrt{-i\omega\mu\sigma_j}$, for $j = 1, \ldots, N$. In order to avoid redundancies and to reduce the length of some formulas, in the sequel we simply write R_j, ψ_j, u_j in place of $R_j(\lambda)$, $\psi_j(\lambda)$, $u_j(\lambda)$.

Therefore, we have

$$H_z^{(N)} = \frac{m}{4\pi} \int_0^\infty (1 + R_0 e^{-2H\lambda}) \lambda^2 J_0(\lambda r) d\lambda, \tag{2.29}$$

$$H_\rho^{(N)} = \frac{m}{4\pi} \int_0^\infty (1 - R_0 e^{-2H\lambda}) \lambda^2 J_1(\lambda r) d\lambda, \tag{2.30}$$

with R_0 as in (2.28). We observe that, if $N = 1$, representing the situation of homogeneous earth, and $H = 0$, then $R_1 = 0$, $R_0 = \Psi_1$ and analytic expressions for (2.29) and (2.30) are given by (cf. (1.82) and (1.85) with $\rho = r$)

$$\begin{aligned} H_z^{(1)} &= \frac{m}{2\pi k_1^2 r^5} \left[9 - (9 + 9ik_1 r - 4k_1^2 r^2 - ik_1^3 r^3) e^{-ik_1 r} \right], \\ H_\rho^{(1)} &= -\frac{mk_1^2}{4\pi r} \left[I_1\left(\frac{ik_1 r}{2}\right) K_1\left(\frac{ik_1 r}{2}\right) - I_2\left(\frac{ik_1 r}{2}\right) K_2\left(\frac{ik_1 r}{2}\right) \right]. \end{aligned}$$

Other two common configurations (see again Figure 2.1) consist in vertical coplanar loop (both axes are horizontal and parallel, VCP configuration), and in vertical coaxial loops (VCX configuration). In the VCX configuration the measured field is the horizontal $H_x^{(N)}$ given by equation (1.87) with $y = 0$, $\rho = r$ and then $x = r$. Hence, we have

$$H_x^{(N)} = -\frac{m}{4\pi} \int_0^\infty (1 - R_0 e^{-2H\lambda}) \lambda^2 J_0(\lambda r) d\lambda + \frac{m}{4\pi r} \int_0^\infty (1 - R_0 e^{-2H\lambda}) \lambda J_1(\lambda r) d\lambda. \tag{2.31}$$

Moreover, for $N = 1$ and $H = 0$, from (1.93) we obtain

$$H_x^{(1)} = -\frac{m}{2\pi k_1^2 r^5} \left[-2k_1^2 r^2 - 12 + (-ik_1^3 r^3 - 5k_1^2 r^2 + 12ik_1 r + 12) e^{-ik_1 r} \right]$$

In the VCP geometry we are in the case of y-directed horizontal magnetic dipole. By Remark 5, the fields can be obtained by following the same analysis of Section 1.7.2, but with a permutation of coordinates. Therefore, in this configuration, the measured magnetic field at the receiver is the horizontal $H_y^{(N)}$ component given by setting $x = 0$ in equation (1.87), in which x should be read y. Then, we obtain

$$H_y^{(N)} = -\frac{m}{4\pi r}\int_0^\infty (1 - R_0 e^{-2H\lambda})\lambda J_1(\lambda r)d\lambda \tag{2.32}$$

and, for $N = 1$ and $H = 0$ (see (1.93)),

$$H_y^{(1)} = -\frac{m}{2\pi k_1^2 r^5}\left[3 + k_1^2 r^2 - (3 + 3ik_1 r - k_1^2 r^2)e^{-ik_1 r}\right]. \tag{2.33}$$

In this section, for simplicity, we assume $H = 0$, i.e., that the dipole is located at the surface of the earth, even if, with some further complications, the following analysis can be generalized also for $H \neq 0$. Defining for $l = 0, 1$

$$g_l(\lambda) = (R_0 - \Psi_1)\lambda^2 J_l(\lambda r), \tag{2.34}$$
$$q_l(\lambda) = [1 + (-1)^l \Psi_1]\lambda^2 J_l(\lambda r), \tag{2.35}$$
$$p_l(\lambda) = [1 - \Psi_1(\lambda)]\lambda^{2-l} J_l(\lambda r), \tag{2.36}$$

we can write (see (2.29), (2.30), (2.31), (2.32))

$$\begin{aligned}
(1 + R_0)\lambda^2 J_0(\lambda r) &= g_0(\lambda) + q_0(\lambda),\\
(1 - R_0)\lambda^2 J_1(\lambda r) &= q_1(\lambda) - g_1(\lambda),\\
(1 - R_0)\lambda^2 J_0(\lambda r) &= p_0(\lambda) - g_0(\lambda),\\
(1 - R_0)\lambda J_1(\lambda r) &= p_1(\lambda) - \lambda^{-1} g_1(\lambda).
\end{aligned}$$

Since $q_l(\lambda)$ and $p_l(\lambda)$ represent the integrand functions in the case $N = 1$ ($R_1 = 0$ and hence $g_l(\lambda) = 0$), we have that

$$\begin{aligned}
\frac{m}{4\pi}\int_0^\infty q_0(\lambda)d\lambda &= H_z^{(1)},\\
\frac{m}{4\pi}\int_0^\infty q_1(\lambda)d\lambda &= H_\rho^{(1)},\\
-\frac{m}{4\pi}\int_0^\infty p_0(\lambda)d\lambda + \frac{m}{4\pi r}\int_0^\infty p_1(\lambda)d\lambda &= H_x^{(1)},\\
-\frac{m}{4\pi r}\int_0^\infty p_1(\lambda)d\lambda &= H_y^{(1)},
\end{aligned}$$

and therefore

$$H_z^{(N)} = \frac{m}{4\pi}\int_0^\infty g_0(\lambda)\,d\lambda + H_z^{(1)}, \tag{2.37}$$

$$H_\rho^{(N)} = -\frac{m}{4\pi}\int_0^\infty g_1(\lambda)\,d\lambda + H_\rho^{(1)}, \tag{2.38}$$

$$H_x^{(N)} = \frac{m}{4\pi}\int_0^\infty g_0(\lambda)d\lambda - \frac{m}{4\pi r}\int_0^\infty \lambda^{-1}g_1(\lambda)d\lambda + H_x^{(1)}, \tag{2.39}$$

$$H_y^{(N)} = \frac{m}{4\pi r}\int_0^\infty \lambda^{-1}g_1(\lambda)d\lambda + H_y^{(1)}. \tag{2.40}$$

Our strategy for the computation of $H_z^{(N)}$, $H_\rho^{(N)}$, $H_x^{(N)}$ and $H_y^{(N)}$ in the general case of N layers is based on the observation that the functions $g_l(\lambda)$, $l = 0, 1$, exponentially decay with respect to λ. To prove this behavior, some preliminary results are necessary.

Lemma 2 *It holds*

$$R_0 - \Psi_1 = R_1\left(1 + \mathcal{O}\left(\frac{1}{\lambda^2}\right)\right), \quad \text{as } \lambda \to +\infty.$$

Proof. Using the definitions of R_0 and Ψ_1 we have

$$R_0 - \Psi_1 = \frac{4R_1u_1}{R_1k_1^2 + (\lambda + u_1)^2}\lambda. \tag{2.41}$$

Since

$$u_1 = \lambda\sqrt{1 - \frac{k_1^2}{\lambda^2}} = \lambda\left(1 - \frac{k_1^2}{2\lambda^2} + \mathcal{O}\left(\frac{1}{\lambda^4}\right)\right),$$

as $\lambda \to +\infty$, we can write

$$\begin{aligned} R_0 - \Psi_1 = \frac{4R_1u_1\lambda}{R_1k_1^2 + (\lambda + u_1)^2} &= \frac{4R_1\lambda^2\left(1 - \frac{k_1^2}{2\lambda^2} + \mathcal{O}\left(\frac{1}{\lambda^4}\right)\right)}{R_1k_1^2 + \lambda^2\left(2 - \frac{k_1^2}{2\lambda^2} + \mathcal{O}\left(\frac{1}{\lambda^4}\right)\right)^2} \\ &= R_1\left(1 + \mathcal{O}\left(\frac{1}{\lambda^2}\right)\right). \end{aligned}$$

■

Lemma 3 *The function R_1 can be written in the following form*

$$R_1 = \sum\nolimits_{k=1}^{N-1}\delta_k(\lambda)\exp\left(-\gamma_k\lambda\right), \tag{2.42}$$

where

$$\gamma_k = \sum_{i=1}^{k} c_i > 0, \quad k = 1, \ldots, N-1,$$
$$c_i = 2h_i\sqrt{1 + \frac{i\omega\mu\sigma_i}{\lambda^2}}, \quad i = 1, \ldots, N-1. \tag{2.43}$$

Proof. In order to demonstrate (2.42), starting from $j = 1$, by induction we show that

$$R_{N-j} = \sum_{k=1}^{j} \delta_k^{(N-j)} \exp(-(\gamma_{N+k-(j+1)} - \gamma_{N-(j+1)})\lambda), \quad \text{for } j = 1, \ldots, N-1, \tag{2.44}$$

in which $\gamma_0 = 0$. We first observe that

$$2u_ih_i = 2h_i\sqrt{\lambda^2 + i\omega\mu\sigma_i} = 2h_i\sqrt{1 + \frac{i\omega\mu\sigma_i}{\lambda^2}} \cdot \lambda = c_i\lambda.$$

Let $j = 1$. By (2.28) and defining

$$\delta_1^{(N-1)} = \Psi_N = \frac{\sqrt{\lambda^2 - k_{N-1}^2} - \sqrt{\lambda^2 - k_N^2}}{\sqrt{\lambda^2 - k_{N-1}^2} + \sqrt{\lambda^2 - k_N^2}}, \tag{2.45}$$

we have that (2.44) is correct for $j = 1$ because $R_N = 0$. Assuming that (2.44) is also correct for a given $j < N-1$, by (2.28)

$$\begin{aligned} R_{N-(j+1)} &= \frac{R_{N-j} + \Psi_{N-j}}{R_{N-j}\Psi_{N-j} + 1} e^{-c_{N-(j+1)}\lambda} \\ &= \sum_{k=1}^{j+1} \delta_k^{(N-(j+1))} \exp(-(\gamma_{N+k-(j+2)} - \gamma_{N-(j+2)})\lambda), \end{aligned} \tag{2.46}$$

in which we have defined

$$\begin{aligned} \delta_1^{(N-(j+1))} &= \frac{\Psi_{N-j}}{R_{N-j}\Psi_{N-j} + 1}, \\ \delta_k^{(N-(j+1))} &= \frac{\delta_{k-1}^{(N-j)}}{R_{N-j}\Psi_{N-j} + 1}, \quad k = 2, \ldots, j+1. \end{aligned} \tag{2.47}$$

Finally, setting $\delta_j = \delta_j^{(1)}$, $j = 1, \ldots, N-1$, we obtain the result. ■

Lemma 4 *For $\lambda \to +\infty$,*

$$R_1 = \sum_{k=1}^{N-1} \frac{k_{k+1}^2 - k_k^2}{4\lambda^2} \left(1 + \mathcal{O}\left(\frac{1}{\lambda^2}\right)\right) \exp(-\gamma_k\lambda). \tag{2.48}$$

Proof. Starting from $j = 1$, by induction we show that

$$R_{N-j} = \sum_{k=1}^{j} \frac{k_{N+k-j}^2 - k_{N+k-(j+1)}^2}{4\lambda^2} \left(1 + \mathcal{O}\left(\frac{1}{\lambda^2}\right)\right) \exp(-(\gamma_{N+k-(j+1)} - \gamma_{N-(j+1)})\lambda), \tag{2.49}$$

for $j = 1, \ldots, N-1$. We observe that, for $i = 1, \ldots, N$

$$\begin{aligned}
\Psi_i &= \frac{\sqrt{\lambda^2 - k_{i-1}^2} - \sqrt{\lambda^2 - k_i^2}}{\sqrt{\lambda^2 - k_{i-1}^2} + \sqrt{\lambda^2 - k_i^2}} \\
&= \frac{k_i^2 - k_{i-1}^2}{\left[\lambda\left(1 + \frac{k_{i-1}^2}{2\lambda^2} + \mathcal{O}\left(\frac{1}{\lambda^4}\right)\right) + \lambda\left(1 + \frac{k_{i-1}^2}{2\lambda^2} + \mathcal{O}\left(\frac{1}{\lambda^4}\right)\right)\right]^2} \\
&= \frac{k_i^2 - k_{i-1}^2}{4\lambda^2\left(1 + \mathcal{O}\left(\frac{1}{\lambda^2}\right)\right)} = \frac{k_i^2 - k_{i-1}^2}{4\lambda^2}\left(1 + \mathcal{O}\left(\frac{1}{\lambda^2}\right)\right).
\end{aligned}$$

By (2.44) with $j = 1$ and (2.45), we have that

$$\begin{aligned}
R_{N-1} &= \delta_1^{(N-1)} \exp(-(\gamma_{N-1} - \gamma_{N-2})\lambda) \\
&= \frac{k_N^2 - k_{N-1}^2}{4\lambda^2}\left(1 + \mathcal{O}\left(\frac{1}{\lambda^2}\right)\right) \exp(-(\gamma_{N-1} - \gamma_{N-2})\lambda).
\end{aligned}$$

Therefore, (2.49) holds true for $j = 1$. Assuming that (2.49) is also correct for a given $j < N - 1$, by (2.46) we have

$$R_{N-(j+1)} = \sum_{k=1}^{j+1} \delta_k^{(N-(j+1))} \exp(-(\gamma_{N+k-(j+2)} - \gamma_{N-(j+2)})\lambda),$$

where by (2.47) and using the induction hypothesis on R_{N-j}

$$\begin{aligned}
\delta_1^{(N-(j+1))} &= \frac{\Psi_{N-j}}{R_{N-j}\Psi_{N-j}+1} \\
&= \frac{\frac{k_{N-j}^2-k_{N-j-1}^2}{4\lambda^2}\left(1+\mathcal{O}\left(\frac{1}{\lambda^2}\right)\right)}{\mathcal{O}\left(\frac{1}{\lambda^2}\right)\frac{k_{N-j}^2-k_{N-j-1}^2}{4\lambda^2}\left(1+\mathcal{O}\left(\frac{1}{\lambda^2}\right)\right)+1} \\
&= \frac{k_{N-j}^2-k_{N-j-1}^2}{4\lambda^2}\left(1+\mathcal{O}\left(\frac{1}{\lambda^2}\right)\right), \\
\delta_k^{(N-(j+1))} &= \frac{\delta_{k-1}^{(N-j)}}{R_{N-j}\Psi_{N-j}+1} \\
&= \frac{\frac{k_{N+k-(j+1)}^2-k_{N+k-(j+2)}^2}{4\lambda^2}\left(1+\mathcal{O}\left(\frac{1}{\lambda^2}\right)\right)}{\mathcal{O}\left(\frac{1}{\lambda^2}\right)\frac{k_{N+k-(j+1)}^2-k_{N+k-(j+2)}^2}{4\lambda^2}\left(1+\mathcal{O}\left(\frac{1}{\lambda^2}\right)\right)+1} \\
&= \frac{k_{N+k-(j+1)}^2-k_{N+k-(j+2)}^2}{4\lambda^2}\left(1+\mathcal{O}\left(\frac{1}{\lambda^2}\right)\right), \quad k=2,\dots,j+1.
\end{aligned}$$

■

By using the above Lemmas we can prove the following result, which finally expresses the asymptotic behavior of R_1, and hence the one of $R_0-\Psi_1$ by Lemma 2.

Proposition 9 *For $\lambda \to +\infty$,*

$$R_1 = \sum_{k=1}^{N-1} \frac{k_{k+1}^2-k_k^2}{4\lambda^2}\exp(-\tilde{\gamma}_k\lambda)\left(1+\mathcal{O}\left(\frac{1}{\lambda}\right)\right), \tag{2.50}$$

where $\tilde{\gamma}_k = 2\sum_{i=1}^k h_i$.

Proof. First of all, by (2.43) we have

$$\gamma_k = \sum_{i=1}^k c_i = 2\sum_{i=1}^k h_i\left(1+\mathcal{O}\left(\frac{1}{\lambda^2}\right)\right) = \tilde{\gamma}_k\left(1+\mathcal{O}\left(\frac{1}{\lambda^2}\right)\right), \quad \text{for } k=1,\dots,N-1. \tag{2.51}$$

Therefore

$$\begin{aligned}
\exp(-\gamma_k\lambda) &= \exp\left(-\tilde{\gamma}_k\lambda\left(1+\mathcal{O}\left(\frac{1}{\lambda^2}\right)\right)\right) \\
&= \exp(-\tilde{\gamma}_k\lambda)\left(1+\mathcal{O}\left(\frac{1}{\lambda}\right)\right),
\end{aligned}$$

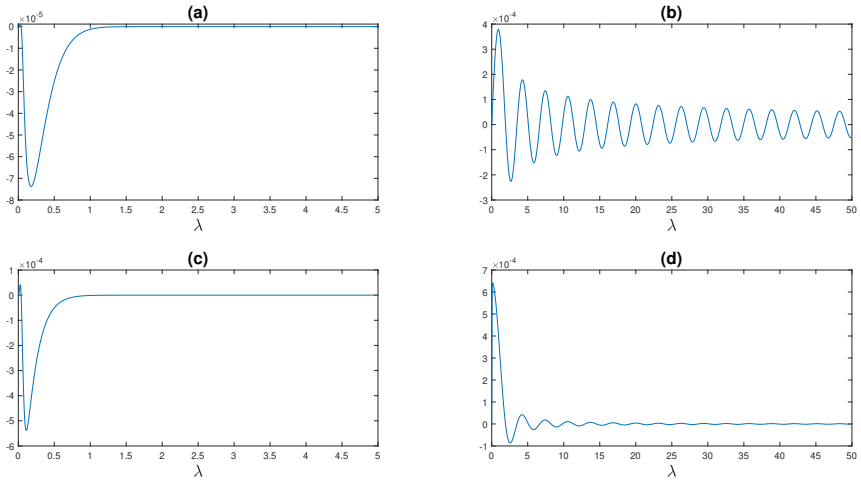

Figure 2.2: The imaginary part of the functions $g_1(\lambda)$ (a), $q_1(\lambda)$ (b), $\lambda^{-1}g_1(\lambda)$ (c) and $p_1(\lambda)$ (d), in the case of a 3-layered underground model with $r = 2$ m, $\nu = 10$ kHz, $m = 1$ A/m^2 $\sigma_1 = 33$ mS/m, $\sigma_2 = 20$ mS/m, $\sigma_3 = 100$ mS/m, $h_1 = 2.5$ m, $h_2 = 0.5$ m.

where the last equality comes from

$$\exp\left(-\tilde{\gamma}_k \mathcal{O}\left(\frac{1}{\lambda}\right)\right) = 1 + \mathcal{O}\left(\frac{1}{\lambda}\right).$$

The result then follows straighfully from Lemma 4. ■

By Lemma 2 and Proposition 9, we have that the functions g_l (see (2.37), (2.38), (2.39) and (2.40)), can be written as

$$\begin{aligned} g_l &= (R_0 - \Psi_1)\lambda^2 J_l(\lambda r) \\ &= \sum_{k=1}^{N-1} \frac{k_{k+1}^2 - k_k^2}{4} \exp(-\tilde{\gamma}_k \lambda) J_l(\lambda r) \left(1 + \mathcal{O}\left(\frac{1}{\lambda}\right)\right), \end{aligned} \tag{2.52}$$

so that the oscillations due to the Bessel functions are rapidly damped.

Just to provide an example, in Figure 2.2 we plot the imaginary part of $g_1(\lambda)$, $q_1(\lambda)$, $\lambda^{-1}g_1(\lambda)$ and $p_1(\lambda)$ for a given subsoil model. It is clear that the oscillations are only retained by the terms $q_1(\lambda)$ and $p_1(\lambda)$.

This situation holds true in general and therefore, for suitable positive

scalars s_l, $l = 0, 1$, we can consider the following approximations

$$H_z^{(N)} \approx \frac{m}{4\pi} \int_0^{s_0} g_0(\lambda)\, d\lambda + H_z^{(1)}, \tag{2.53}$$

$$H_\rho^{(N)} \approx -\frac{m}{4\pi} \int_0^{s_1} g_1(\lambda)\, d\lambda + H_\rho^{(1)}, \tag{2.54}$$

$$H_x^{(N)} \approx \frac{m}{4\pi} \int_0^{s_0} g_0(\lambda) d\lambda - \frac{m}{4\pi r} \int_0^{s_1} \lambda^{-1} g_1(\lambda) d\lambda + H_x^{(1)}, \tag{2.55}$$

$$H_y^{(N)} \approx \frac{m}{4\pi r} \int_0^{s_1} \lambda^{-1} g_1(\lambda) d\lambda + H_y^{(1)}, \tag{2.56}$$

in which we neglect the tail of the integrals.

Theoretically, the truncation error can be bounded as follows.

Proposition 10 *For $l = 0, 1$ there exist constants c_1 and c_2 such that, for s_l large enough,*

$$\left| \int_{s_l}^{\infty} g_l(\lambda) d\lambda \right| \leq c_1 \sqrt{\frac{1}{8\pi r}} \sum_{k=1}^{N-1} |k_{k+1}^2 - k_k^2| \tilde{\gamma}_k^{-1} e^{-\tilde{\gamma}_k s_l} s_l^{-\frac{1}{2}},$$

and

$$\left| \int_{s_1}^{\infty} \lambda^{-1} g_1(\lambda) d\lambda \right| \leq c_2 \sqrt{\frac{1}{8\pi r}} \sum_{k=1}^{N-1} |k_{k+1}^2 - k_k^2| \tilde{\gamma}_k^{-1} e^{-\tilde{\gamma}_k s_1} s_1^{-\frac{3}{2}},$$

In order to prove Proposition 10 we need the following lemma.

Lemma 5 *For $u \to +\infty$,*

$$\int_u^{\infty} e^{-x} x^{-\nu} dx = u^{-\nu} e^{-u} \left(1 + \mathcal{O}\left(\frac{1}{u}\right)\right).$$

Proof. By using [29, p.318, 3.381, n.6] and [1, p.505-504] respectively, we have that

$$\begin{aligned} \int_u^{\infty} \frac{e^{-x}}{x^\nu} dx &= u^{-\frac{\nu}{2}} e^{-\frac{u}{2}} \mathcal{W}_{-\frac{\nu}{2}, \frac{1-\nu}{2}}(u) \\ &= u^{1-\nu} e^{-u} \mathcal{U}(1, 2-\nu, u) \\ &= u^{-\nu} e^{-u} \left(1 + \mathcal{O}\left(\frac{1}{u}\right)\right), \end{aligned}$$

where $\mathcal{W}$ is the Whittaker function and $\mathcal{U}$ is the Kummer's confluent hypergeometric function. ■

Now we can prove Proposition 10.

Proof. By (2.52) for $l = 0, 1$, we have

$$\left| \int_{s_l}^{\infty} g_l(\lambda) d\lambda \right| \lesssim \sum_{k=1}^{N-1} \frac{|k_{k+1}^2 - k_k^2|}{4} \int_{s_l}^{\infty} e^{-\tilde{\gamma}_k \lambda} |J_l(\lambda r)| d\lambda,$$

$$\left| \int_{s_1}^{\infty} \lambda^{-1} g_1(\lambda) d\lambda \right| \lesssim \sum_{k=1}^{N-1} \frac{|k_{k+1}^2 - k_k^2|}{4} \int_{s_1}^{\infty} \lambda^{-1} e^{-\tilde{\gamma}_k \lambda} |J_1(\lambda r)| d\lambda.$$

Using the relation (see [1, p.364])

$$J_l(t) = \sqrt{\frac{2}{\pi t}} \left[\cos\left(t - \frac{1}{2} l\pi - \frac{1}{4}\pi \right) + \mathcal{O}\left(\frac{1}{t} \right) \right], \quad \text{for } t \to +\infty,$$

and Lemma 5, we obtain

$$\begin{aligned} \int_{s_l}^{\infty} e^{-\tilde{\gamma}_k \lambda} |J_l(\lambda r)| d\lambda &\lesssim \sqrt{\frac{2}{\pi r}} \int_{s_l}^{\infty} e^{-\tilde{\gamma}_k \lambda} \lambda^{-\frac{1}{2}} d\lambda \\ &= \sqrt{\frac{2}{\pi r}} \int_{\tilde{\gamma}_k s_l}^{\infty} e^{-t} t^{-\frac{1}{2}} dt \\ &\approx \sqrt{\frac{2}{\pi r}} \tilde{\gamma}_k^{-1} e^{-\tilde{\gamma}_k s_l} s_l^{-\frac{1}{2}}, \end{aligned}$$

and

$$\begin{aligned} \int_{s_1}^{\infty} \lambda^{-1} e^{-\tilde{\gamma}_k \lambda} |J_1(\lambda r)| d\lambda &\lesssim \sqrt{\frac{2}{\pi r}} \int_{s_1}^{\infty} e^{-\tilde{\gamma}_k \lambda} \lambda^{-\frac{3}{2}} d\lambda \\ &\approx \sqrt{\frac{2}{\pi r}} \tilde{\gamma}_k^{-1} e^{-\tilde{\gamma}_k s_1} s_1^{-\frac{3}{2}}, \end{aligned}$$

where we have used the symbols $\approx$ and $\lesssim$ to neglect the factor $1 + \mathcal{O}\left(\frac{1}{\lambda}\right)$. ■

In practice, s_l can be taken relatively small to obtain reliable results by a traditional quadrature formula on finite intervals, e.g., $s_l = 2 \div 3$, for $l = 0, 1$.

Table 2.1 shows, for example, the results obtained with $r = 2\ m$ and $\nu = 10\ kHz$, in the case of a subsurface model composed by 3 layers: $\sigma_1 = 333\ mS/m$, $\sigma_2 = 20\ mS/m$, $\sigma_3 = 100\ mS/m$, $h_1 = 2.5\ m$, $h_2 = 0.5\ m$. In Table 2.1, as well as in the sequel of this work, we have used the Gauss-Kronrod quadrature technique, described in [52]. We refer to Appendix C for the general theory concerning Gaussian quadrature rules and in particular to C.4 for the Gauss-Kronrod method. Specifically, the algorithm is based on a popular scheme (see [35]) which combines a 7-point Gauss rule with a 15-point

s_l (m^{-1})	$\int_0^{s_0} \Im(g_0(\lambda))d\lambda$ (A/m)	$\int_0^{s_1} \Im(g_1(\lambda))d\lambda$ (A/m)	$\int_0^{s_1} \Im(\lambda^{-1}g_1(\lambda))d\lambda$ (A/m)
0.5	$0.2340 \cdot 10^{-3}$	$0.7103 \cdot 10^{-4}$	$0.3000 \cdot 10^{-3}$
1.0	$0.2632 \cdot 10^{-3}$	$0.9482 \cdot 10^{-4}$	$0.3632 \cdot 10^{-3}$
1.5	$0.2634 \cdot 10^{-3}$	$0.9610 \cdot 10^{-4}$	$0.3665 \cdot 10^{-3}$
2.0	$0.2633 \cdot 10^{-3}$	$0.9613 \cdot 10^{-4}$	$0.3665 \cdot 10^{-3}$
2.5	$0.2633 \cdot 10^{-3}$	$0.9613 \cdot 10^{-4}$	$0.3665 \cdot 10^{-3}$
3.0	$0.2633 \cdot 10^{-3}$	$0.9613 \cdot 10^{-4}$	$0.3665 \cdot 10^{-3}$
3.5	$0.2633 \cdot 10^{-3}$	$0.9613 \cdot 10^{-4}$	$0.3665 \cdot 10^{-3}$
4.0	$0.2633 \cdot 10^{-3}$	$0.9613 \cdot 10^{-4}$	$0.3665 \cdot 10^{-3}$

Table 2.1: Results of the Gauss-Kronrod quadrature for different values of s_l, with $r = 2\ m$ and $\nu = 10\ kHz$, in the case of a subsurface model composed by 3 layers: $\sigma_1 = 333\ mS/m$, $\sigma_2 = 20\ mS/m$, $\sigma_3 = 100\ mS/m$, $h_1 = 2.5\ m$, $h_2 = 0.5\ m$.

Kronrod rule. Because the Gauss points are incorporated into the Kronrod points, a total of only 15 function evaluations are needed. Moreover, the following adaptive procedure is implemented. Given a prescribed error tolerance, the Gauss-Kronrod quadrature is applied in the interval $[0, s_l]$ and then the error is estimated as the modulus of the difference between the 7-point Gaussian rule and the 15-point Gauss-Kronrod formula. If the tolerance is not achieved, the interval $[0, s_l]$ is divided in 2 subintervals. For each subinterval the corresponding integral is calculated by using the Gauss-Kronrod scheme and the error is estimated as described above. This procedure is repeated until the error tolerance or a given maximum number of intervals is reached. In the example of Table 2.1 and in the sequel of the work, for the Gauss-Kronrod method the relative error tolerance is set to $1e-8$.

We remark that, respect to the digital filtering approach, the method described above allows, first of all, to estimate the quadrature error at each step, and hence to achieve any prescribed accuracy. Moreover, by using an adaptive procedure, the nodes and weights strongly depend on the behavior of the integrand function, while for the digital filtering algorithms they are fixed, independently of the values of the parameters.

In Figure 2.3 we compare, for two different underground models, the imaginary part in logarithmic scale of the fields $H_z^{(3)}$, $H_\rho^{(3)}$, $H_x^{(3)}$ and $H_y^{(3)}$, computed by using the Gauss Kronrod technique from the integral formulations (2.53), (2.54), (2.55) and (2.56), with the results of the digital filtering algorithm provided by Singh and Mogi [54]. The plots show the very good

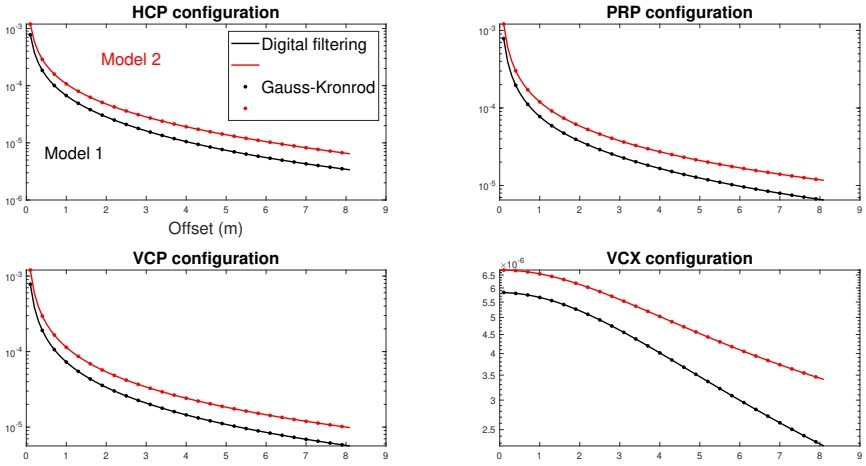

Figure 2.3: Comparison between the imaginary part of the fields $H_z^{(3)}$ (a), $H_\rho^{(3)}$ (b), $H_y^{(3)}$ (c) and $H_x^{(3)}$ (d), in logarithmic scale, computed adopting the Gauss-Kronrod quadrature technique (solid lines) and the numerical digital filtering algorithm provided by Singh and Mogi [54] (symbols). Two underground models are considered: $\sigma_1 = 50.0\ mS/m$, $\sigma_2 = 4.9\ mS/m$, $\sigma_3 = 18.2\ mS/m$, $h_1 = 2.5\ m$, $h_2 = 0.5\ m$ (Model 1) and $\sigma_1 = 76.9\ mS/m$, $\sigma_2 = 32.3\ mS/m$, $\sigma_3 = 50.0\ mS/m$, $h_1 = 2.5\ m$, $h_2 = 0.5\ m$ (Model 2). In all cases $\nu = 10\ kHz$ and $m = 1\ A/m^2$.

concordance of the two numerical approaches for both models. In particular, the curves differ by less than 10^{-8} in absolute error. Using more subintervals the error further decreases, but with higher computational costs.

2.3 An ad-hoc Gaussian rule for the EM fields

Let us consider the general integral solutions of Maxwell's equations for vertical and horizontal magnetic dipoles, placed at $z = -H$ above the surface of the earth, given by equations (2.29), (2.30), (2.31) and (2.32). By taking the imaginary part of the fields and using the change of variable $\lambda r = x$, we

obtain

$$\Im\left(H_z^{(N)}\right) = \frac{m}{4\pi r^3}\int_0^\infty \Im\left(R_0\left(\frac{x}{r}\right)\right) e^{-\frac{2H}{r}x} x^2 J_0(x)dx, \tag{2.57}$$

$$\Im\left(H_\rho^{(N)}\right) = -\frac{m}{4\pi r^3}\int_0^\infty \Im\left(R_0\left(\frac{x}{r}\right)\right) e^{-\frac{2H}{r}x} x^2 J_1(x)dx, \tag{2.58}$$

$$\begin{aligned}\Im\left(H_x^{(N)}\right) = \frac{m}{4\pi r^3}\Bigg[&\int_0^\infty \Im\left(R_0\left(\frac{x}{r}\right)\right) e^{-\frac{2H}{r}x} x^2 J_0(x)dx \\ &- \int_0^\infty \Im\left(R_0\left(\frac{x}{r}\right)\right) e^{-\frac{2H}{r}x} x J_1(x)dx\Bigg],\end{aligned} \tag{2.59}$$

$$\Im\left(H_y^{(N)}\right) = \frac{m}{4\pi r^3}\int_0^\infty \Im\left(R_0\left(\frac{x}{r}\right)\right) e^{-\frac{2H}{r}x} x J_1(x)dx, \tag{2.60}$$

where the symbol $\Im$ indicates the imaginary part. We notice that the integrals in (2.57), (2.58), (2.59) and (2.60) can be written as

$$I_{\nu,\alpha,c}(f) = \int_0^\infty f(x)x^\alpha e^{-cx} J_\nu(x)dx, \tag{2.61}$$

with $f(x) = \Im\left(R_0\left(\frac{x}{r}\right)\right)$, $\alpha = 1, 2$, $c = \frac{2H}{r}$ and $\nu = 0, 1$. In this section we present a Gaussian quadrature rule, developed in [11], for the computation of integrals of type (2.61). Again, we refer to Appendix C for more details concerning Gaussian quadrature formulae.

In particular, we use the following strategy. First of all, since for the Bessel functions it holds $|J_\nu(x)| \leq 1$, for $\nu \geq 0$, $x \in \mathbb{R}$ (see [1, p.362]), we consider weight functions of the type

$$w_{\nu,\alpha,c}(x) = x^\alpha e^{-cx}[J_\nu(x) + 1] \quad \text{on } [0, +\infty). \tag{2.62}$$

Then, we rewrite (2.61) as

$$I^J_{\nu,\alpha,c}(f) - I^L_{\alpha,c}(f),$$

where

$$\begin{aligned} I^J_{\nu,\alpha,c}(f) &= \int_0^\infty f(x)x^\alpha e^{-cx}[J_\nu(x) + 1]dx, \\ &= \int_0^\infty f(x)w_{\nu,\alpha,c}(x)dx, \end{aligned} \tag{2.63}$$

and

$$I^L_{\alpha,c}(f) = \int_0^\infty f(x)x^\alpha e^{-cx}dx. \tag{2.64}$$

At this point, we notice that integral (2.64) can be accurately computed using a slight modification of the Gauss-Laguerre quadrature rule (see (C.4)). In this setting, our aim is to construct a Gaussian rule with respect to the function $w_{\nu,\alpha,c}$. Since we do not know the explicit expression of the corresponding monic orthogonal polynomials, that we denote by π_k, $k \geq 0$, we employ the Chebyshev and modified Chebyshev algorithm to derive the recurrence coefficients α_k and β_k. Moreover, in addition to these standard techniques, we present an alternative approach that is based on the preconditioning of the moment matrix (that will be defined in what follows). In particular, since the three-term recurrence coefficients can be written in terms of ratios of determinants of the moment matrix or slight modifications of them (see [10, Sect.2.7]), we exploit the Cramer rule to show that these coefficients can be computed by solving a linear system with the moment matrix. Since the weight function (2.62) can be interpreted as a perturbation of the weight function of the generalized Laguerre polynomials, we use the moment matrix of these polynomials as preconditioner. The numerical experiments show that this technique is always (independently of the parameters ν, α, c) much more stable than the modified Chebyshev algorithm.

Finally, for the computation of (2.61), we use the approximation

$$I^J_{\nu,\alpha,c}(f) \approx I^J_n(f) = \sum_{i=1}^{n} w_i f(x_i),$$

for integral (2.63). Then, denoting by t^L_i, w^L_i respectively the nodes and the weights of the Gauss-Laguerre rule with respect to the weight function $w_\alpha(t) = t^\alpha e^{-t}$, $\alpha > -1$, integral (2.64) is approximated by

$$\begin{aligned} I^L_{\alpha,c}(f) &= \frac{1}{c^{\alpha+1}} \int_0^\infty f\left(\frac{t}{c}\right) t^\alpha e^{-t} dt \\ &\approx I^L_n(f) = \frac{1}{c^{\alpha+1}} \sum_{i=1}^{n} w^L_i f\left(\frac{t^L_i}{c}\right). \end{aligned}$$

Finally, we thus have

$$I_{\nu,\alpha,c}(f) \approx I^J_n(f) - I^L_n(f). \tag{2.65}$$

In the next section we derive a recursive relation for the practical evaluation of the power moments.

2.3.1 Computation of the moments

The moments relative to weight function (2.62) are defined as (see (C.5))

$$\mu_k = \mu_k^{\nu,\alpha,c} = \int_0^\infty x^{k+\alpha} e^{-cx} [J_\nu(x) + 1] dx, \quad k \geq 0. \tag{2.66}$$

First of all, we derive a recursive relation for the so called core moments

$$\mu_{k,0} = \mu_{k,0}^{\nu,\alpha,c} = \int_0^\infty x^{k+\alpha} e^{-cx} J_\nu(x) dx, \quad k \geq 0. \tag{2.67}$$

We remark that the term core moment was first introduced by Gautschi in [23, Sect.2.1].

Proposition 11 *For $k \geq 0$ it holds*

$$\mu_{k,0} = \frac{1}{(\sqrt{c^2+1})^{k+\alpha+1}} \Gamma(k+\alpha+\nu+1) P_{k+\alpha}^{-\nu} \left(\frac{c}{\sqrt{c^2+1}} \right), \tag{2.68}$$

where Γ is the Gamma function and $P_{k+\alpha}^{-\nu}$ is the associated Legendre function (see e.g. [1, ch.8]) of order $-\nu$ and degree $k+\alpha$.

Proof. We start from the general relation [29, p.713]

$$\int_0^\infty e^{-t\cos\theta} J_\nu(t\sin\theta) t^{k+\alpha} dt = \Gamma(k+\alpha+\nu+1) P_{k+\alpha}^{-\nu}(\cos\theta),$$

which holds for each $k \geq 0$ whenever $\alpha > -1$, $\nu \geq 0$. By the change of variable $s = t\sin\theta$, we have that

$$\int_0^\infty e^{-s\frac{\cos\theta}{\sin\theta}} J_\nu(s) s^{k+\alpha} ds = \sin^{k+\alpha+1}(\theta) \Gamma(k+\alpha+\nu+1) P_{k+\alpha}^{-\nu}(\cos\theta).$$

Setting $\theta = \arctan\left(\frac{1}{c}\right)$, $0 < \theta < \frac{\pi}{2}$, so that $c = \frac{\cos\theta}{\sin\theta}$, and using the relations

$$\sin(\arctan x) = \frac{x}{\sqrt{1+x^2}}, \quad \cos(\arctan x) = \frac{1}{\sqrt{1+x^2}},$$

we obtain the result. ■

Proposition 12 *The following three-term recursion holds*

$$\mu_{k+1,0} = \frac{1}{c^2+1} \{ c\,[2(k+\alpha)+1]\,\mu_{k,0} - [(k+\alpha)^2 - \nu^2] \mu_{k-1,0} \}, \quad k \geq 1, \tag{2.69}$$

with

$$\begin{aligned}\mu_{0,0} = &\frac{\Gamma(\alpha+\nu+1)}{(\sqrt{c^2+1})^{\alpha+1}\Gamma(\nu+1)}\left(\sqrt{c^2+1}+c\right)^{-\nu}\times \\ &{}_2F_1\left(-\alpha,\alpha+1;1+\nu;\frac{1}{2\sqrt{c^2+1}\left(\sqrt{c^2+1}-c\right)}\right),\end{aligned} \tag{2.70}$$

$$\begin{aligned}\mu_{1,0} = &\frac{\Gamma(\alpha+\nu+2)}{(\sqrt{c^2+1})^{\alpha+2}\Gamma(\nu+1)}\left(\sqrt{c^2+1}+c\right)^{-\nu}\times \\ &{}_2F_1\left(-\alpha-1,\alpha+2;1+\nu;\frac{1}{2\sqrt{c^2+1}\left(\sqrt{c^2+1}-c\right)}\right),\end{aligned} \tag{2.71}$$

where ${}_2F_1$ *is the hypergeometric function.*

Proof. From equation (2.68) and using the following three-term recursive relation for the associated Legendre functions ([1, p.334])

$$(k+\alpha+\nu+1)P^{-\nu}_{k+\alpha+1}(z) = (2k+2\alpha+1)zP^{-\nu}_{k+\alpha}(z) - (k+\alpha-\nu)P^{-\nu}_{k+\alpha-1}(z),$$

we can write

$$\begin{aligned}\mu_{k+1,0} &= \frac{1}{(\sqrt{c^2+1})^{k+\alpha+2}}\Gamma(k+\alpha+\nu+2)P^{-\nu}_{k+\alpha+1}\left(\frac{c}{\sqrt{c^2+1}}\right) \\ &= \frac{\Gamma(k+\alpha+\nu+2)}{(\sqrt{c^2+1})^{k+\alpha+2}}\left[\frac{2(k+\alpha)+1}{k+\alpha+\nu+1}\frac{c}{\sqrt{c^2+1}}P^{-\nu}_{k+\alpha}\left(\frac{c}{\sqrt{c^2+1}}\right)\right. \\ &\left. - \frac{k+\alpha-\nu}{k+\alpha+\nu+1}P^{-\nu}_{k+\alpha-1}\left(\frac{c}{\sqrt{c^2+1}}\right)\right].\end{aligned} \tag{2.72}$$

Rearranging (2.72) and using again (2.68) for $\mu_{k,0}$ and $\mu_{k-1,0}$, we obtain relation (2.69). Equations (2.70) and (2.71) follow directly from (2.68) with $k=0$ and $k=1$, respectively, and from the relation [29, p.999]

$$P^{-\nu}_{k+\alpha}(x) = \frac{1}{\Gamma(\nu+1)}\left(\frac{1+x}{1-x}\right)^{-\frac{\nu}{2}}{}_2F_1\left(-k-\alpha,k+\alpha+1;1+\nu;\frac{1-x}{2}\right),$$

for $x\in(0,1)$. ■

Finally, we can derive a recursive relation for the moments.

Proposition 13 *For* $k\geq 1$ *it holds*

$$\begin{aligned}\mu_{k+1} = \frac{1}{c^2+1}\Big\{&c\left[2(k+\alpha)+1\right]\mu_k - \left[(k+\alpha)^2-\nu^2\right]\mu_{k-1} \\ &+ \frac{\Gamma(k+\alpha)[(k+\alpha)^2+(k+\alpha)-c^2\nu^2]}{c^{k+\alpha+2}}\Big\},\end{aligned} \tag{2.73}$$

with

$$\mu_0 = \mu_{0,0} + \frac{\Gamma(\alpha+1)}{c^{\alpha+1}}, \quad \mu_1 = \mu_{1,0} + \frac{\Gamma(\alpha+2)}{c^{\alpha+2}}.$$

Proof. By definition (2.66), the moments μ_k are given by

$$\begin{aligned}\mu_k &= \int_0^\infty x^{k+\alpha} e^{-cx} J_\nu(x) dx + \int_0^\infty x^{k+\alpha} e^{-cx} dx \\ &= \mu_{k,0} + \frac{\Gamma(k+\alpha+1)}{c^{k+\alpha+1}},\end{aligned}$$

where we have used [29, Sect.3.381, n.4]. Therefore, from relation (2.69) for $k \geq 1$, we can write

$$\begin{aligned}\mu_{k+1} &= \mu_{k+1,0} + \frac{\Gamma(k+\alpha+2)}{c^{k+\alpha+2}} \\ &= \frac{c[2(k+\alpha)+1]}{c^2+1}\left(\mu_k - \frac{\Gamma(k+\alpha+1)}{c^{k+\alpha+1}}\right) - \frac{(k+\alpha)^2-\nu^2}{c^2+1}\left(\mu_{k-1} - \frac{\Gamma(k+\alpha)}{c^{k+\alpha}}\right) \\ &+ \frac{\Gamma(k+\alpha+2)}{c^{k+\alpha+2}}.\end{aligned}$$

After some simple manipulations, we obtain the result. ■

At this point, we employ the Chebyshev algorithm for the computation of the coefficients α_k and β_k of the recurrence relation

$$\begin{aligned}\pi_{k+1}(x) &= (x-\alpha_k)\pi_k(x) - \beta_k \pi_{k-1}(x), \quad k \geq 0 \qquad (2.74)\\ \pi_{-1}(x) &= 0, \quad \pi_0(x) = 1,\end{aligned}$$

with $\beta_k > 0$.

Below we present the results of some numerical experiments. The Matlab routines that implement the Chebyshev algorithm and the Gauss-Laguerre quadrature rule are taken from [24] and [59], respectively. Since for integrals involving Bessel functions, exponentials and powers the exact solution is known, in our simulations we choose $f(x) = e^{-0.5x}$. In Figure 2.4 we consider two examples, for different values of the parameters ν, α and c, and plot the absolute error between the approximation obtained with the developed Gaussian rule and the exact solution (see [29, Sect.6.624, n.6] and [29, Sect.8.704]) given by

$$\begin{aligned}I_{\nu,\alpha,d}(f) = \frac{\Gamma(d+\nu+1)}{(\sqrt{c^2+1})^{d+1}\Gamma(\nu+1)}\left(\frac{\sqrt{c^2+1}+c}{\sqrt{c^2+1}-c}\right)^{-\frac{\nu}{2}} \times \\ {}_2F_1\left(-d, d+1; 1+\nu; \frac{1}{2} - \frac{c}{2\sqrt{c^2+1}}\right),\end{aligned}$$

where $d = c + 0.5$.

Moreover, since for the truncation error it holds (see [10, Sect.4.4])

$$\begin{aligned} E_n(f) &= I_{\nu,\alpha,c}(f) - (I_n^J(f) - I_n^L(f)) \\ &= (I_{\nu,\alpha,c}^J(f) - I_n^J(f)) - (I_{\alpha,c}^L(f)) - I_n^L(f)) \\ &= \frac{f^{(2n)}(\eta^J)}{(2n)!(k_n^J)^2} - \frac{f^{(2n)}(\eta^L)}{(2n)!(k_n^L)^2}, \quad \eta^J, \eta^L \in (0, \infty), \end{aligned}$$

where k_n^J and k_n^L are the leading coefficients of the corresponding orthonormal polynomials of degree n, in Figure 2.4 we also provide the plot of the upper bound of $E_n(f)$ given by

$$|E_n(f)| \leq \frac{\|f^{(2n)}\|_\infty}{(2n)!} \left(\frac{1}{(k_n^J)^2} + \frac{1}{(k_n^L)^2} \right). \tag{2.75}$$

The coefficients k_n^J are numerically evaluated by using the relation (see [10, Sect.2.7])

$$k_n^J = \frac{1}{\prod_{j=0}^n \sqrt{\beta_j}},$$

while for k_n^L we employ the known explicit formulation

$$k_n^L = \frac{1}{\sqrt{n!\Gamma(n+\alpha+1)}}.$$

2.3.2 The modified Chebyshev algorithm

The picture on the right of Figure 2.4 shows the stability problem when working with the power moments μ_k. Indeed the Chebyshev algorithm typically starts to produce negative values of β_k for k around 20 or even before. This behavior is rather common and has been observed by many authors in the past ([22], [28], [67]). As already mentioned, the problem is that the coefficients α_k and β_k are extremely sensitive to small changes in the moments. In fact, the nonlinear map

$$\begin{aligned} K_n \colon \mathbb{R}^{2n} &\to \mathbb{R}^{2n} \\ \mu &\mapsto \rho \end{aligned}$$

which maps the moment vector $\mu = [\mu_0, \mu_1, \ldots, \mu_{2n-1}]^T$ to the vector $\rho = [\alpha_0, \ldots, \alpha_{n-1}, \beta_0, \ldots, \beta_{n-1}]^T$ of recursion coefficients becomes extremely ill conditioned as n increases (see [22] for the complete analysis). To overcome

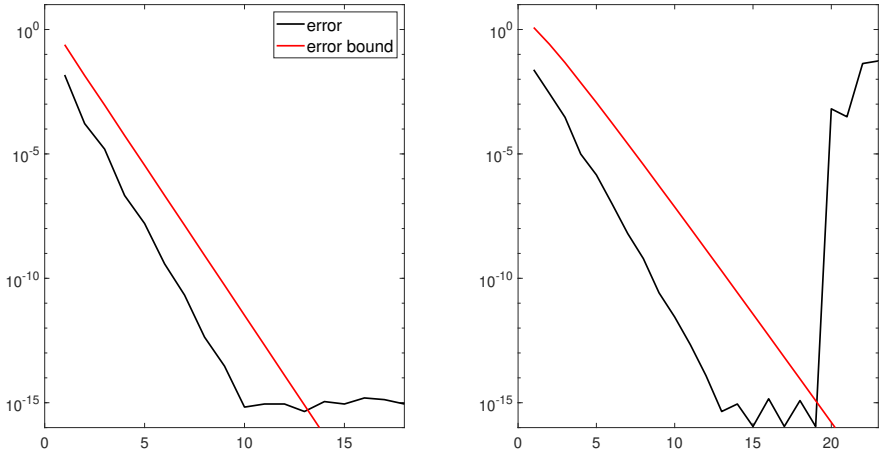

Figure 2.4: Error behavior of (2.65) and error bound (2.75) with respect to n for $\nu = 1$, $\alpha = -0.5$, $c = 1$ on the left and for $\nu = 0.5$, $\alpha = 0.5$, $c = 0.2$ on the right. In both cases $f(x) = e^{-0.5x}$.

this difficulty, in this section we employ the modified Chebyshev algorithm with modified moments (see (C.6))

$$m_k = m_k^{\nu,\alpha,c} = \int_0^\infty p_k(x) w_{\nu,\alpha,c}(x) dx, \quad k \geq 0, \tag{2.76}$$

and mixed moments (see (C.7))

$$\tilde{\sigma}_{kl} = \int_0^\infty \phi_k(x) p_l(x) w_{\nu,\alpha,c}(x) dx, \quad k, l \geq -1.$$

In our case, since the weight function can be interpreted as a perturbation of the weight function relative to the generalized Laguerre polynomials $\{L_k^\alpha\}_{k\geq 0}$, we choose as $\{p_k\}_{k\geq 0}$ the system $\{L_k^{\alpha,c}\}_{k\geq 0}$ of the monic polynomials

$$L_k^{\alpha,c}(x) = \frac{1}{c^k} \tilde{L}_k^\alpha(cx), \tag{2.77}$$

where $\tilde{L}_k^\alpha(t) = (-1)^k k! L_k^\alpha(t)$ is the monic generalized Laguerre polynomial of degree k. This system satisfies the relation

$$\tilde{L}_{k+1}^\alpha(t) = (t - A_k)\, \tilde{L}_k^\alpha(t) - B_k \tilde{L}_{k-1}^\alpha(t),$$

with

$$A_k = 2k + \alpha + 1, \quad B_k = k(k+\alpha) \quad k \geq 1. \tag{2.78}$$

Proposition 14 *The monic polynomials $\{L_k^{\alpha,c}\}_{k\geq 0}$ defined by (2.77) are orthogonal with respect to the weight function $x^\alpha e^{-cx}$ and satisfy the three-term recurrence relation*

$$L_{k+1}^{\alpha,c}(x) = \left(x - \frac{A_k}{c}\right) L_k^{\alpha,c}(x) - \frac{B_k}{c^2} L_{k-1}^{\alpha,c}(x), \tag{2.79}$$

in which A_k and B_k are defined in (2.78).

Proof. The orthogonality follows from the change of variable $cx = t$, that leads to

$$\begin{aligned}\int_0^\infty L_k^{\alpha,c}(x) L_l^{\alpha,c}(x) x^\alpha e^{-cx} dx &= \frac{1}{c^{k+l}}(-1)^{k+l} k!l! \int_0^\infty L_k^\alpha(cx) L_l^\alpha(cx) x^\alpha e^{-cx} dx \\ &= \frac{(-1)^{k+l} k!l!}{c^{k+l+1-\alpha}} \int_0^\infty L_k^\alpha(t) L_l^\alpha(t) t^\alpha e^{-t} dt.\end{aligned}$$

Now, from the recursive relation for the monic generalized Laguerre polynomials $\{\tilde{L}_k^\alpha\}_{k\geq 0}$

$$\tilde{L}_{k+1}^\alpha(cx) = (cx - A_k)\tilde{L}_k^\alpha(cx) - B_k \tilde{L}_{k-1}^\alpha(cx), \tag{2.80}$$

by (2.77) we obtain

$$c^{k+1} L_{k+1}^{\alpha,c}(x) = c\left(x - \frac{A_k}{c}\right) c^k L_k^{\alpha,c}(x) - B_k c^{k-1} L_{k-1}^{\alpha,c}(x),$$

and then (2.79). ■

Using the polynomials $\{L_k^{\alpha,c}\}_{k\geq 0}$, the modified moments (see (2.76)) can be written as

$$m_k = \int_0^\infty L_k^{\alpha,c}(x) x^\alpha e^{-cx} J_\nu(x) dx + \int_0^\infty L_k^{\alpha,c}(x) x^\alpha e^{-cx} dx.$$

Clearly, by orthogonality, the second integral is zero for $k \geq 1$. Hence, for $k \geq 1$, by (2.77) and the following explicit expression for the generalized Laguerre polynomials (see [1, p.775])

$$L_k^\alpha(x) = \sum_{j=0}^k (-1)^j \binom{k+\alpha}{k-j} \frac{1}{j!} x^j,$$

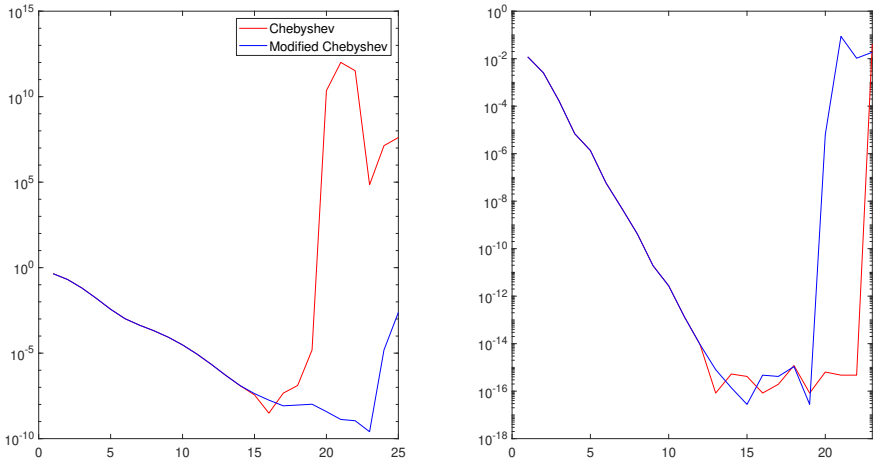

Figure 2.5: Error behavior with respect to n for $\nu = 0.5$, $\alpha = 0.5$, $c = 0.2$ on the left and for $\nu = 1$, $\alpha = 0.5$, $c = 0.7$ on the right. In both cases $f(x) = e^{-0.5x}$.

we have that

$$\begin{aligned} m_k &= \int_0^\infty L_k^{\alpha,c}(x) x^\alpha e^{-cx} J_\nu(x) dx \\ &= \frac{(-1)^k k!}{c^k} \int_0^\infty L_k^\alpha(cx) x^\alpha e^{-cx} J_\nu(x) dx \\ &= \frac{(-1)^k k!}{c^k} \sum_{j=0}^k (-1)^j \binom{k+\alpha}{k-j} \frac{1}{j!} c^j \int_0^\infty x^{\alpha+j} e^{-cx} J_\nu(x) dx \\ &= \frac{(-1)^k k!}{c^k} \sum_{j=0}^k (-1)^j \binom{k+\alpha}{k-j} \frac{1}{j!} c^j \mu_{j,0}, \end{aligned} \tag{2.81}$$

where the last equality comes from (2.67). Finally, for $k = 0$ we obtain

$$m_0 = \mu_{0,0} + \frac{\Gamma(\alpha+1)}{c^{\alpha+1}},$$

by [29, Sect.3.381, n.4]. In Figure 2.5 we compare the results of Algorithm 6 and 7. We provide only two representative examples that, nevertheless, are sufficient to say that Algorithm 7 in general allows to gain stability for further $5 \div 10$ iterations but in many cases there is no effective improvement. In the next section we present the alternative approach based on the preconditioning of the moment matrix, using again the generalized Laguerre polynomials.

2.3.3 A preconditioned Cramer based approach

Let

$$M_k = \begin{bmatrix} \mu_0 & \mu_1 & \cdots & \mu_{k-1} \\ \mu_1 & \mu_2 & \cdots & \mu_k \\ \vdots & \vdots & & \vdots \\ \mu_{k-1} & \mu_k & \cdots & \mu_{2k-2} \end{bmatrix} \in \mathbb{R}^{k\times k},$$

be the moment matrix, and

$$N_k = \begin{bmatrix} \mu_0 & \mu_1 & \cdots & \mu_{k-2} & \mu_k \\ \mu_1 & \mu_2 & \cdots & \mu_{k-1} & \mu_{k+1} \\ \vdots & \vdots & & \vdots & \vdots \\ \mu_{k-1} & \mu_k & \cdots & \mu_{2k-3} & \mu_{2k-1} \end{bmatrix} \in \mathbb{R}^{k\times k}.$$

It is known (see [10], [58]) that the recurrence coefficients in (2.74) can also be written as

$$\alpha_k = \frac{F_{k+1}}{D_{k+1}} - \frac{F_k}{D_k}, \quad \beta_k = \frac{D_{k-1}D_{k+1}}{D_k^2} \quad k \geq 0, \tag{2.82}$$

where

$$\begin{aligned} D_k &= \det(M_k), \quad \text{for} \quad k \geq 1, \\ F_k &= \det(N_k), \quad \text{for} \quad k \geq 2, \end{aligned}$$

and

$$\begin{aligned} D_0 &= D_{-1} = 1, \\ F_0 &= 0,\ F_1 = \mu_1. \end{aligned}$$

Consider the linear system

$$M_{k+1}x^{(k+1)} = e_{k+1}, \tag{2.83}$$

where $e_{k+1} = (0, \ldots, 0, 1)^T \in \mathbb{R}^{k+1}$. In the following, we denote by $x_i^{(k+1)}$ the i-th component of the solution of (2.83). First of all, we observe that, by Cramer's rule,

$$\frac{D_k}{D_{k+1}} = x_{k+1}^{(k+1)}.$$

Moreover, since

$$\det(N_k) = -\det M_{k+1,(k)},$$

in which $M_{k+1,(k)}$ is the matrix M_{k+1} with the k-th column substituted by the vector e_{k+1}, we have that

$$\frac{F_k}{D_{k+1}} = -\frac{\det M_{k+1,(k)}}{\det M_{k+1}} = -x_k^{(k+1)}.$$

Hence, we obtain

$$\frac{F_k}{D_k} = \frac{F_k}{D_{k+1}}\frac{D_{k+1}}{D_k} = -\frac{x_k^{(k+1)}}{x_{k+1}^{(k+1)}}.$$

In this setting, the coefficients α_k and β_k can be expressed in terms of the components of the solutions of appropriate linear systems as follows:

$$\alpha_k = -\frac{x_{k+1}^{(k+2)}}{x_{k+2}^{(k+2)}} + \frac{x_k^{(k+1)}}{x_{k+1}^{(k+1)}}, \quad \beta_k = \frac{x_k^{(k)}}{x_{k+1}^{(k+1)}}, \quad k \geq 1, \tag{2.84}$$

with

$$\alpha_0 = \frac{\mu_1}{\mu_0}, \quad \beta_0 = \mu_0.$$

System (2.83) rapidly becomes severely ill conditioned, so that the procedure does not offer any improvement with respect to the Chebyshev algorithm. Nevertheless, since M_{k+1} is a symmetric positive definite matrix, the idea is to consider a matrix $C = H^T H$, called bilateral preconditioner, where H is non singular. Then, the matrix $H^{-T} M_{k+1} H^{-1}$ is symmetric positive definite and the system

$$H^{-T} M_{k+1} H^{-1} y^{(k+1)} = H^{-T} e_{k+1}, \tag{2.85}$$

with $x^{(k+1)} = H^{-1} y^{(k+1)}$, is equivalent to (2.83). Analogously to the choice made for the modified Chebyshev approach, here we want to use as preconditioner C the moment matrix corresponding to the generalized Laguerre polynomials and as H its Cholesky decomposition.

Let η_k, $k \geq 0$, be the moments relative to the weight function $x^\alpha e^{-cx}$, given by

$$\eta_k = \eta_k^{\alpha,c} = \int_0^\infty x^{k+\alpha} e^{-cx} dx = \frac{\Gamma(k+\alpha+1)}{c^{k+\alpha+1}},$$

where we have used again [29, Sect.3.381, n.4]. We can write

$$\eta_k = \frac{1}{c^{\alpha+1}} \frac{\gamma_k}{c^k},$$

where

$$\gamma_k = \gamma_k^\alpha = \int_0^\infty x^{k+\alpha} e^{-x} dx = \Gamma(k+\alpha+1) \tag{2.86}$$

are the moments relative to the generalized Gauss-Laguerre rule. Hence, we can write the corresponding moment matrix

$$M_k^{\alpha,c} = \begin{bmatrix} \eta_0 & \eta_1 & \cdots & \eta_{k-1} \\ \vdots & \vdots & & \vdots \\ \eta_{k-1} & \eta_k & \cdots & \eta_{2k-2} \end{bmatrix} \in \mathbb{R}^{k\times k},$$

as

$$M_k^{\alpha,c} = \frac{1}{c^{\alpha+1}} E_k M_k^{\alpha} E_k,$$

where

$$M_k^{\alpha} = \begin{bmatrix} \gamma_0 & \gamma_1 & \cdots & \gamma_{k-1} \\ \vdots & \vdots & & \vdots \\ \gamma_{k-1} & \gamma_k & \cdots & \gamma_{2k-2} \end{bmatrix} \in \mathbb{R}^{k\times k},$$

and $E_k = \text{diag}\left(c^0, c^{-1}, \ldots, c^{1-k}\right)$.

At this point, if we consider the Cholesky decomposition of M_k^{α}

$$M_k^{\alpha} = (R_k^{\alpha})^T R_k^{\alpha},$$

we have

$$M_k^{\alpha,c} = \frac{1}{c^{\alpha+1}} E_k (R_k^{\alpha})^T R_k^{\alpha} E_k = (R_k^{\alpha,c})^T R_k^{\alpha,c},$$

where

$$R_k^{\alpha,c} = \frac{1}{(\sqrt{c})^{\alpha+1}} R_k^{\alpha} E_k.$$

The following proposition provides the explicit expression for R_k^{α}, and therefore for $R_k^{\alpha,c}$.

Proposition 15 *The Cholesky decomposition of the matrix M_k^{α} is*

$$M_k^{\alpha} = (R_k^{\alpha})^T R_k^{\alpha},$$

with

$$R_{ij}^{\alpha} = \frac{(j-1)!}{(j-i)!} \frac{\Gamma(\alpha+j)}{\sqrt{\Gamma(i)\Gamma(\alpha+i)}}, \quad \text{for} \quad i \le j \le k.$$

Proof. Since the matrix M_k^{α} is symmetric, we can restrict the analysis to the case $i \le j$. By (2.86) we know that

$$(M_k^{\alpha})_{ij} = \Gamma(i+\alpha+j-1).$$

Now,

$$((R_k^\alpha)^T R_k^\alpha)_{ij} = \sum_{l=1}^{i} R_{lj}^\alpha R_{li}^\alpha$$
$$= \Gamma(j)\Gamma(\alpha+j)\Gamma(i)\Gamma(\alpha+i)\sum_{l=1}^{i}\frac{1}{(j-l)!(i-l)!\Gamma(l)\Gamma(\alpha+l)}.$$

Writing

$$\binom{x}{y} = \frac{\Gamma(x+1)}{\Gamma(y+1)\Gamma(x-y+1)}, \tag{2.87}$$

with $x = \alpha + i - 1$ and $y = l - i$, we have

$$\frac{1}{\Gamma(\alpha+l)(i-l)!} = \binom{\alpha+i-1}{i-l}\frac{1}{\Gamma(\alpha+i)}.$$

Moreover,

$$\frac{1}{(j-l)!(l-1)!} = \binom{j-1}{l-1}\frac{1}{(j-1)!}.$$

Using the above relations, we obtain

$$((R_k^\alpha)^T R_k^\alpha)_{ij} = \Gamma(\alpha+j)\Gamma(i)\sum_{l=1}^{i}\binom{\alpha+i-1}{i-l}\binom{j-1}{l-1}.$$

At this point, by the following slight modification of the Chu-Vandermonde identity (see [4]),

$$\sum_{u=1}^{q}\binom{t}{u-1}\binom{s-t}{q-u} = \binom{s}{q-1},$$

we obtain

$$((R_k^\alpha)^T R_k^\alpha)_{ij} = \Gamma(\alpha+j)\Gamma(i)\binom{\alpha+j+i-2}{i-1}.$$

Using again (2.87), with $x = \alpha + j + i - 2$ and $y = i + 1$, it holds

$$\binom{\alpha+j+i-2}{i-1} = \frac{\Gamma(i+j+\alpha-1)}{\Gamma(\alpha+j)\Gamma(i)},$$

and finally

$$((R_k^\alpha)^T R_k^\alpha)_{ij} = \Gamma(i+\alpha+j-1).$$

■

We observe that the matrix R_k^α can be written as

$$R_k^\alpha = D_k \tilde{R}_k^\alpha,$$

with

$$(\tilde{R}_k^\alpha)_{ij} = \frac{(j-1)!\Gamma(\alpha+j)}{(j-i)!\Gamma(i)\Gamma(\alpha+i)}, \quad \text{for} \quad i \leq j,$$

and D_k diagonal matrix such that

$$(D_k)_{ii} = \sqrt{\Gamma(i)\Gamma(\alpha+i)}.$$

Since

$$(R_k^\alpha)^{-1} = (\tilde{R}_k^\alpha)^{-1}(D_k^\alpha)^{-1},$$

and

$$(\tilde{R}_k^\alpha)_{ij}^{-1} = (-1)^{i+j}(\tilde{R}_k^\alpha)_{ij},$$

we have that the explicit expression for $(R_k^\alpha)^{-1}$ is given by

$$(R_k^\alpha)_{ij}^{-1} = (-1)^{i+j}\frac{\sqrt{(j-1)!\Gamma(\alpha+j)}}{(j-i)!\Gamma(i)\Gamma(\alpha+i)}, \quad \text{for} \quad i \leq j.$$

Therefore, the matrix $(R_k^{\alpha,c})^{-1}$ can be written as

$$(R_k^{\alpha,c})^{-1} = (\sqrt{c})^{\alpha+1}E_k^{-1}(\tilde{R}_k^\alpha)^{-1}(D_k^\alpha)^{-1},$$

with

$$(R_k^{\alpha,c})_{ij}^{-1} = \frac{\sqrt{c}^{\alpha+1}c^{i-1}(-1)^{i+j}\sqrt{(j-1)!\Gamma(\alpha+j)}}{(j-i)!\Gamma(i)\Gamma(\alpha+i)}. \tag{2.88}$$

Finally, the linear system (2.83) can be preconditioned as

$$(R_{k+1}^{\alpha,c})^{-T}M_{k+1}(R_{k+1}^{\alpha,c})^{-1}y^{(k+1)} = (R_{k+1}^{\alpha,c})^{-T}e_{k+1}, \tag{2.89}$$

with

$$x^{(k+1)} = (R_{k+1}^{\alpha,c})^{-1}y^{(k+1)}. \tag{2.90}$$

Since the matrix M_{k+1} can be written as $M_{k+1} = M_{k+1}^{\alpha,c} + M_{k+1,0}^{\alpha,c}$, where $M_{k+1,0}^{\alpha,c}$ is the matrix of the core moments defined by equation (2.67), we have that

$$\begin{aligned}(R_{k+1}^{\alpha,c})^{-T}M_{k+1}(R_{k+1}^{\alpha,c})^{-1} &= (R_{k+1}^{\alpha,c})^{-T}(M_{k+1}^{\alpha,c} + M_{k+1,0}^{\alpha,c})(R_{k+1}^{\alpha,c})^{-1} \\ &= (R_{k+1}^{\alpha,c})^{-T}M_{k+1}^{\alpha,c}(R_{k+1}^{\alpha,c})^{-1} + (R_{k+1}^{\alpha,c})^{-T}M_{k+1,0}^{\alpha,c}(R_{k+1}^{\alpha,c})^{-1} \\ &= I_{k+1} + (R_{k+1}^{\alpha,c})^{-T}M_{k+1,0}^{\alpha,c}(R_{k+1}^{\alpha,c})^{-1} := Q_{k+1}, \end{aligned} \tag{2.91}$$

k	5	10	15	20	25	30
$\kappa_2(M_k)$	$2.4e+13$	$7.8e+32$	$1.0e+51$	$2.2e+69$	$4.6e+88$	$1.1e+107$
$\kappa_2(Q_k)$	$1.0e+00$	$1.3e+00$	$1.4e+00$	$1.4e+00$	$1.5e+00$	$1.6e+00$

Table 2.2: The Euclidean condition number of the matrix M_k and of the preconditioned matrix Q_k, defined in (2.91), for different values of k. In this example $\nu = 0.9$, $\alpha = 0.1$ and $c = 0.1$.

where I_{k+1} is the identity matrix. The system (2.89) becomes

$$(I_{k+1} + (R_{k+1}^{\alpha,c})^{-T} M_{k+1,0}^{\alpha,c} (R_{k+1}^{\alpha,c})^{-1}) y^{(k+1)} = (R_{k+1}^{\alpha,c})^{-T} e_{k+1}.$$

In Table 2.2 we show the remarkable effect of the preconditioning.

We observe that, since $(R_{k+1}^{\alpha,c})^{-1}$ is an upper triangular matrix, the components of the solution used in (2.82) can be written as

$$x_k^{(k+1)} = (R_{k+1}^{\alpha,c})_{kk}^{-1} y_k^{(k+1)} + (R_{k+1}^{\alpha,c})_{k,k+1}^{-1} y_{k+1}^{(k+1)}, \tag{2.92}$$

$$x_{k+1}^{(k+1)} = (R_{k+1}^{\alpha,c})_{k+1,k+1}^{-1} y_{k+1}^{(k+1)}. \tag{2.93}$$

We notice that the numerical implementation of the procedure to calculate α_k and β_k as in (2.84), by using expressions (2.92) and (2.93), starts to show instability around $k = 60 \div 70$, depending on the parameters, when $x_k^{(k+1)}$ and $x_{k+1}^{(k+1)}$ are close to the underflow. In order to gain more stability the idea is to rewrite the coefficients α_k and β_k, for $k \geq 1$, in terms of the components of the vectors $y^{(k)}, y^{(k+1)}, y^{(k+2)}$, defined in (2.90), and exploits relation (2.88). Indeed, we observe that for $i \sim j \sim k$,

$$(R_k^{\alpha,c})_{ij}^{-1} \sim \frac{c^k}{k!},$$

and therefore $y_i^{(k+1)} \gg x_i^{(k+1)}$, for $i = k, k+1$. By (2.82) and (2.88), we obtain

$$\begin{aligned} \alpha_k = & -\frac{\sqrt{(k+1)(\alpha+k+1)}}{c} \left(\frac{y_{k+1}^{(k+2)}}{y_{k+2}^{(k+2)}} - \sqrt{(k+1)(\alpha+k+1)} \right) \\ & + \frac{\sqrt{k(\alpha+k)}}{c} \left(\frac{y_k^{(k+1)}}{y_{k+1}^{(k+1)}} - \sqrt{k(\alpha+k)} \right), \end{aligned} \tag{2.94}$$

$$\beta_k = \frac{\sqrt{k(\alpha+k)}}{c} \left(\frac{y_k^{(k)}}{y_{k+1}^{(k+1)}} \right). \tag{2.95}$$

The final procedure, explained in Algorithm 1, allows to work with $80 \div 90$ points, dependently on the parameters.

Algorithm 1 *Define* α_0, β_0, β_1, $y^{(1)}$, $y^{(2)}$.
for $k = 2, \ldots, n-1$
calculate $y^{(k+1)}$ *by solving (2.89)*
$\beta_k \leftarrow y^{(k+1)}$, $y^{(k)}$ *by (2.95)*
$\alpha_{k-1} \leftarrow y^{(k+1)}$, $y^{(k)}$ *by (2.94)*
end

In Figure 2.6 we compare the results of Algorithm 6-7 (see Appendix C) and Algorithm 1. For all the examples we can say that only the preconditioned Cramer based approach allows to achieve an absolute error around the machine precision, while the Chebyshev and modified Chebyshev algorithms lose stability much earlier. In fact, as shown in Figure 2.7, Algorithm 6 and 7 start to provide inaccurate values of the coefficients α_k and β_k for k around $15 \div 25$, while Algorithm 1 is definitely more stable. Since the plot is in logarithmic scale, the missing parts of the curves are relative to negative entries. In conclusion, we can say that the numerical experiments confirm the reliability of the preconditioned Cramer based approach and shows that it is definitely more stable than the modified Chebyshev algorithm, since it allows to work with further $40 \div 60$ points, depending on the parameters.

We remark that, in principle, the approach can be applied to each weight function that is not so far to the standard ones, because it is necessary to be able to construct the preconditioner.

2.3.4 Application to electromagnetic fields

In the numerical experiments we use Algorithm 1 to evaluate fields (2.57), (2.58), (2.59) and (2.60). As before, we still consider the case of a 3-layered underground model with the same values of frequency and magnetic moment as in the previous section. However, this time the dipole height H is such that $H \neq 0$. Referring to (2.61), in our examples we set $\nu = 0, 1$, $\alpha = 0$, $c = \frac{2H}{r}$ and $f_i(x) = \Im\left(R_0\left(\frac{x}{r}\right)\right) x^i$, $i = 1, 2$. Regarding the choice of the parameters σ_i and h_i, i.e. of the underground models, we consider real life values of river levees (see e.g. [17]). We point out that for these parameters and by using double-precision arithmetic the method works with $k_{\max} \sim 85$, but in order to get closer to the machine precision more points are necessary. To overcome this issue, we adopt the symbolic computation and variable-precision arithmetic (see e.g. [23]), as supplied, e.g., by the current release

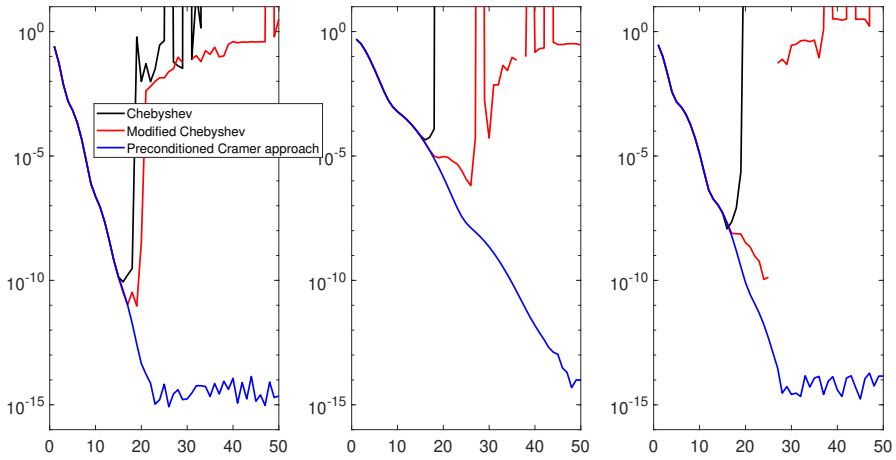

Figure 2.6: Error histories for $\nu = 1$, $\alpha = 0.7$, $c = 0.3$ on the left, for $\nu = 0.9$, $\alpha = 0.1$, $c = 0.1$ in the middle and for $\nu = 1.5$, $\alpha = 0.5$, $c = 0.2$ on the right. In all cases $f(x) = e^{-0.5x}$.

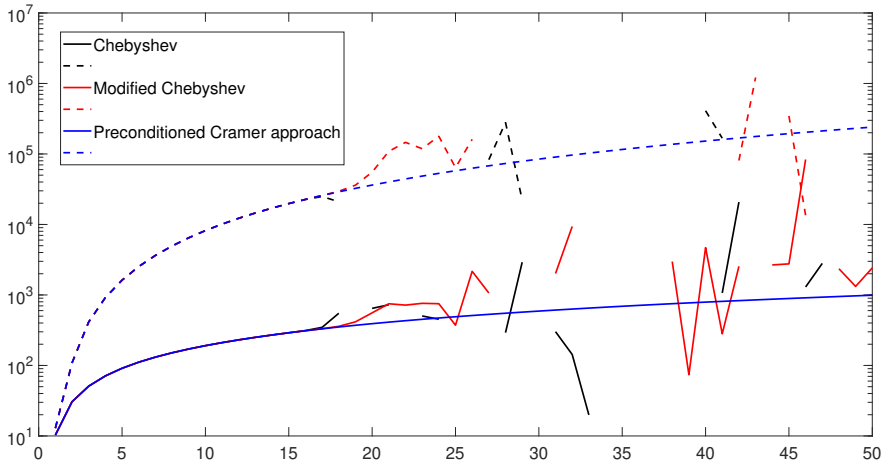

Figure 2.7: Plot of the coefficients α_k (solid lines) and β_k (dashed lines) for $\nu = 0.9$, $\alpha = 0.1$ and $c = 0.1$.

of Matlab. In this setting, we modify the routine that implements the preconditioned Cramer based approach by using `d`-decimal digit arithmetic to generate the first n recurrence coefficients. We remark that the number of digits depends on the model parameters and increase with n. Finally, we also point out that, similarly to the Gauss Laguerre rule, the weights decay exponentially and therefore a truncated approach can also be introduced as well. The idea is to fix a certain level of accuracy ϵ that we want to achieve and then to find $m_n < n$ such that we can neglect the tails of the quadrature formula. In particular, for each $k = 1, \ldots, n$, we truncate the weights w_i such that $w_i < \frac{\epsilon}{10}$, $i = 1, \ldots, k$, and define m_k as the number of remaining nodes. Alternatively, the quadrature error can be estimated by using the averaged and generalized averaged Gaussian rules (see [41, 56]), which are easy to construct and typically lead to quite accurate approximations of the error ([48]). Moreover, to further improve the truncated approach, we remark that, having at disposal a Gaussian quadrature rule allows to develop an a priori analysis of the error behavior. In particular, following the work of Barrett [5], it is possible to derive quite sharp error estimates, and hence to known a priori the rate of convergence of the error. These ideas are currently under development in [12].

In Figure 2.8-2.9-2.10-2.11 we provide the absolute error between the approximated fields $\Im(H_z^{(3)})$, $\Im(H_\rho^{(3)})$, $\Im(H_x^{(3)})$ and $\Im(H_y^{(3)})$, and a corresponding reference solution (see e.g. [31], [54]), with respect to the number of quadrature points m_n.

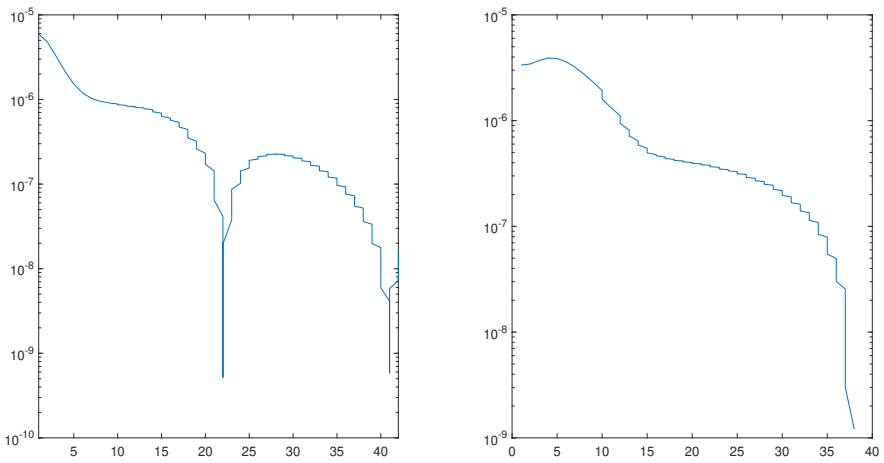

Figure 2.8: Error history for the computation of $\Im(H_z^{(3)})$ with respect to m_n for parameters $H = 0.4\ m$, $r = 8\ m$, $h_1 = 2.5\ m$, $h_2 = 0.5\ m$, $\sigma_1 = 0.05\ S/m$, $\sigma_2 = 0.0049\ S/m$, $\sigma_3 = 0.0182\ S/m$ on the left and for parameters $H = 0.2\ m$, $r = 8\ m$, $h_1 = 2.5\ m$, $h_2 = 0.5\ m$, $\sigma_1 = 0.033\ S/m$, $\sigma_2 = 0.1\ S/m$, $\sigma_3 = 0.01\ S/m$ on the right.

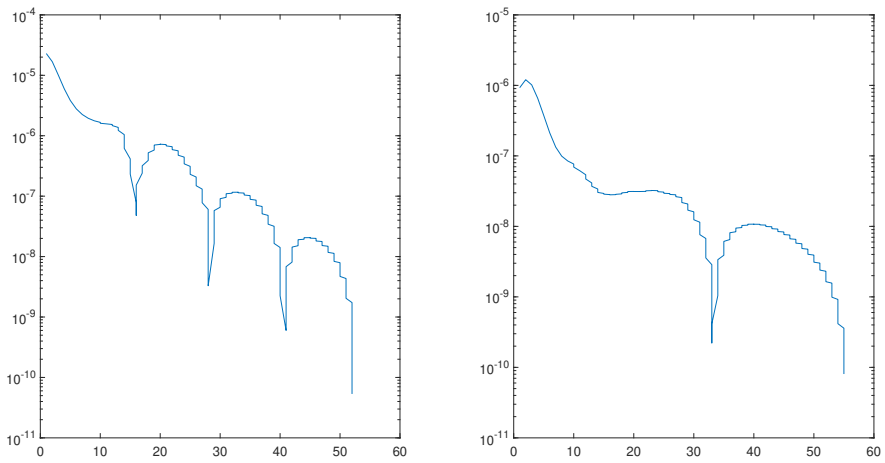

Figure 2.9: Error history for the computation of $\Im(H_\rho^{(3)})$ with respect to m_n for parameters $H = 0.4\ m$, $r = 8\ m$, $h_1 = 2.5\ m$, $h_2 = 0.5\ m$, $\sigma_1 = 0.333\ S/m$, $\sigma_2 = 0.02\ S/m$, $\sigma_3 = 0.1\ S/m$ on the left and for parameters $H = 0.4\ m$, $r = 8\ m$, $h_1 = 2.5\ m$, $h_2 = 0.5\ m$, $\sigma_1 = 0.033\ S/m$, $\sigma_2 = 0.1\ S/m$, $\sigma_3 = 0.01\ S/m$ on the right.

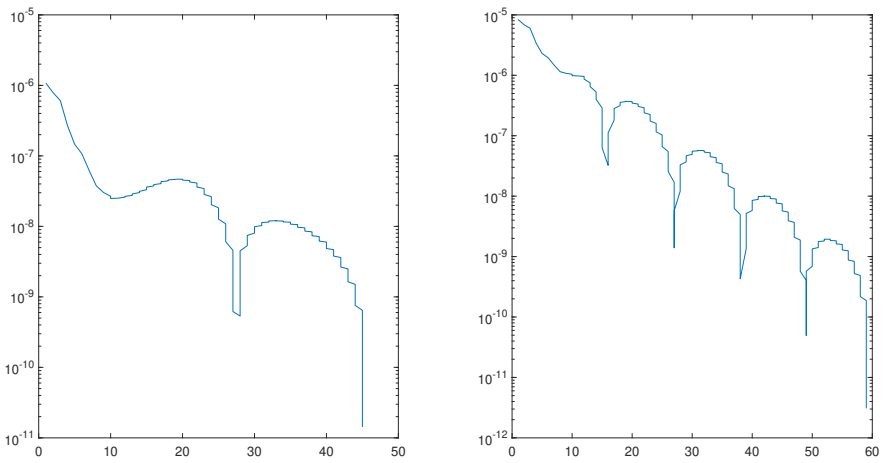

Figure 2.10: Error history for the computation of $\Im(H_x^{(3)})$ with respect to m_n for parameters $H = 0.2\ m$, $r = 8\ m$, $h_1 = 3\ m$, $h_2 = 2\ m$, $\sigma_1 = 0.033\ S/m$, $\sigma_2 = 0.2\ S/m$, $\sigma_3 = 0.01\ S/m$ on the left and for parameters $H = 0.1\ m$, $r = 4\ m$, $h_1 = 2.5\ m$, $h_2 = 0.5\ m$, $\sigma_1 = 0.05\ S/m$, $\sigma_2 = 0.0049\ S/m$, $\sigma_3 = 0.0182\ S/m$ on the right.

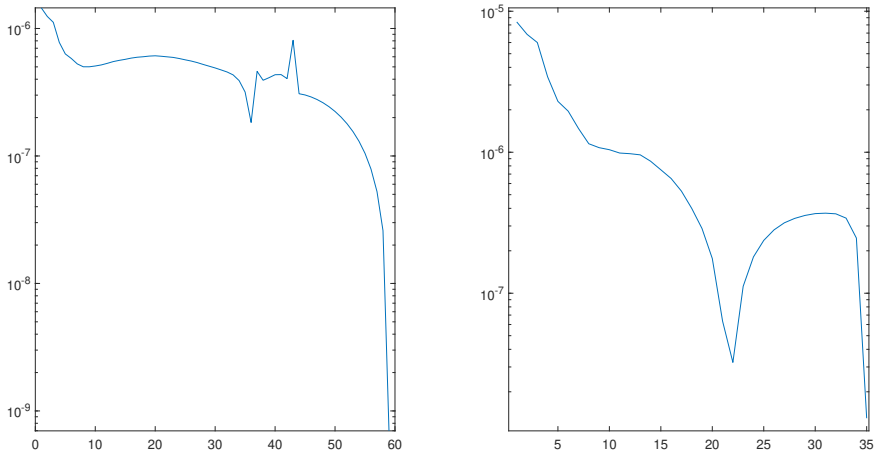

Figure 2.11: Error history for the computation of $\Im(H_y^{(3)})$ with respect to m_n for parameters $H = 0.5\ m$, $r = 2\ m$, $h_1 = 3\ m$, $h_2 = 2\ m$, $\sigma_1 = 0.0769\ S/m$, $\sigma_2 = 0.0323\ S/m$, $\sigma_3 = 0.05\ S/m$ on the left and for parameters $H = 0.5\ m$, $r = 2\ m$, $h_1 = 3\ m$, $h_1 = 2\ m$, $\sigma_1 = 0.333\ S/m$, $\sigma_2 = 0.02\ S/m$, $\sigma_3 = 0.01\ S/m$ on the right.

Chapter 3

Approximations of the EM fields

In this chapter, with the number of ground layers $N = 2, 3$ and the height of the receptor $H = 0$, we derive useful analytical approximations of the fields $H_z^{(N)}$, $H_\rho^{(N)}$, $H_x^{(N)}$ and $H_y^{(N)}$, expressed by equations (2.37), (2.38), (2.39) and (2.40). While these approximations can be used in general to have an idea of the main features of the fields, our basic aim is to employ them for the inverse problem, in which we want to compute the underground model parameters from a set of observed data (see Chapter 4). We remark that, with some efforts, the analysis can be extended to the case $H \neq 0$.

3.1 General analytical approximations

In this section we provide an analytical approximation of the fields, only based on mathematical considerations and without further hypothesis on the physical properties of the underground model.

First, from (2.41) we have

$$g_l(\lambda) = \frac{4R_1u_1}{R_1k_1^2 + (\lambda + u_1)^2}\lambda^3 J_l(\lambda r), \quad l = 0, 1.$$

Moreover, for $0 \leq i, j, \ell \leq N$

$$\begin{aligned}(u_i - u_j)e^{-2u_\ell h_\ell} &= \frac{k_j^2 - k_i^2}{\sqrt{\lambda^2 - k_i^2} + \sqrt{\lambda^2 - k_j^2}} e^{-2\sqrt{\lambda^2 - k_\ell^2}h_\ell} \\ &= \mathcal{O}\left(\frac{e^{-2\lambda h_\ell}}{\lambda}\right), \quad \text{for} \quad \lambda \to \infty, \end{aligned} \tag{3.1}$$

and the same holds true for $(\lambda-u_j)e^{-2u_\ell h_\ell}$. Actually, this asymptotic behavior is observed already for λ relatively small, because also the quantities k_i are very small. In order to derive approximations of $H_z^{(N)}$, $H_\rho^{(N)}$, $H_x^{(N)}$ and $H_y^{(N)}$, in what follows whenever possible we neglect the terms involving these factors.

$\mathbf{N=2}$ - In this case we have

$$R_2 = 0, \quad R_1 = \Psi_2 e^{-2u_1h_1} = \frac{u_1-u_2}{u_1+u_2}e^{-2u_1h_1},$$

and therefore

$$\frac{4R_1u_1}{R_1k_1^2+(\lambda+u_1)^2} = \frac{4u_1(u_1-u_2)}{(\lambda^2-u_1^2)(u_1-u_2)e^{-2u_1h_1}+(\lambda+u_1)^2(u_1+u_2)}e^{-2u_1h_1}.$$

By (3.1) we can consider the approximation

$$(\lambda^2-u_1^2)(u_1-u_2)e^{-2u_1h_1} \approx 0.$$

Moreover, using the first order approximation

$$u_1 = \sqrt{\lambda^2+i\omega\mu\sigma_1} = \lambda\sqrt{1+\frac{i\omega\mu\sigma_1}{\lambda^2}} \approx \lambda\left(1+\frac{i\omega\mu\sigma_1}{2\lambda^2}\right), \tag{3.2}$$

we obtain

$$\begin{aligned}\frac{4R_1u_1}{R_1k_1^2+(\lambda+u_1)^2} &\approx \frac{4u_1(u_1-u_2)}{(\lambda+u_1)^2(u_1+u_2)}e^{-2u_1h_1} &(3.3)\\ &= \frac{4u_1(u_1-u_2)^2(\lambda-u_1)^2}{(\lambda^2-u_1^2)^2(u_1^2-u_2^2)}e^{-2u_1h_1}\\ &\approx \frac{i\omega\mu(\sigma_1-\sigma_2)}{4\lambda^3}\left(1+\frac{i\omega\mu\sigma_1}{2\lambda^2}\right)e^{-2u_1h_1}. &(3.4)\end{aligned}$$

At this point, we use the non standard approximation

$$u_1 = \sqrt{\lambda^2+i\omega\mu\sigma_1} \approx \lambda+\sqrt{i\omega\mu\sigma_1}. \tag{3.5}$$

The main reason for this choice is that the standard (3.2) leads to final approximation that does not allow to simplify the integrals with the existing formulas. Anyway, approximation (3.5) is partially justified by observing that

$$\frac{u_1}{\lambda+\sqrt{i\omega\mu\sigma_1}} \to 1, \quad \text{for} \quad \lambda\to 0 \text{ and } \lambda\to+\infty.$$

Now, since

$$\lambda+\sqrt{i\omega\mu\sigma_1} = \lambda+\frac{\sqrt{2}}{2}\sqrt{\omega\mu\sigma_1}+i\frac{\sqrt{2}}{2}\sqrt{\omega\mu\sigma_1},$$

we obtain

$$\begin{aligned} e^{-2u_1h_1} &\approx e^{-2\lambda h_1 - h_1\sqrt{2\omega\mu\sigma_1}}[\cos(h_1\sqrt{2\omega\mu\sigma_1}) - i\sin(h_1\sqrt{2\omega\mu\sigma_1})] \\ &\approx e^{-2\lambda h_1 - h_1\sqrt{2\omega\mu\sigma_1}}. \end{aligned} \tag{3.6}$$

Using the above approximation in (3.4) we have

$$\Im\left(\frac{4R_1u_1}{R_1k_1^2 + (\lambda+u_1)^2}\right) \approx \frac{\omega\mu(\sigma_1-\sigma_2)e^{-2\lambda h_1 - h_1\sqrt{2\omega\mu\sigma_1}}}{4\lambda^3}.$$

Moreover, by the general formulas (see [29, p.707, 6.611, n.1] and [29, p.702, 6.623, n.3])

$$\begin{aligned} &\int_0^\infty e^{-\alpha x}J_\nu(\beta x)dx = \frac{\beta^{-\nu}[\sqrt{\alpha^2+\beta^2}-\alpha]^\nu}{\sqrt{\alpha^2+\beta^2}}, \quad \Re(\nu) > -1,\ \Re(\alpha \pm i\beta) > 0, \\ &\int_0^\infty \frac{e^{-\alpha x}}{x}J_\nu(\beta x)dx = \frac{(\sqrt{\alpha^2+\beta^2}-\alpha)^\nu}{\nu\beta^\nu}, \quad \Re(\nu) > 0,\ \Re(\alpha) > |\Im(\beta)|, \end{aligned}$$

where the symbol $\Re$ indicates the real part, we finally obtain, for the integral in equation (2.37) and the first integral in equation (2.39), the approximation

$$\begin{aligned} &\Im\left(\int_0^\infty \frac{4R_1u_1}{R_1k_1^2+(\lambda+u_1)^2}\lambda^3 J_0(\lambda r)d\lambda\right) \\ &\approx \frac{\omega\mu(\sigma_1-\sigma_2)e^{-h_1\sqrt{2\omega\mu\sigma_1}}}{4}\int_0^\infty e^{-2\lambda h_1}J_0(\lambda r)d\lambda \\ &= \frac{\omega\mu(\sigma_1-\sigma_2)e^{-h_1\sqrt{2\omega\mu\sigma_1}}}{4\sqrt{4h_1^2+r^2}}, \end{aligned}$$

while, for the integral in equation (2.40) and the second integral in equation (2.39), we have

$$\begin{aligned} &\Im\left(\int_0^\infty \frac{4R_1u_1}{R_1k_1^2+(\lambda+u_1)^2}\lambda^2 J_1(\lambda r)d\lambda\right) \\ &\approx \frac{\omega\mu(\sigma_1-\sigma_2)e^{-h_1\sqrt{2\omega\mu\sigma_1}}}{4}\int_0^\infty \frac{e^{-2\lambda h_1}}{\lambda}J_1(\lambda r)d\lambda \\ &= \frac{\omega\mu(\sigma_1-\sigma_2)e^{-h_1\sqrt{2\omega\mu\sigma_1}}(\sqrt{4h_1^2+r^2}-2h_1)}{4r}. \end{aligned}$$

Using the same arguments for $H_\rho^{(2)}$, the integral in equation (2.38) can be

approximated as

$$\begin{aligned}
&\Im\left(\int_0^\infty \frac{-4R_1u_1}{R_1k_1^2+(\lambda+u_1)^2}\lambda^3 J_1(\lambda r)d\lambda\right) \approx \\
&\approx -\frac{\omega\mu(\sigma_1-\sigma_2)e^{-h_1\sqrt{2\omega\mu\sigma_1}}}{4}\int_0^\infty e^{-2\lambda h_1}J_1(\lambda r)d\lambda \\
&= -\frac{\omega\mu(\sigma_1-\sigma_2)e^{-h_1\sqrt{2\omega\mu\sigma_1}}(\sqrt{4h_1^2+r^2}-2h_1)}{4r\sqrt{4h_1^2+r^2}}.
\end{aligned}$$

Finally,

$$\begin{aligned}
\Im(H_z^{(2)}) &\approx \frac{m}{4\pi}\left(\frac{\omega\mu(\sigma_1-\sigma_2)e^{-h_1\sqrt{2\omega\mu\sigma_1}}}{4\sqrt{4h_1^2+r^2}}\right)+\Im\left(H_z^{(1)}\right), \\
\Im(H_\rho^{(2)}) &\approx -\frac{m}{4\pi}\left(\frac{\omega\mu(\sigma_1-\sigma_2)e^{-h_1\sqrt{2\omega\mu\sigma_1}}(\sqrt{4h_1^2+r^2}-2h_1)}{4r\sqrt{4h_1^2+r^2}}\right)+\Im\left(H_\rho^{(1)}\right), \\
\Im(H_x^{(2)}) &\approx \frac{m}{4\pi}\frac{\omega\mu(\sigma_1-\sigma_2)e^{-h_1\sqrt{2\omega\mu\sigma_1}}}{4}\left(\frac{1}{\sqrt{4h_1^2+r^2}}-\frac{\sqrt{4h_1^2+r^2}-2h_1}{r^2}\right)+\Im(H_x^{(1)}), \\
\Im(H_y^{(2)}) &\approx \frac{m}{4\pi r}\left(\frac{\omega\mu(\sigma_1-\sigma_2)e^{-h_1\sqrt{2\omega\mu\sigma_1}}(\sqrt{4h_1^2+r^2}-2h_1)}{4r}\right)+\Im\left(H_y^{(1)}\right).
\end{aligned}$$

N = 3 - In this case we have

$$\begin{aligned}
R_3 &= 0, \\
R_2 &= \Psi_3 e^{-2u_2h_2} = \frac{u_2-u_3}{u_2+u_3}e^{-2u_2h_2}, \\
R_1 &= \frac{\frac{u_2-u_3}{u_2+u_3}e^{-2u_2h_2}+\frac{u_1-u_2}{u_1+u_2}}{\frac{u_2-u_3}{u_2+u_3}\frac{u_1-u_2}{u_1+u_2}e^{-2u_2h_2}+1}e^{-2u_1h_1} \\
&= \frac{(u_1+u_2)(u_2-u_3)e^{-2u_2h_2}+(u_1-u_2)(u_2+u_3)}{(u_2-u_3)(u_1-u_2)e^{-2u_2h_2}+(u_1+u_2)(u_2+u_3)}e^{-2u_1h_1} \\
&\approx \frac{(u_1+u_2)(u_2-u_3)e^{-2u_2h_2}+(u_1-u_2)(u_2+u_3)}{(u_1+u_2)(u_2+u_3)}e^{-2u_1h_1},
\end{aligned}$$

where, as before, we have used (3.1). We obtain

$$\begin{aligned}
&\frac{4R_1u_1}{R_1k_1^2+(\lambda+u_1)^2} = \\
= \;& 4u_1[(u_1+u_2)(u_2-u_3)e^{-2(u_1h_1+u_2h_2)}+(u_1-u_2)(u_2+u_3)e^{-2u_1h_1}]\times \\
& [(u_1+u_2)(u_2-u_3)(\lambda^2-u_1^2)e^{-2(u_1h_1+u_2h_2)}+(u_1-u_2)(u_2+u_3)(\lambda^2-u_1^2)e^{-2u_1h_1} \\
& +(\lambda+u_1)^2(u_1-u_2)(u_2-u_3)e^{-2u_2h_2}+(\lambda+u_1)^2(u_1+u_2)(u_2+u_3)]^{-1} \\
\approx \;& 4u_1\frac{(u_1+u_2)(u_2-u_3)e^{-2(u_1h_1+u_2h_2)}+(u_1-u_2)(u_2+u_3)e^{-2u_1h_1}}{(\lambda+u_1)^2(u_1+u_2)(u_2+u_3)} \qquad (3.7)\\
= \;& \frac{4u_1(u_2-u_3)e^{-2(u_1h_1+u_2h_2)}}{(\lambda+u_1)^2(u_2+u_3)}+\frac{4u_1(u_1-u_2)e^{-2u_1h_1}}{(\lambda+u_1)^2(u_1+u_2)}, \qquad (3.8)
\end{aligned}$$

where approximation (3.7) arises again from (3.1). We observe that the two terms of (3.8) are very similar and, in particular, the second one corresponds to (3.3) for $N=2$. Therefore, using approximations (3.2) and (3.5) for u_1, u_2 and u_3, we obtain

$$\Im\left(\int_0^\infty \frac{4R_1u_1}{R_1k_1^2+(\lambda+u_1)^2}\lambda^3J_0(\lambda r)d\lambda\right)\approx\frac{\omega\mu e^{-h_1\sqrt{2\omega\mu\sigma_1}}}{4}\left(\frac{(\sigma_2-\sigma_3)e^{-h_2\sqrt{2\omega\mu\sigma_2}}}{\sqrt{4(h_1+h_2)^2+r^2}}+\frac{\sigma_1-\sigma_2}{\sqrt{4h_1^2+r^2}}\right),$$

and

$$\begin{aligned}
&\Im\left(\int_0^\infty \frac{4R_1u_1}{R_1k_1^2+(\lambda+u_1)^2}\lambda^2J_1(\lambda r)d\lambda\right)\approx \\
&\approx\frac{\omega\mu e^{-h_1\sqrt{2\omega\mu\sigma_1}}}{4r}\Big((\sigma_2-\sigma_3)e^{-h_2\sqrt{2\omega\mu\sigma_2}}\left[\sqrt{4(h_1+h_2)^2+r^2}-2(h_1+h_2)\right] \\
&+(\sqrt{4h_1^2+r^2}-2h_1)(\sigma_1-\sigma_2)\Big).
\end{aligned}$$

Analogously,

$$\begin{aligned}
&\Im\left(\int_0^\infty \frac{-4R_1u_1}{R_1k_1^2+(\lambda+u_1)^2}\lambda^3J_1(\lambda r)d\lambda\right)\approx \\
\approx\;& \frac{\omega\mu e^{-h_1\sqrt{2\omega\mu\sigma_1}}}{-4r}\left(\frac{(\sigma_2-\sigma_3)e^{-h_2\sqrt{2\omega\mu\sigma_2}}[\sqrt{4(h_1+h_2)^2+r^2}-2(h_1+h_2)]}{\sqrt{4(h_1+h_2)^2+r^2}}\right. \\
&\left.+\frac{(\sqrt{4h_1^2+r^2}-2h_1)(\sigma_1-\sigma_2)}{\sqrt{4h_1^2+r^2}}\right).
\end{aligned}$$

Finally,

$$\Im(H_z^{(3)}) \approx \frac{m}{4\pi}\frac{\omega\mu e^{-h_1\sqrt{2\omega\mu\sigma_1}}}{4}\left(\frac{(\sigma_2-\sigma_3)e^{-h_2\sqrt{2\omega\mu\sigma_2}}}{\sqrt{4(h_1+h_2)^2+r^2}}+\frac{\sigma_1-\sigma_2}{\sqrt{4h_1^2+r^2}}\right)+\Im\left(H_z^{(1)}\right), \tag{3.9}$$

$$\Im(H_\rho^{(3)}) \approx -\frac{m}{4\pi}\frac{\omega\mu e^{-h_1\sqrt{2\omega\mu\sigma_1}}}{4r}\Big(\frac{(\sigma_2-\sigma_3)e^{-h_2\sqrt{2\omega\mu\sigma_2}}[\sqrt{4(h_1+h_2)^2+r^2}-2(h_1+h_2)]}{\sqrt{4(h_1+h_2)^2+r^2}} + \frac{(\sqrt{4h_1^2+r^2}-2h_1)(\sigma_1-\sigma_2)}{\sqrt{4h_1^2+r^2}}\Big)+\Im(H_\rho^{(1)}), \tag{3.10}$$

$$\Im(H_x^{(3)}) \approx \frac{m}{4\pi}\frac{\omega\mu e^{-h_1\sqrt{2\omega\mu\sigma_1}}}{4}\Bigg[(\sigma_2-\sigma_3)e^{-h_2\sqrt{2\omega\mu\sigma_2}}\left(\frac{1}{\sqrt{4(h_1+h_2)^2+r^2}} - \frac{\sqrt{4(h_1+h_2)^2+r^2}-2(h_1+h_2)}{r^2}\right)+(\sigma_1-\sigma_2)\left(\frac{1}{\sqrt{4h_1^2+r^2}} - \frac{\sqrt{4h_1^2+r^2}-2h_1}{r^2}\right)\Bigg]+\Im(H_x^{(1)}) \tag{3.11}$$

and

$$\Im(H_y^{(3)}) \approx \frac{m}{4\pi r}\frac{\omega\mu e^{-h_1\sqrt{2\omega\mu\sigma_1}}}{4r}\Bigg((\sigma_2-\sigma_3)e^{-h_2\sqrt{2\omega\mu\sigma_2}}\left[\sqrt{4(h_1+h_2)^2+r^2}-2(h_1+h_2)\right] + \left(\sqrt{4h_1^2+r^2}-2h_1\right)(\sigma_1-\sigma_2)\Bigg)+\Im(H_y^{(1)}). \tag{3.12}$$

3.2 Low-frequency response and LIN approximations

In this section we describe the commonly employed approximations of the fields under the low induction numbers assumption.

In the case of a N-layered earth, when the frequency is sufficiently low, more precisely at low induction numbers (LIN), the reflection term can be approximated in order to obtain explicit expressions for the fields $H_z^{(N)}$, $H_\rho^{(N)}$, $H_x^{(N)}$ and $H_y^{(N)}$, given by equations (2.29), (2.30), (2.31) and (2.32) (see [61], [62] and [44]). In particular, the induction number is defined as

$$B = \frac{r}{d},$$

where

$$d = \sqrt{\frac{2}{\omega\mu\sigma}}$$

is the skin depth and r is the source-receiver distance (offset). At LIN, $B \ll 1$ and the eddy currents of each layer do not interact. Moreover, the secondary field measured at the receiver is the sum of the independent fields from each individual current loop. The approximation is equivalent to assume that the frequency is low (around $10\,kHz$) and that the current flow at any point is independent of the current flow at any other point, since the magnetic coupling between all current loops is negligible.

As before, we work with $N = 2, 3$ and $H = 0$.

$\mathbf{N = 2}$ - From (2.28) we have

$$R_2 = 0, R_1 = \Psi_2 e^{-2u_1 h_1} = \frac{u_1 - u_2}{u_1 + u_2} e^{-2u_1 h_1}$$

and therefore

$$R_0 = \frac{R_1 + \Psi_1}{R_1\Psi_1 + 1} = \frac{(\lambda + u_1)(u_1 - u_2)e^{-2u_1 h_1} + (\lambda - u_1)(u_1 + u_2)}{(u_1 - u_2)(\lambda - u_1)e^{-2u_1 h_1} + (u_1 + u_2)(\lambda + u_1)}.$$

By (3.1) we can consider

$$(u_1 - u_2)(\lambda - u_1)e^{-2u_1 h_1} \approx 0.$$

Moreover, using the first order approximation

$$u_j = \sqrt{\lambda^2 + i\omega\mu\sigma_j} = \lambda\sqrt{1 + \frac{i\omega\mu\sigma_j}{\lambda^2}} \approx \lambda\left(1 + \frac{i\omega\mu\sigma_j}{2\lambda^2}\right), \quad j = 1, 2$$

and since

$$\left|\frac{i\omega\mu\sigma_j}{\lambda^2}\right| \ll 1, \quad j = 1, 2,$$

we obtain

$$\begin{aligned} R_0 &\approx \frac{(\lambda + u_1)(u_1 - u_2)e^{-2u_1 h_1} + (\lambda - u_1)(u_1 + u_2)}{(u_1 + u_2)(\lambda + u_1)} \\ &\approx \frac{-i\omega\mu\sigma_1 + i\omega\mu\sigma_1 e^{-2u_1 h_1} - i\omega\mu\sigma_2 e^{-2u_1 h_1}}{4\lambda^2}. \end{aligned}$$

Finally, by the approximation

$$e^{-2u_1 h_1} \approx e^{-2h_1\lambda}, \tag{3.13}$$

we have that

$$R_0 \approx \frac{-i\omega\mu\sigma_1(1 - e^{-2h_1\lambda}) - i\omega\mu\sigma_2 e^{-2h_1\lambda}}{4\lambda^2}. \tag{3.14}$$

Remark 6 *We notice that approximation (3.13) represent the main difference with respect to the general analytical approximation of Section 3.1 (c.f. formula (3.6)).*

Using result (3.14) in (2.29), (2.30), (2.31) and (2.32), we obtain

$$\Im\left(H_z^{(2)}\right) \approx -\frac{\omega\mu m}{16\pi}\left[\sigma_1\int_0^\infty J_0(\lambda r)d\lambda + (\sigma_2-\sigma_1)\int_0^\infty e^{-2h_1\lambda}J_0(\lambda r)d\lambda\right],$$

$$\Im\left(H_\rho^{(2)}\right) \approx \frac{\omega\mu m}{16\pi}\left[\sigma_1\int_0^\infty J_1(\lambda r)d\lambda + (\sigma_2-\sigma_1)\int_0^\infty e^{-2h_1\lambda}J_1(\lambda r)d\lambda\right],$$

$$\begin{aligned}\Im\left(H_x^{(2)}\right) \approx &-\frac{\omega\mu m}{16\pi}\left[\sigma_1\int_0^\infty J_0(\lambda r)d\lambda + (\sigma_2-\sigma_1)\int_0^\infty e^{-2h_1\lambda}J_0(\lambda r)d\lambda\right]\\ &+\frac{\omega\mu m}{16\pi r}\left[\sigma_1\int_0^\infty \frac{J_1(\lambda r)}{\lambda}d\lambda + (\sigma_2-\sigma_1)\int_0^\infty \frac{e^{-2h_1\lambda}}{\lambda}J_1(\lambda r)d\lambda\right]\end{aligned}$$

and

$$\Im\left(H_y^{(2)}\right) \approx -\frac{\omega\mu m}{16\pi r}\left[\sigma_1\int_0^\infty \sigma_1\frac{J_1(\lambda r)}{\lambda}d\lambda + (\sigma_2-\sigma_1)\int_0^\infty \frac{e^{-2h_1\lambda}}{\lambda}J_1(\lambda r)d\lambda\right].$$

At this point, from [29, p.665, 6.511, n.1], [29, p.707, 6.611, n.1], [29, p.702, 6.623, n.3] and [29, p.676, 6.561, n.14], we have

$$\Im\left(H_z^{(2)}\right) \approx -\frac{\omega\mu m}{16\pi}\left(\frac{\sigma_1}{r} + \frac{\sigma_2-\sigma_1}{\sqrt{r^2+4h_1^2}}\right),$$

$$\Im\left(H_\rho^{(2)}\right) \approx \frac{\omega\mu m}{16\pi r}\left[\sigma_1 + (\sigma_2-\sigma_1)\left(1-\frac{2h_1}{\sqrt{r^2+4h_1^2}}\right)\right],$$

$$\Im\left(H_x^{(2)}\right) \approx \frac{\omega\mu m}{16\pi}\left[(\sigma_2-\sigma_1)\left(\frac{\sqrt{4h_1^2+r^2}-2h_1}{r^2} - \frac{1}{\sqrt{4h_1^2+r^2}}\right)\right]$$

and

$$\Im\left(H_y^{(2)}\right) \approx -\frac{\omega\mu m}{16\pi r}\left[\sigma_1 + (\sigma_2-\sigma_1)\frac{\sqrt{4h_1^2+r^2}-2h_1}{r}\right].$$

$\mathbf{N=3}$ - From (2.28) we have

$$R_3 = 0,$$

$$R_2 = \Psi_3 e^{-2u_2h_2} = \frac{u_2-u_3}{u_2+u_3}e^{-2u_2h_2},$$

$$\begin{aligned}R_1 &= \frac{\frac{u_2-u_3}{u_2+u_3}e^{-2u_2h_2} + \frac{u_1-u_2}{u_1+u_2}}{\frac{u_2-u_3}{u_2+u_3}\frac{u_1-u_2}{u_1+u_2}e^{-2u_2h_2}+1}e^{-2u_1h_1}\\ &= \frac{(u_1+u_2)(u_2-u_3)e^{-2(u_1h_1+u_2h_2)} + (u_1-u_2)(u_2+u_3)e^{-2u_1h_1}}{(u_1-u_2)(u_2-u_3)e^{-2u_2h_2} + (u_1+u_2)(u_2+u_3)}.\end{aligned}$$

Therefore, following the same kind of approximations of the case $N = 2$, we obtain

$$R_0 \approx \frac{2\lambda i\omega\mu(\sigma_2-\sigma_3)e^{-2(h_1+h_2)\lambda} + 2\lambda i\omega\mu(\sigma_1-\sigma_2)e^{-2h_1\lambda} - 2\lambda i\omega\mu\sigma_1}{8\lambda^3}$$
$$= -i\omega\mu\frac{\sigma_1\left(1-e^{-2h_1\lambda}\right) + \sigma_2\left(e^{-2h_1\lambda} - e^{-2(h_1+h_2)\lambda}\right) + \sigma_3 e^{-2(h_1+h_2)\lambda}}{4\lambda^2}.$$

Finally, by substituting the above expression in (2.29), (2.30), (2.31) and (2.32) and by using again [29, p.665, 6.511, n.1], [29, p.707, 6.611, n.1], [29, p.702, 6.623, n.3] and [29, p.676, 6.561, n.14], we have

$$\Im\left(H_z^{(3)}\right) \approx -\frac{\omega\mu m}{16\pi}\left(\frac{\sigma_1}{r} + \frac{\sigma_2-\sigma_1}{\sqrt{r^2+4h_1^2}} + \frac{\sigma_3-\sigma_2}{\sqrt{r^2+4(h_1+h_2)^2}}\right), \tag{3.15}$$

$$\Im\left(H_\rho^{(3)}\right) \approx \frac{\omega\mu m}{16\pi r}\left[\sigma_1 + (\sigma_2-\sigma_1)\left(1-\frac{2h_1}{\sqrt{r^2+4h_1^2}}\right)\right.$$
$$\left. + (\sigma_3-\sigma_2)\left(1-\frac{2(h_1+h_2)}{\sqrt{r^2+4(h_1+h_2)^2}}\right)\right], \tag{3.16}$$

$$\Im\left(H_x^{(3)}\right) \approx \frac{\omega\mu m}{16\pi}\left[(\sigma_2-\sigma_1)\left(\frac{\sqrt{4h_1^2+r^2}-2h_1}{r^2} - \frac{1}{\sqrt{4h_1^2+r^2}}\right)\right.$$
$$\left. + (\sigma_3-\sigma_2)\left(\frac{\sqrt{4(h_1+h_2)^2}-2(h_1+h_2)}{r^2} - \frac{1}{\sqrt{4(h_1+h_2)^2+r^2}}\right)\right] \tag{3.17}$$

and

$$\Im\left(H_y^{(3)}\right) \approx -\frac{\omega\mu m}{16\pi r}\left[\sigma_1 + (\sigma_2-\sigma_1)\frac{\sqrt{4h_1^2+r^2}-2h_1}{r}\right.$$
$$\left. + (\sigma_3-\sigma_2)\frac{\sqrt{4(h_1+h_2)^2}-2(h_1+h_2)}{r}\right]. \tag{3.18}$$

3.3 Some numerical examples

To conclude this chapter, in Figure 3.1 we compare the imaginary part of the fields $H_z^{(3)}$, $H_\rho^{(3)}$, $H_y^{(3)}$ and $H_x^{(3)}$, in logarithmic scale, computed from the integral formulations (2.53), (2.54), (2.55) and (2.56) by using the Gauss Kronrod technique, with the analytical approximations (3.9), (3.10), (3.11),

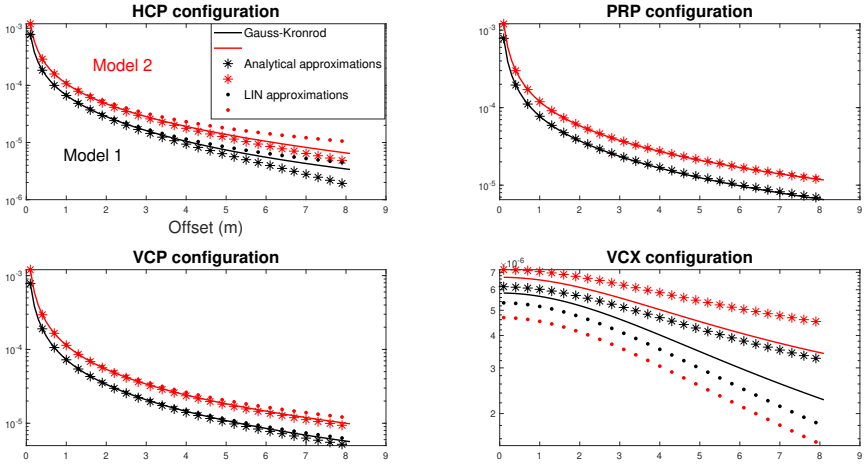

Figure 3.1: Comparison between the imaginary part of the fields $H_z^{(3)}$ (a), $H_\rho^{(3)}$ (b), $H_y^{(3)}$ (c) and $H_x^{(3)}$ (d), in logarithmic scale, computed adopting the Gauss-Kronrod quadrature technique (solid lines) and the approximations of Section 3.1 and 3.2 (symbols). Two underground models are considered: $\sigma_1 = 50.0\ mS/m$, $\sigma_2 = 4.9\ mS/m$, $\sigma_3 = 18.2\ mS/m$, $h_1 = 2.5\ m$, $h_2 = 0.5\ m$ (Model 1) and $\sigma_1 = 76.9\ mS/m$, $\sigma_2 = 32.3\ mS/m$, $\sigma_3 = 50.0\ mS/m$, $h_1 = 2.5\ m$, $h_2 = 0.5\ m$ (Model 2). In all cases $\nu = 10\ kHz$ and $m = 1\ A/m^2$.

(3.12) of Section 3.1 and the LIN approximations (3.15), (3.16), (3.17), (3.18) of Section 3.2, for two different underground models. In particular, the plots relative to the fields $H_\rho^{(3)}$ and $H_y^{(3)}$ (Figure 3.1 (b)-(c)) show a very good concordance between the numerical representation and the two approximations. As for the field $H_z^{(3)}$ (Figure 3.1 (a)), we have that the approximations are rather good for small offsets but not so much for greater offsets. Finally, Figure 3.1 (d) shows a bad concordance between the numerical representation of the field $H_x^{(3)}$ and the approximations, especially for increasing offsets.

Chapter 4

The inverse problem

4.1 Mathematical formulation

In this final chapter we deal with the inverse problem of computing the model parameters (i.e., conductivity and thickness of the layers) from a set of measured field values at different offsets, in the case of a homogeneous layered earth. Specifically, we consider the electromagnetic response of the DUALEM (DUAL-geometry Electro-Magnetic) system placed at the surface of the earth. For this instrument the dipole geometry consists of a transmitter loop (T) and many dual receiver loops (Rz, Rρ) that are horizontal co-planar (HCP configuration) and perpendicular (PRP configuration). Figure 4.1 represents an example of dual-coil configuration inside the DUALEM, where the offset is 2 m and 2.1 m between T and the first couple of receivers Rz, Rρ, respectively. Other couples of receivers are located at 4, 6 and 8 m offset. In this setting, the theoretical components of the magnetic field at the receiver location on the surface are given by (cf. (2.29) and (2.30) with $H = 0$)

$$H_z^{(N)} = \frac{m}{4\pi} \int_0^\infty (1 + R_0)\lambda^2 J_0(\lambda r) d\lambda, \tag{4.1}$$

$$H_\rho^{(N)} = \frac{m}{4\pi} \int_0^\infty (1 - R_0)\lambda^2 J_1(\lambda r) d\lambda. \tag{4.2}$$

In this case, it is possible to generalize the inversion procedure for $H \neq 0$, by extending the results of Section 3.1 and 2.2. Alternatively, one can consider an air layer, with conductivity almost zero, that separates the DUALEM from the ground and work with $H = 0$. We remark that usually, in practice, the DUALEM system is $40 \div 50$ cm above the surface of the earth. However, the instrument can also be placed directly on the ground to take repeated measurements. So it is not restrictive to consider the case $H = 0$.

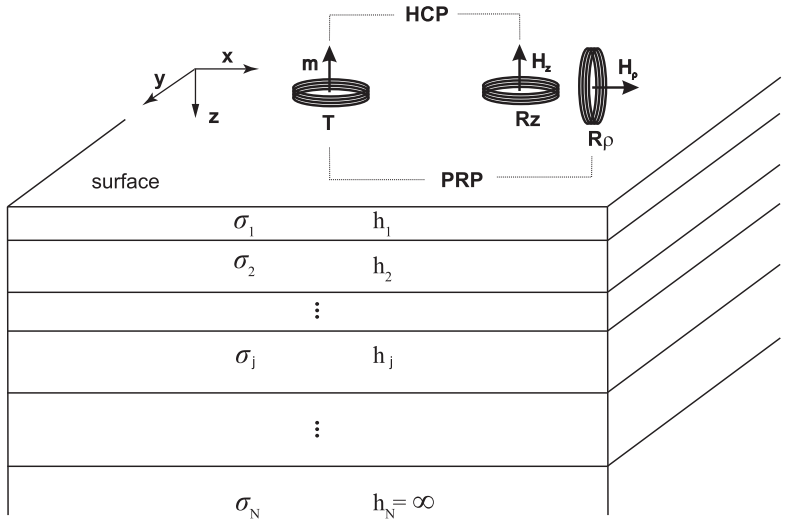

Figure 4.1: Layered underground conductivity model and dual-coil configuration inside the DUALEM instrument.

Now, let $p = (\sigma_1, ..., \sigma_N, h_1, ..., h_{N-1}) \in \mathbb{R}^{2N-1}$ be the vector of underground parameters. The components of the magnetic field at the surface are functions of these parameters and the offset r, thus $H_z^{(N)} = H_z^{(N)}(p, r)$ and $H_\rho^{(N)} = H_\rho^{(N)}(p, r)$. Given a vector of observations $d = (d_{z,1}, ..., d_{z,k}, d_{\rho,1}, ..., d_{\rho,k})^T$, corresponding to distances $r_1, ..., r_k$ $(2k > 2N - 1)$, the inverse problem can be formulated as

$$\min_p \sum_{i=1}^{k} \left\{ \left[\Im(H_z^{(N)}(p, r_i)) - d_{z,i} \right]^2 + \left[\Im(H_\rho^{(N)}(p, r_i)) - d_{\rho,i} \right]^2 \right\}. \tag{4.3}$$

We remark that other kinds of minimization are of course possible, that is, by using a different norm, and possibly a regularization term may be included to reduce the effect of noise on the measurements. By defining $\mathcal{H} : \mathbb{R}^{2N-1} \to \mathbb{R}^{2k}$ as

$$\mathcal{H}(p) = \left(\Im(H_z^{(N)}(p, r_1)), ..., \Im(H_z^{(N)}(p, r_k)), \Im(H_\rho^{(N)}(p, r_1)), ..., \Im(H_\rho^{(N)}(p, r_k)) \right)^T, \tag{4.4}$$

problem (4.3) can be rewritten in the compact form

$$\min_p \left\| \mathcal{H}(p) - d \right\|^2, \tag{4.5}$$

where $\| \cdot \|$ denotes the Euclidean norm.

	$\sigma(S/m)$
Clay	0.2 [8]
Sand/Silt grains	0.01 [8]
Tap water	0.1 [63]
Air	0.0001 [47]

Table 4.1: Material electrical conductivity

4.2 Underground models

Regarding the choice of the underground models for the simulations, we consider a specific application related to the internal composition of river levees, which may collapse due to the condition of the soils that form the embankments. Particularly, the presence of gravel lenses inside the embankment body constitutes a critical factor for the structural levee stability. We assume that the subsoil models are composed by three layers (referring to previous section, $N = 3$), representing a highly porous gravel level embedded in sediments of clay and silty sands. Two (extreme) cases are considered (see Table 4.2): the first case (Models 1 and 3) represents a dry levee (summer conditions) and the second case (Models 2 and 4) represents a wet levee (winter conditions). Moreover, different layer thicknesses are taken into account. The subsoil conductivities are computed with the complex refractive index model (CRIM) and the material properties shown in Table 4.1 and Table 4.2. The CRIM model for a shaly sandstone with negligible permittivity and partially saturated with gas, can be expressed as [51, 7]

$$\sigma = [(1-\phi)(1-C)\sigma_q^\gamma + (1-\phi)C\sigma_c^\gamma + \phi S_w \sigma_w^\gamma + \phi(1-S_w)\sigma_a^\gamma]^{1/\gamma}, \quad (4.6)$$

with $\gamma = 1/2$ and where σ_q, σ_c, σ_w and σ_a are the sand-grain (quartz), clay, water and air conductivities, C is the clay content, ϕ is the porosity and S_w is the water saturation. If γ is a free parameter, the equation is termed Lichtnecker-Rother formula. It is based on the ray approximation. The travel time in each medium is inversely proportional to the electromagnetic velocity, which in turn is inversely proportional to the square root of the complex dielectric constant. At low frequencies, displacement currents can be neglected and equation (4.6) is obtained. For zero clay content, and neglecting σ_q and σ_c, equation (4.6) is exactly Archie's law [32]. The computed values in Table 4.2 represent typical conductivities of shallow sediments, frequently measured on river embankments (e.g., [68, 17]).

Medium	Layer	C (%)	ϕ (%)	S_w (%)	σ (mS/m)	h (m)	Lithology
Model 1	1	50	20	3	50.0	2.5	Dry silt and clay
	2	1	37	1	4.9	0.5	Dry gravel lens
	3	25	30	2	18.2		Dry sand/silt and clay
Model 2	1	50	20	92	76.9	2.5	Wet silt and clay
	2	1	37	98	32.3	0.5	Wet gravel lens
	3	25	30	98	50.0		Wet sand/silt and clay
Model 3	1	50	20	3	50.0	3.0	Dry silt and clay
	2	1	37	1	4.9	2.0	Dry gravel lens
	3	25	30	2	18.2		Dry sand/silt and clay
Model 4	1	50	20	92	76.9	3.0	Wet silt and clay
	2	1	37	98	32.3	2.0	Wet gravel lens
	3	25	30	98	50.0		Wet sand/silt and clay

Table 4.2: Petrophysical properties of the river levees models used in the numerical forward simulations.

4.3 The BFGS approach

Due to the complexity of the function $\mathcal{H}(p)$ (see (4.4)), whose computation requires the evaluation of integrals, it is necessary to employ a derivative free minimization algorithm based, for example, on a BFGS (Broyden-Fletcher-Goldfarb-Shanno) line-search method ([6, 16, 26, 53]). In particular, starting from an initial guess $p_0 \in \mathbb{R}^{2N-1}$ and letting $f(p) = \|\mathcal{H}(p) - d\|^2$, the method is defined by the iteration

$$p_{j+1} = p_j - \lambda_j A_j^{-1} \nabla f(p_j), \tag{4.7}$$

where A_j is a symmetric positive definite approximation of the Hessian matrix of f at p_j, given by the BFGS update

$$A_{j+1} = A_j + \frac{y_j y_j^T}{y_j s_j} - \frac{A_j s_j s_j^T A_j}{s_j^T A_j s_j}, \tag{4.8}$$

with $s_j = p_{j+1} - p_j$, $y_j = \nabla f(p_{j+1}) - \nabla f(p_j)$ and A_0 a generic approximation of the Hessian matrix at the initial guess. Moreover, the parameters $\lambda_j > 0$ in (4.7) represent the steps and are chosen to satisfy the Armijo-Goldstein conditions [3, 27]

$$f(p_{j+1}) \leq f(p_j) + \alpha \nabla f(p_j)^T (p_{j+1} - p_j), \tag{4.9}$$

$$\nabla f(p_{j+1})^T (p_{j+1} - p_j) \geq \beta \nabla f(p_j)^T (p_{j+1} - p_j), \tag{4.10}$$

for some $\alpha \in (0, 1)$ and $\beta \in (\alpha, 1)$ suitable chosen. The above conditions prevent the use of steps too large or too small. Specifically, the term line search refers to any procedure for selecting λ_j. In practice, (4.10) generally is not necessary if a backtracking strategy, described by the following algorithm, is used.

Algorithm 2 (Backtracking line search) *Given $\alpha \in (0, 1)$, $0 < l < u < 1$,*

1. *set $\lambda_j = 1$,*
2. *while (4.9) does not hold, set $\lambda_j = \rho \lambda_j$, for some $\rho \in [l, u]$,*
3. *calculate p_{j+1} as in (4.7).*

Since the line search is included, Algorithm 2 is proven to be globally convergent if it is applied to a strictly convex function (see e.g., [14, Theorem 9.5.1]). However, the method is very demanding in terms of computational resources and elaboration time. In order to overcome this issue, by using the

approximations given in the previous chapter (see Section 3.1), we present below a more efficient algorithm to solve (4.5) for the underground models of Section 4.2, in which $N = 3$.

Let $p = (\sigma_1, \sigma_2, \sigma_3, h_1, h_2) \in \mathbb{R}^5$ be the vector of the underground parameters and consider the fields $H_z^{(3)} = H_z$ and $H_\rho^{(3)} = H_\rho$, defined by equations (4.1) and (4.2). From the previous chapter, $\Im(H_z)$ and $\Im(H_\rho)$ can be approximated using equations (3.9) and (3.10) at different offsets $r_1, \ldots, r_k$. We indicate these approximations as L_z and L_ρ.

Suppose the underground model to be characterized by the parameters vector $p^\star = (\sigma_1^\star, \sigma_2^\star, \sigma_3^\star, h_1^\star, h_2^\star) \in \mathbb{R}^5$. The observations vector d is computed using integral formulations (2.53) and (2.54), being numerical simulations the best representation of realistic EM surveys. Given an initial guess p_0 of $p^\star$, we search for a certain $\bar{p} \in \mathbb{R}^5$ such that

$$\bar{p} = (\bar{\sigma}_1, \bar{\sigma}_2, \bar{\sigma}_3, \bar{h}_1, \bar{h}_2) = \arg\min_p \left\| \bar{\mathcal{H}}(p) - d \right\|^2, \tag{4.11}$$

where $\bar{\mathcal{H}} : \mathbb{R}^5 \to \mathbb{R}^{2k}$ is defined as

$$\bar{\mathcal{H}}(p) = (L_z(p, r_1)), ..., L_z(p, r_k)), L_\rho(p, r_1)), ..., L_\rho(p, r_k)))^T.$$

At this point we use $\bar{p}$ as initial guess for a second minimization procedure with integral formulations (2.53) and (2.54) instead of analytical approximations (3.9) and (3.10). Therefore, we look for $\hat{p} \in \mathbb{R}^5$ such that

$$\hat{p} = (\hat{\sigma}_1, \hat{\sigma}_2, \hat{\sigma}_3, \hat{h}_1, \hat{h}_2) = \arg\min_p \left\| \mathcal{H}(p) - d \right\|^2, \tag{4.12}$$

where $\mathcal{H} : \mathbb{R}^5 \to \mathbb{R}^{2k}$ is defined by (4.4). Finally, the approximate solution of the inverse problem is given by the vector $\hat{p} \in \mathbb{R}^5$.

The above procedure can be summarized by the following algorithm.

Algorithm 3 *Given $p_0 \in \mathbb{R}^5$ and $d \in \mathbb{R}^{2k}$, using the BFGS iteration (4.7)*

1. *solve problem (4.11) to find $\bar{p}$,*

2. *solve problem (4.12), with $\bar{p}$ as initial guess, to find $\hat{p}$.*

Since $\bar{\mathcal{H}}(p) \approx \mathcal{H}(p)$ is a quite good approximation (see the examples in the previous chapter), the double step minimization allows to considerably reduce the computational cost because $\bar{\mathcal{H}}$ does not require the evaluation of integrals.

4.3.1 Numerical examples

To solve minimization problems (4.11) and (4.12), we use the quasi-Newton method BFGS together with the line search technique explained by Algorithm 2, with step tolerance and termination tolerance in the order of the machine precision. As initial guess A_0 in (4.8) we take the identity matrix and empirically set $\alpha = 0.01$, $\rho = 0.9$ as parameters of the line search in Algorithm 2. Moreover, the gradient ∇f (cf. (4.7)) is calculated by partial derivatives using a numerical differentiation method via finite differences. We apply Algorithm 3 to the observations vector d, obtained from the models defined in Table 4.2, and calculate the relative percentage error between the approximate solution $\hat{p}$ and the real underground model parameters $p^\star$. The examples aim to simulate an EM acquisition on river levees using the DUALEM system (https://dualem.com), for which the offsets are $r_1 = 2\ m$, $r_2 = 4\ m$, $r_3 = 6\ m$ and $r_4 = 8\ m$, and the frequency is about $f = 10\ kHz$. The observation data vector $d \in \mathbb{R}^8$ is generated by

$$d = \mathcal{H}(p^\star) + \eta,$$

where η is a random white noise vector such that the Noise-to-Signal Ratio (NSR) is $\epsilon = \frac{\|\eta\|}{\|d\|}$. We first consider a noise free example (i.e., $\epsilon = 0$) and then two values of percentage NSR, $\epsilon = 0.1\%, 0.5\%$. These values are compatible with the results of laboratory test, showing that environmental RMS noise levels, in terms of apparent conductivity measurements at 8 m offset, are typically less than 1 mS/m (see https://dualem.com). The solution errors are averaged over 20 simulations for each model, in order to have an estimate of the parameters expectation values. The results of the simulations are shown in Tables 4.3-4.4-4.5, where we report the mean relative error over 20 experiments for each model in order to reduce the random dependence on the data. The optimization solver always converges for all the simulations and the errors are mainly due to the presence of a large number of local minima in the objective function. The simulations without random noise (Table 4.3) show the best results, with the maximum average error around 5 %. Then, as expected, the errors increase with increasing NSR, reaching an average maximum error of $\approx 35\%$ for $NSR = 0.5$ (Table 4.5). The conductivity and thickness of the intermediate layer are affected by the larger errors. Moreover, thinner layers show larger errors.

4.4 The Gauss-Newton approach

The BFGS method is known to be very sensitive to the choice of the initial guess A_0 in (4.8) (see [14, Theorem 9.5.1]). In order to overcome this issue,

	Mean relative error	
	Conductivity (%)	Thickness (%)
Model 1	0.1 5.4 0.1	0.0 5.4
Model 2	0.1 2.0 0.1	0.2 1.1
Model 3	0.7 53.0 1.8	1.0 23.8
Model 4	0.0 1.7 0.5	0.3 6.2
Average error	5.4	4.75

Table 4.3: Results of the EM inversions using the BFGS method. The NSR is $\epsilon = 0$.

	Mean relative error	
	Conductivity (%)	Thickness (%)
Model 1	16.3 24.2 9.2	11.2 5.5
Model 2	8.3 7.6 2.6	9.5 14.8
Model 3	9.4 15.2 3.4	7.5 21.0
Model 4	5.2 1.8 6.2	4.0 7.0
Average error	9.12	10.0

Table 4.4: Results of the EM inversions using the BFGS method. The NSR is $\epsilon = 0.1\%$.

	Mean relative error	
	Conductivity (%)	Thickness (%)
Model 1	21.0 35.2 12.6	16.2 4.5
Model 2	11.0 21.5 4.5	13.2 20.7
Model 3	16.7 29.1 4.8	12.3 19.2
Model 4	15.7 13.7 18.4	11.6 8.5
Average error	17.02	13.28

Table 4.5: Results of the EM inversions using the BFGS method. The NSR is $\epsilon = 0.5\%$

we consider a second minimization strategy based on the observation that (4.5) is actually a nonlinear least-squares problem.

As before, let $p = (\sigma_1, \dots, \sigma_N, h_1, \dots, h_{N-1}) \in \mathbb{R}^{2N-1}$ be the vector of underground parameters, $H_z^{(N)}(p, r)$, $H_\rho^{(N)}(p, r)$ the components of the magnetic field at the surface and $d = (d_{z,1}, \dots, d_{z,k}, d_{\rho,1}, \dots, d_{\rho,k})^T$ a vector of observations. Then, given the residual function $R\colon \mathbb{R}^{2N-1} \to \mathbb{R}^{2k}$ defined by

$$R(p) = \mathcal{H}(p) - d, \tag{4.13}$$

with $\mathcal{H}(p)$ as in (4.4), we consider the nonlinear least-squares problem, equivalent to the one in (4.5),

$$\min_p \mathcal{R}(p) = \min_p \frac{1}{2} R(p)^T R(p) = \frac{1}{2} \sum_{i=1}^{2k} R_i(p)^2, \tag{4.14}$$

where $R_i(p)$ denotes the i-th component of $R(p)$. In order to solve (4.14), we employ the Gauss-Newton method with line search, whose generic iteration is defined as

$$p_{j+1} = p_j - \lambda_j (J(p_j)^T J(p_j))^{-1} J(p_j)^T R(p_j), \tag{4.15}$$

in which λ_j is selected by the backtracking procedure (steps 1-2 of Algorithm 2) and $J(p) \in \mathbb{R}^{(2N-1)\times 2j}$ is the Jacobian matrix relative to R. The above method, commonly named damped Gauss-Newton algorithm, is usually globally convergent but may be very slow. Moreover, it is not well defined if $J(p_j)$ does not have full column rank. We refer to [14, Chapter 10] for more details.

Before going on, we observe that the experiments presented in Section 4.3.1 strongly depend on the initial guess p_0 (see also Algorithm 3). In order to avoid this empirical choice, we decide to solve problem (4.14), for the underground models described in Section 4.2, starting from a grid of values of p_0.

As before, let $p = (\sigma_1, \sigma_2, \sigma_3, h_1, h_2) \in \mathbb{R}^5$ and $p^\star = (\sigma_1^\star, \sigma_2^\star, \sigma_3^\star, h_1^\star, h_2^\star) \in \mathbb{R}^5$ be the vector of the underground parameters and the real subsoil model, respectively. Moreover, consider the fields $H_z^{(3)} = H_z$ and $H_\rho^{(3)} = H_\rho$ and a noise free observation data vector d, computed by using integral formulations (2.53) and (2.54). Then, we search for $\bar{p} \in \mathbb{R}^5$ such that

$$\bar{p} = \left(\bar{\sigma}_1, \bar{\sigma}_2, \bar{\sigma}_3, \bar{h}_1, \bar{h}_2\right) = \arg\min_p \frac{1}{2} R(p)^T R(p), \tag{4.16}$$

where R is defined in (4.13). At this point, for each parameter (i.e., the components of the vector p) we consider a grid tabulation. Particularly,

we set a minimum and a maximum value $\sigma_{\min}, \sigma_{\max}$ and $h_{\min}, h_{\max}$ for conductivities and thicknesses, respectively, and then, for each of the five parameters, we generate a vector of M linearly spaced points between these values. In this way, we obtain M^5 possible combinations of initial models $\left\{p_0^{(i)}\right\}_{i=1,\dots,M^5}$. Then, we employ each $p_0^{(i)}$ as initial guess for method (4.15) and call $\left\{\tilde{p}^{(i)}\right\}_{i=1,\dots,M^5}$ the set of results of the minimization procedures. Finally, we find the approximate solution $\bar{p}$ by solving the problem

$$\min_{\tilde{p}^{(i)} \in \left\{\tilde{p}^{(i)}\right\}_{i=1,\dots,M^5}} \frac{1}{2} R\left(\tilde{p}^{(i)}\right)^T R\left(\tilde{p}^{(i)}\right). \tag{4.17}$$

The above strategy is summarized in the following algorithm.

Algorithm 4 *Given $\sigma_{min}, \sigma_{max}, h_{min}, h_{max}, M, d \in \mathbb{R}^{2k}$,*

1. *tabulate the parameters $\sigma_1, \sigma_2, \sigma_3, h_1, h_2$ and generate the set $\left\{p_0^{(i)}\right\}_{i=1,\dots,M^5}$ of possible initial models,*
2. *for each $p_0^{(i)}$, solve problem (4.16) to find the set $\left\{\tilde{p}^{(i)}\right\}_{i=1,\dots,M^5}$,*
3. *find $\bar{p}$ by solving (4.17).*

4.5 Numerical experiments

In order to solve minimization problem (4.16), we implement the damped Gauss-Newton method (4.15), with $\alpha = 0.01$ and $\rho = 0.5$ as parameters of the line search (see Algorithm 2). The Jacobian matrix is numerically evaluated via finite differences and $d = \mathcal{H}(p^\star)$ is the noise free observation data vector. As in Section 4.3.1, the examples aim to simulate the DUALEM system, hence $d \in \mathbb{R}^8$. Moreover, the procedure stops if a given tolerance on the residual $\|R(p) - d\|$ (in the order of $1e-6$) or a maximum number of iterations (50) is achieved. Then, we apply Algorithm 4, with $\sigma_{\min} = 2$ mS/m, $\sigma_{\max} = 85$ mS/m, $h_{\min} = 0.04$ m, $h_{\max} = 4$ m and $M = 7$, to the observations vector d, obtained from the models defined in Table 4.2, and calculate the relative percentage error between the approximate solution $\bar{p}$ and the real underground model parameters $p^\star$. We notice that, respect to the previous experiments in which there was a single inversion to perform (see Section 4.3.1), this time we deal with $7^5 = 16807$ inversion procedures. Therefore, in this case, the employment of a virtual machine equipped with

	Relative error	
	Conductivity (%)	Thickness (%)
Model 1	$2.7e-11$ $7.5e-6$ $4.6e-9$	$6.8e-8$ $2.0e-6$
Model 2	$1.2e-9$ $2.8e-5$ $5.7e-8$	$1.7e-6$ $4.0e-5$
Model 3	$1.2e-10$ $6.7e-8$ $1.7e-8$	$1.6e-9$ $8.8e-8$
Model 4	$6.0e-12$ $1.0e-6$ $2.0e-7$	$1.3e-7$ $2.7e-6$
Average error	$3.0e-6$	$5.8e-6$

Table 4.6: Results of the noise free EM inversions using the damped Gauss-Newton method.

the NVIDIA A100 Tensor Core GPU is fundamental to accelerate the computational performance. By using this resource, the average running time of Algorithm 4 is less than 30 minutes.

The results of the simulations are shown in Table 4.6 and confirm the reliability of Algorithm 4. In fact the average errors of the models considered are in the order of 10^{-6} and the value of the objective function $\mathcal{R}(p)$ at the solution is less than 10^{-30}.

At this point, we want to add noise to the simulations, but, this time we can not look for $\bar{p}$ by solving problem (4.17). Hence, we should modify the inversion procedure. Before going on, some further observations are necessary.

First of all, we notice that $\mathcal{R}(p)$ is characterized by the presence of many local minima, even in the noise free case. This behavior is confirmed by the histograms plots of the results of the inversions. Specifically, given the set $\left\{\tilde{p}^{(i)}\right\}_{i=1,\dots,M^5}$, we consider the histogram in frequency of each underground parameter. An example, relative to Model 2 (cf. Table 4.2) and $M = 3$, is

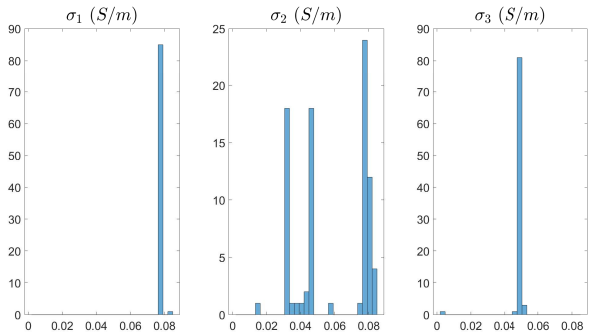

(a)

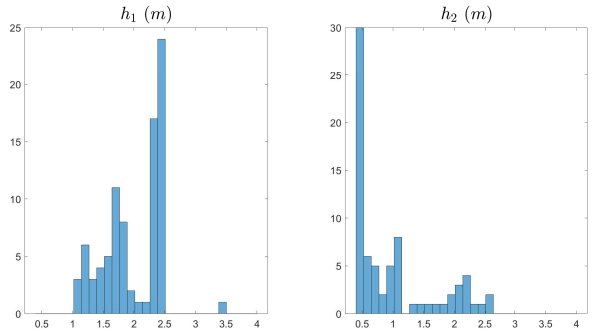

(b)

Figure 4.2: Histogram plots of the frequency distribution of conductivities (a) and thicknesses (b), in the case of Model 2.

provided in Figure 4.2, where we can see the presence of more than one peak of frequency, corresponding to a local minimum. Nevertheless, we notice that for some parameters, e.g. σ_1, σ_3 and h_1, there is only one clear distribution of values around the exact solution.

Hence, to have a clear view of the behavior of the objective function, we set $\sigma_1 = \sigma_1^\star, \sigma_3 = \sigma_3^\star, h_1 = h_1^\star$ and then plot $\mathcal{R}(p)$ with respect to σ_2 and h_2. An example, still in the case of Model 2, is shown in Figure 4.3. In particular, we can identify the presence of a global minimum of the objective function (inside the red rectangle), provided by a pair of underground parameters σ_2, h_2 that corresponds to the exact solution.

After these considerations, the idea is to follow the first two steps of Algorithm 4, with d affected by a certain noise, then analyze the histograms, fix in some way the values of σ_1, σ_3, h_1 and finally study the plot of the objective function to determine a confidence zone of the remaining parameters σ_2, h_2. As for the solution of problem (4.16), we still employ the damped Gauss-Newton method but with the addition of a regularization parameter

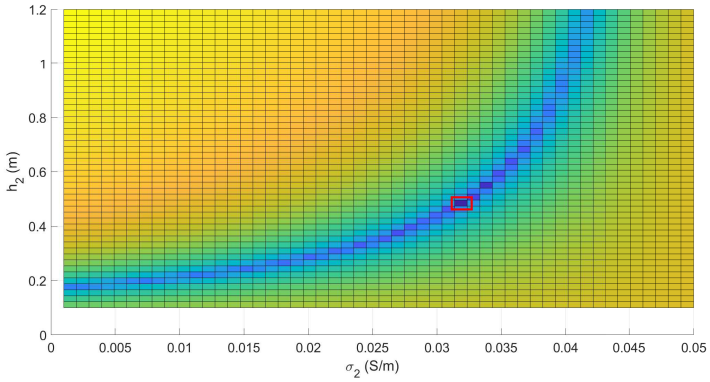

Figure 4.3: The objective function $\mathcal{R}(p)$, with respect to σ_2 and h_2, in the case of Model 2.

$\ell > 0$, that is (cf. (4.15)),

$$p_{j+1} = p_j - \lambda_j (J(p_j)^T J(p_j) - \ell^2 I_j)^{-1} J(p_j)^T R(p_j), \tag{4.18}$$

where $I_j \in \mathbb{R}^{2j \times 2j}$ is the identity matrix. This strategy is summarized by the following algorithm.

Algorithm 5 *Given $\sigma_{min}, \sigma_{max}, h_{min}, h_{max}, M, d \in \mathbb{R}^{2k}$,*

1. *tabulate the parameters $\sigma_1, \sigma_2, \sigma_3, h_1, h_2$ and generate the set $\left\{p_0^{(i)}\right\}_{i=1,\dots,M^5}$ of possible initial models,*
2. *for each $p_0^{(i)}$, solve problem (4.16) to find the set $\left\{\tilde{p}^{(i)}\right\}_{i=1,\dots,M^5}$,*
3. *retrieve the parameters σ_1, σ_3, h_1 from the histogram plots,*
4. *plot the objective function $\mathcal{R}(p)$, with respect to σ_2 and h_2, and look for its minimum.*

To solve problem (4.16) in presence of noise, we apply Algorithm 5 to the models described in Table 4.2. The parameters of the line search, the stopping criteria and the values of $\sigma_{\min}, \sigma_{\max}, h_{\min}, h_{\max}$ and M are the same of the noise free experiments. As for the regularization parameter in (4.18), we empirically take $\ell = 1e-6$, while the observation vector is obtained as in Section 4.3.1 with NSR $\epsilon = 0.1\%$. In Figure 4.4 we report the histogram plots, relative to Model 3, that we obtained after the inversion procedures. We notice that we can deduce only the values of σ_1, σ_3, h_1 (see Table 4.7). Specifically, for each of these parameters, we consider the bin with highest

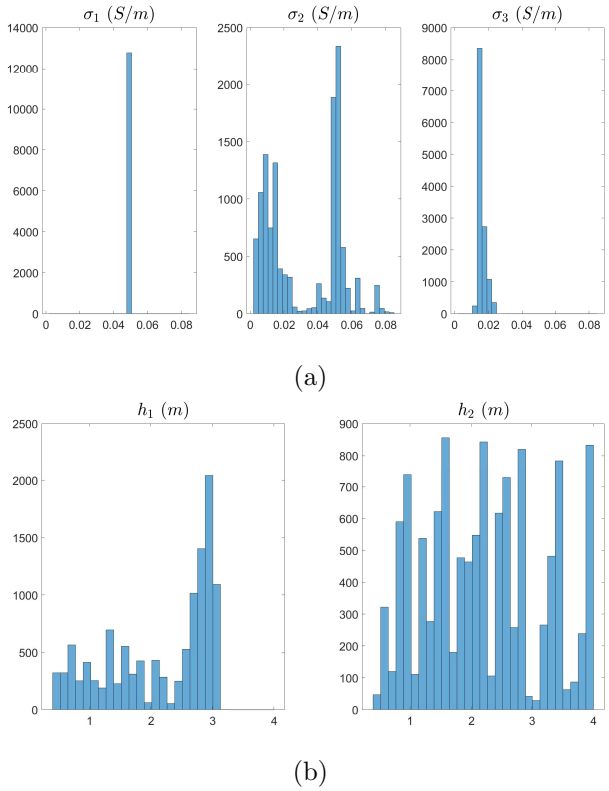

Figure 4.4: Histogram plots of the frequency distribution of conducivities (a) and thicknesses (b), in the case of Model 3, with NSR $\epsilon = 0.1\%$.

	Retrieved values		
	σ_1 (mS/m)	σ_3 (mS/m)	h_1 (m)
Model 1	49	18.1	2.46
Model 2	76.8	49	2.4
Model 3	49.5	17.9	3.02
Model 4	76.9	49.5	3.03

Table 4.7: Retrieved values of the parameters σ_1, σ_3, h_1 after the inversions.

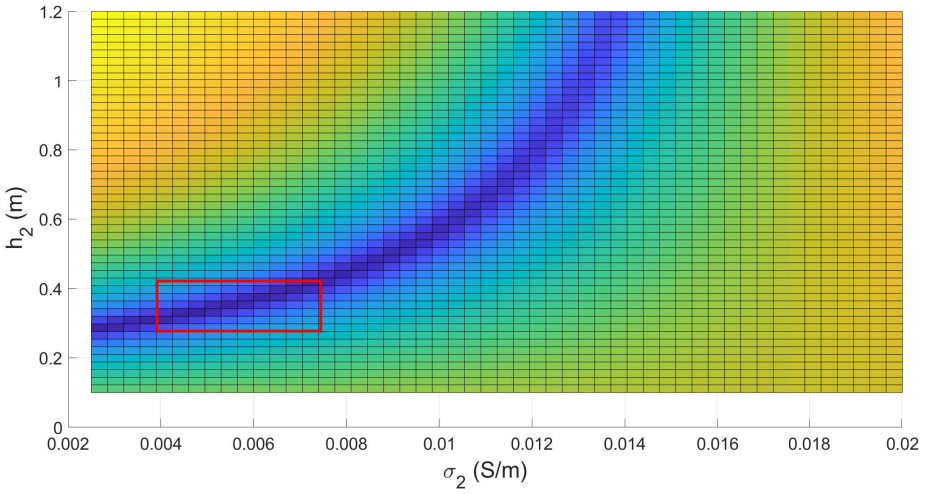

Figure 4.5: The objective function $\mathcal{R}(p)$, with respect to σ_2, h_2, in the case of Model 1.

frequency and take the average of the values inside the bin. At this point, we fix these values and plot the objective function $\mathcal{R}(p)$ with respect to σ_2, h_2. The results are shown in Figure 4.5-4.6-4.7-4.8. We observe that, unlike the noise free example (Figure 4.3), in this case we can only identify a confidence zone (the red rectangle in Figure 4.5-4.7-4.8) around the exact solution, corresponding to the area in which the objective function assumes the lowest values. Particularly, for Model 2 (Figure 4.6) it is not even possible to locate the confidence region, but only a curve of possible solutions. Furthermore, thinner layers show larger errors. In conclusion, Figures 4.5-4.6-4.7-4.8 reveal the ill-conditioning of the inverse problem respect to the parameters σ_2, h_2.

Finally, we point out that, for the detection of the confidence zone of the exact solution, some imaging techniques can be introduced as well.

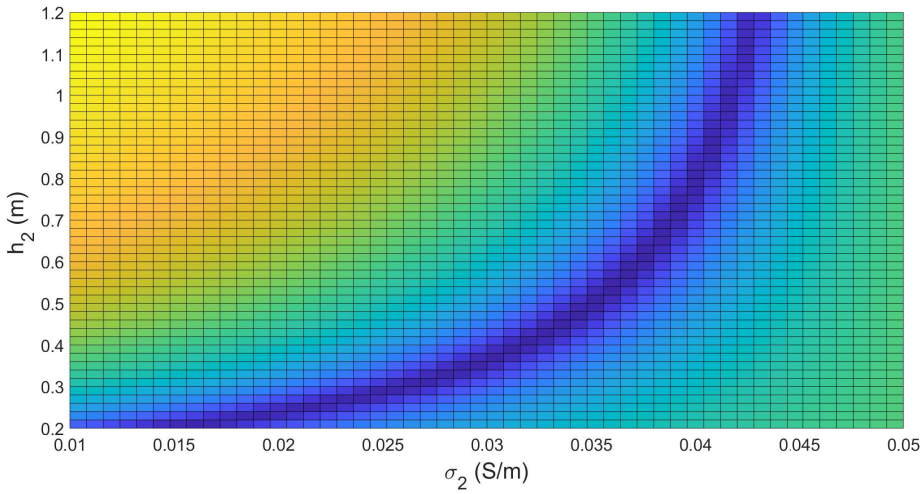

Figure 4.6: The objective function $\mathcal{R}(p)$, with respect to σ_2, h_2, in the case of Model 2.

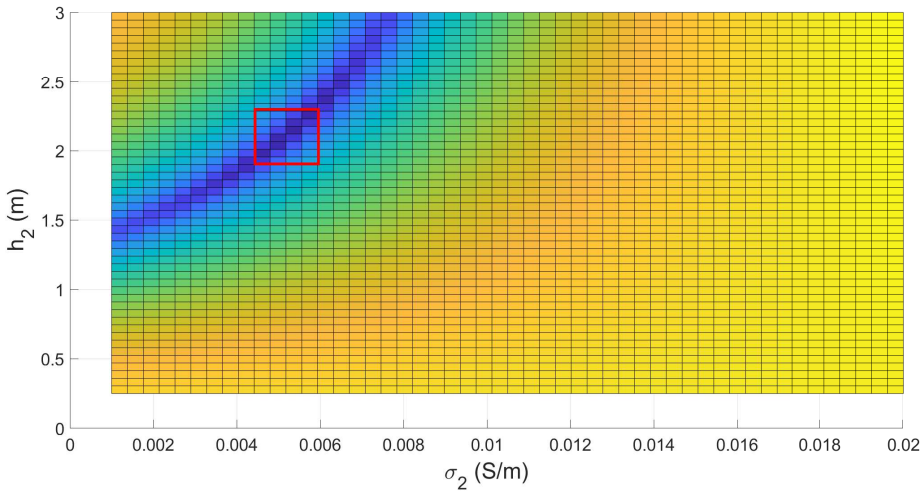

Figure 4.7: The objective function $\mathcal{R}(p)$, with respect to σ_2, h_2, in the case of Model 3.

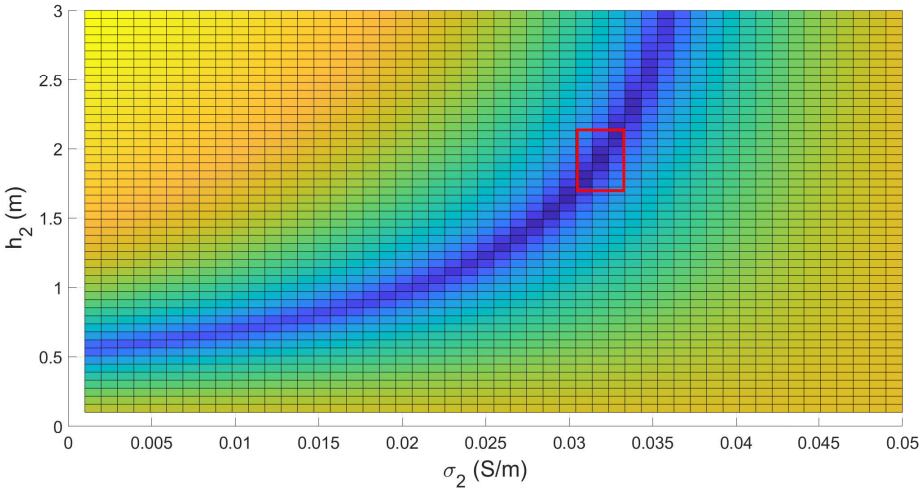

Figure 4.8: The objective function $\mathcal{R}(p)$, with respect to σ_2, h_2, in the case of Model 4.

Conclusions

In this thesis we have studied the numerical and analytical estimation of the electromagnetic fields in a stratified medium, together with the inverse problem of retrieving the underground parameters from a set of recorded measurements taken at the surface.

For the forward problem, that is, the computation of the integrals involved in the solution of the Maxwell equations, we have presented two novel methodologies. The first one is based on the splitting of the reflection term and on the application of the Gauss-Kronrod technique. The second approach consists in the derivation and application of a Gaussian quadrature formula for weight functions involving fractional powers, exponentials and Bessel functions of the first kind. For the computation of the coefficients of the three-term recurrence relation for the corresponding orthogonal polynomials, we have developed an alternative and very stable approach, based on the preconditioning of the moment matrix. In particular, we have presented an algorithm which exploits the Cramer rule to compute the coefficients by solving a linear system with the moment matrix and that allows to work with further $40 \div 60$ points, depending on the parameters, with respect to the techniques commonly employed (i.e., the standard and modified Chebyshev algorithm). Moreover, in order to work with even more points, we have adopted the symbolic computation and variable-precision arithmetic. We have estimated the validity of both approaches for the computation of the components of the EM field and the results are in good agreement with those of the commonly used digital filtering methods. On the other hand, the approach based on the splitting of the reflection term has also allowed the derivation of general analytical approximations of the integral formulations of the EM fields, that can be employed to speed up the solution of the inverse problem and are only based on mathematical considerations without further hypotheses on the ground's physical properties.

As for the solution of the inverse problem, in the first approach we have considered the specific electromagnetic response of the DUALEM system placed at the surface of the earth, in which the receiver couples are placed

at $2, 4, 6$ and 8 m from the transmitter coil, and typical source-receiver geometries are the HCP and PRP configurations. We have introduced two minimization procedures: the first one, enhanced by the analytical approximations, is based on a line-search BFGS method. For the second approach we have employed the damped Gauss-Newton method. Moreover, we have developed an optimization strategy that allows to avoid the dependence on the initial guess of the iterative procedure. In this setting, the use of the NVIDIA A 100 Tensor Core GPU have been proved to be crucial in accelerating the minimization algorithm. We have carried out numerical simulations to study the integrity of river levees,an important environmental problem in Italy, due to the high hydrological risks. Our results confirmed the reliability of the techniques and pointed out a possible application also to real data.

Appendix A

Vector calculus

Because of the number of vectors operations used in electromagnetic boundary valued problems, we give a quick reference to definitions and expressions for several operators, both in Cartesian and cylindrical coordinates.

First of all, we denote by $\mathbf{x} = (x, y, z)$ the three dimensions Cartesian coordinate system with euclidean metric and by $\mathbf{u}_x = (1, 0, 0)$, $\mathbf{u}_y = (0, 1, 0)$ and $\mathbf{u}_z = (0, 0, 1)$ the unit vectors in the x, y and z directions, respectively. Then, given a scalar-valued function ψ and a vector function $\mathbf{A}$, we have the following definitions.

Definition 1 *Let $\psi\colon \mathbb{R}^3 \to \mathbb{R}$ be a twice-differentiable function. Then, the gradient $\nabla\psi\colon \mathbb{R}^3 \to \mathbb{R}^3$ and the Laplacian $\nabla^2\psi\colon \mathbb{R}^3 \to \mathbb{R}$ are respectively defined by*

$$\nabla\psi = \frac{\partial\psi}{\partial x}\mathbf{u}_x + \frac{\partial\psi}{\partial y}\mathbf{u}_y + \frac{\partial\psi}{\partial z}\mathbf{u}_z \tag{A.1}$$

and

$$\nabla^2\psi = \frac{\partial^2\psi}{\partial x^2} + \frac{\partial^2\psi}{\partial y^2} + \frac{\partial^2\psi}{\partial z^2}. \tag{A.2}$$

Definition 2 *Let $\mathbf{A} = (A_x, A_y, A_z)\colon \mathbb{R}^3 \to \mathbb{R}^3$ be a continuously differentiable function. Then, the divergence $\nabla \cdot \mathbf{A}\colon \mathbb{R}^3 \to \mathbb{R}^3$ and the curl $\nabla \times \mathbf{A}\colon \mathbb{R}^3 \to \mathbb{R}^3$ are respectively defined as*

$$\nabla \cdot \mathbf{A} = \frac{\partial A_x}{\partial x} + \frac{\partial A_y}{\partial y} + \frac{\partial A_z}{\partial z} \tag{A.3}$$

and

$$\nabla \times \mathbf{A} = \left(\frac{\partial A_z}{\partial y} - \frac{\partial A_y}{\partial z}\right)\mathbf{u}_x + \left(\frac{\partial A_x}{\partial z} - \frac{\partial A_z}{\partial x}\right)\mathbf{u}_y + \left(\frac{\partial A_z}{\partial x} - \frac{\partial A_x}{\partial y}\right)\mathbf{u}_z. \tag{A.4}$$

Moreover, the divergence of the curl of any vector vanishes identically, that is,

$$\nabla \cdot (\nabla \times \mathbf{A}) = 0. \tag{A.5}$$

and the following vector identities hold:

$$\nabla \times \nabla \times \mathbf{A} = \nabla(\nabla \cdot \mathbf{A}) - \nabla^2 \mathbf{A}, \tag{A.6}$$

$$\nabla^2(\nabla \cdot \mathbf{A}) = \nabla \cdot (\nabla^2 \mathbf{A}). \tag{A.7}$$

Now, let (ρ, ϕ, z) be a cylindrical polar system such that its reference plane is the Cartesian xy-plane and the cylindrical axis is the Cartesian z-axis. In this setting, the conversion between cylindrical and Cartesian coordinates is

$$\begin{aligned} x &= \rho \cos\phi, \\ y &= \rho \sin\phi, \\ z &= z. \end{aligned}$$

Moreover, if $\mathbf{u}_\rho$, $\mathbf{u}_\phi$ and $\mathbf{u}_z$ are the unit vectors in the ρ, ϕ and z-directions, expressions (A.1), (A.2), (A.3) and (A.4) become

$$\begin{aligned} \nabla\psi &= \frac{\partial\psi}{\partial\rho}\mathbf{u}_\rho + \frac{1}{\rho}\frac{\partial\psi}{\partial\phi}\mathbf{u}_\phi + \frac{\partial\psi}{\partial z}\mathbf{u}_z, \\ \nabla^2\psi &= \frac{1}{\rho}\frac{\partial}{\partial\rho}\left(\rho\frac{\partial\psi}{\partial\rho}\right) + \frac{1}{\rho^2}\frac{\partial^2\psi}{\partial\phi^2} + \frac{\partial^2\psi}{\partial z^2}, \\ \nabla\cdot\mathbf{A} &= \frac{1}{\rho}\frac{\partial}{\partial\rho}(\rho A_\rho) + \frac{1}{\rho}\frac{\partial A_\phi}{\partial\phi} + \frac{\partial A_z}{\partial z}, \\ \nabla\times\mathbf{A} &= \frac{1}{\rho}\left[\frac{\partial A_z}{\partial\phi} - \frac{\partial A_\phi}{\partial z}\right]\mathbf{u}_\rho + \left[\frac{\partial A_\rho}{\partial z} - \frac{\partial A_z}{\partial\rho}\right]\mathbf{u}_\phi + \frac{1}{\rho}\left[\frac{\partial}{\partial\rho}(\rho A_\phi) - \frac{\partial A_\phi}{\partial z}\right]\mathbf{u}_\rho. \end{aligned}$$

Appendix B

Fourier transforms

There are several conventions for defining the Fourier transform of an integrable function both in the time and in the space domain. In this work we employ the following ones.

Definition 3 *Given an integrable function $f\colon \mathbb{R} \to \mathbb{C}$, the Fourier transform of f in the frequency domain and its inverse in the time domain are defined respectively by*

$$F(\omega) = \int_{-\infty}^{+\infty} f(t) e^{-i\omega t} dt, \tag{B.1}$$

and

$$f(t) = \frac{1}{2\pi} \int_{-\infty}^{+\infty} F(\omega) e^{i\omega t} d\omega, \tag{B.2}$$

where t is the time and ω is the angular frequency.

Definition 4 *In an Euclidean space of dimension n, for an integrable function $f(\mathbf{x})$ the Fourier transform and its inverse are respectively defined as*

$$\tilde{f}(\xi) = \int_{\mathbb{R}^n} f(\mathbf{x}) e^{-i\mathbf{x}\cdot\xi} d\mathbf{x} \tag{B.3}$$

and

$$f(\mathbf{x}) = \frac{1}{(2\pi)^n} \int_{\mathbb{R}^n} \tilde{f}(\xi) e^{i\mathbf{x}\cdot\xi} d\xi, \tag{B.4}$$

where $\mathbf{x} \cdot \xi$ is the dot product. Moreover, if f is an absolutely continuous differentiable function, the Fourier transform of the m-th derivative $f^{(m)}$ is given by

$$\tilde{f^{(m)}}(\xi) = \left(\frac{i\xi}{2\pi}\right)^m \tilde{f}(\xi).$$

The following theorem states that the Fourier transform translates between convolution and multiplication of functions.

Theorem 1 (Convolution Theorem) *If $f(x)$ and $g(x)$ are integrable functions with Fourier transforms $\tilde{f}(\xi)$ and $\tilde{g}(\xi)$ respectively, then the Fourier transform of the convolution is given by the product of the Fourier transforms, that is, if*

$$h(x) = (f * g)(x) = \int_{-\infty}^{+\infty} f(y)g(x-y)dy,$$

where $*$ denotes the convolution operation, then

$$\tilde{h}(\xi) = \tilde{f}(\xi) \cdot \tilde{g}(\xi).$$

If we deal with a finite sequence of equally spaced samples of a function, we need the following definition.

Definition 5 *The discrete Fourier transform of a sequence of N complex numbers $\{\mathbf{x}\}_{n=0,\ldots,N-1}$ is the sequence $\{\mathbf{X}_k\}_{k=0,\ldots,N-1}$ defined by*

$$\begin{aligned} X_k &= \sum_{n=0}^{N-1} x_n e^{-i\frac{2\pi}{N}kn} \\ &= \sum_{n=0}^{N-1} x_n \left[\cos\left(\frac{2\pi}{N}kn\right) - i\sin\left(\frac{2\pi}{N}kn\right)\right]. \end{aligned} \tag{B.5}$$

Moreover, the inverse discrete Fourier transform is given by

$$\begin{aligned} x_n &= \frac{1}{N}\sum_{k=0}^{N-1} X_k e^{i\frac{2\pi}{N}kn} \\ &= \frac{1}{N}\sum_{k=0}^{N-1} X_k \left[\cos\left(\frac{2\pi}{N}kn\right) + i\sin\left(\frac{2\pi}{N}kn\right)\right]. \end{aligned}$$

Appendix C

Gaussian integration rules

In this section we give a general background of integration rules of Gauss type (see e.g. [10], [24] for a complete and exhaustive discussion of the covered topics).

Consider integrals of the form

$$I(f) = \int_a^b w(x)f(x)dx,$$

where $w(x)$ is assumed to be continuous, non negative and integrable over a finite or infinite interval $[a, b]$. Such a function $w(x)$ is said to be a weight function. The general idea is to approximate $I(f)$ through th n-point quadrature rule

$$I(f) \cong I_n(f) = \sum_{i=1}^{n} w_i f(x_i), \tag{C.1}$$

where x_i and $w_i > 0$ are respectively the nodes and weights. Denoting by Π_m the class of polynomials of degree at most m, we have that the quadrature formula (C.1) has order m if it is exact for all polynomials of class Π_m, that is,

$$I(f) = I_n(f), \quad \forall f \in \Pi_m.$$

The idea of a Gaussian quadrature rule is to properly define x_i and w_i such that (C.1) has order $2n-1$. In this setting we need some preliminary notions and results.

Let

$$L_{2,w} = \left\{ f\colon [0,\infty) \to \mathbb{R} \;\middle|\; \int_a^b f^2(x)w(x)dx < +\infty \right\},$$

and

$$\langle f, g \rangle_w = \int_a^b f(x)g(x)w(x)dx. \tag{C.2}$$

It is known that (C.2) is a scalar product with corresponding norm

$$\|f\|_w = \langle f, f\rangle_w^{\frac{1}{2}},$$

and hence $L_{2,w}$ is a Hilbert space. Moreover, two functions f and g are orthogonal over $[a, b]$, with respect to the weight $w(x)$, if $\langle f, g\rangle_w = 0$. In particular, for a given weight $w(x)$, it is possible to determine a sequence of polynomials $\{\phi_k\}_{k\geq 0}$, $\phi_k \in \Pi_k$, which are orthogonal, that is,

$$\langle \phi_m, \phi_n\rangle_w = 0, \quad \text{for} \quad m \neq n$$

and

$$\langle \phi_m, \phi_n\rangle_w > 0, \quad \text{for} \quad m = n.$$

They are uniquely defined up to the leading coefficient and are called monic if the leading coefficient is equal to 1. The normalization of each $\phi_k(x)$ with respect to $\|\cdot\|_w$ leads to the set of orthonormal polynomials $\{\phi_k^\star\}_{k\geq 0}$, that is

$$\langle \phi_m^\star, \phi_n^\star\rangle_w = \begin{cases} 0 & \text{if} \quad m \neq n \\ 1 & \text{if} \quad m = n \end{cases}.$$

Moreover, the zeros of orthogonal polynomials are real, simple and located in the interior of $[a, b]$. The following theorem defines the nodes and weights of the n-point Gaussian rule.

Theorem 2 *Let $w(x) \geq 0$ be a weight function defined on $[a, b]$ with corresponding orthonormal polynomials $\{\phi_n^\star\}_{n\geq 0}$. Let the zeros of $\phi_n^\star(x)$ be*

$$a < x_1 < x_2 < \ldots < b.$$

Then, positive constants $w_1, \ldots, w_n$ can be found such that

$$\int_a^b w(x)\phi(x)dx = \sum_{k=1}^{n} w_k \phi(x_k), \tag{C.3}$$

whenever $\phi(x)$ is a polynomial of class Π_{2n-1}. The weights w_k have the explicit representation

$$w_k = -\frac{k_{n+1}}{k_n}\frac{1}{\phi_{n+1}^\star(x_k)(\phi^\star)_n'(x_k)},$$

where k_{n+1} and k_n are the leading coefficients of $\phi_{n+1}^\star$ and $\phi_n^\star$, respectively.

When nodes and weights have been determined as in this theorem, we say that the resulting integration rule (C.1) is of Gauss type. We remark that, by (C.3) rule (C.1) is exact for polynomials of class Π_{2n-1}.

C.1 The Gauss-Legendre quadrature rule

In the case of the weight $w(x) = 1$ over $[-1, 1]$, we have the Gauss-Legendre integration rule, that is,

$$\int_{-1}^{1} f(x)dx \cong \sum_{k=1}^{n} w_k f(x_k),$$

where the nodes x_k, $k = 1, \ldots, n$, are the zeros of the Legendre polynomials $P_n(x)$, recursively defined by

$$\begin{aligned} P_0(x) &= 1, \\ P_1(x) &= x, \\ nP_n(x) &= (2n-1)xP_{n-1}(x) - (n-1)P_{n-2}(x), \quad n \geq 2, \end{aligned}$$

and the weights are given by

$$w_k = \frac{2(1-x_k^2)}{[nP_{n-1}(x_k)]^2}, \quad k = 1, \ldots, n.$$

We remark that, for an arbitrary interval $[a, b]$, the nodes and weights can be scaled as follows:

$$\begin{aligned} \tilde{x}_k &= \frac{x_k + 1}{2}(b-a) + a, \\ \tilde{w}_k &= w_k \frac{b-a}{2}. \end{aligned}$$

C.2 The Gauss-Laguerre quadrature rule

An example of Gaussian rule on $[0, +\infty)$ is the Gauss-Laguerre formula given by

$$\int_{0}^{\infty} e^{-x} f(x)dx \cong \sum_{k=1}^{n} w_k f(x_k),$$

for which $w(x) = e^{-x}$. Here the nodes are the zeros of the Laguerre polynomial $L_n(x)$, recursively defined by

$$\begin{aligned} L_0(x) &= 1, \\ L_1(x) &= 1 - x, \\ L_{n+1}(x) &= \frac{(2n+1-x)L_n(x) - nL_{n-1}(x)}{n+1}, \quad n \geq 1, \end{aligned}$$

whereas the weights are given by

$$w_k = \frac{(n!)^2 x_k}{[L_{n+1}(x_k)]^2}.$$

A generalization of the above rule is obtained by considering the weight function $w(x) = x^\alpha e^{-x}$, $\alpha > -1$. This choice leads to the formula

$$\int_0^\infty x^\alpha e^{-x} f(x) dx \cong \sum_{k=1}^{n} w_k f(x_k), \tag{C.4}$$

where x_k are the zeros of the generalized Laguerre polynomial $L_n^\alpha(x)$, recursively defined by

$$\begin{aligned} L_0^\alpha(x) &= 1, \\ L_1^\alpha(x) &= 1 + \alpha - x, \\ L_{n+1}^\alpha(x) &= \frac{(2n+1+\alpha-x)L_n^\alpha(x) - (n+\alpha)L_{n-1}^\alpha(x)}{n+1}, \quad n \geq 1, \end{aligned}$$

and

$$w_k = \frac{n!\Gamma(n+\alpha+1)x_k}{[L_{n+1}^\alpha(x_k)]^2},$$

in which Γ denotes the Gamma function.

C.3 Construction of a Gaussian rule

We notice that, in order to compute the nodes and weights as in Theorem 2, we need to know the zeros of $\phi_n^\star(x)$ and the explicit representation of the orthogonal polynomials $\phi_k^\star$, $k = 1, \ldots, n+1$. This is not always possible, but a way to overcome such issue is to determine the Gaussian rule through the recurrence relation defined in the following theorem.

Theorem 3 *Given a system $\{\phi_k\}_{k\geq 0}$ of monic orthogonal polynomials, the following three term recurrence relation holds:*

$$\phi_{k+1}(x) = (x - \alpha_k)\phi_k(x) - \beta_k \phi_{k-1}(x), \quad k \geq 0,$$

$$\phi_{-1}(x) = 0, \quad \phi_0(x) = 1,$$

where α_k and $\beta_k > 0$ are called the recurrence coefficients.

Given α_k and β_k, the corresponding matrix

$$J = \begin{bmatrix} \alpha_0 & \sqrt{\beta_1} & & & 0 \\ \sqrt{\beta_1} & \alpha_1 & \sqrt{\beta_2} & & \\ & \sqrt{\beta_2} & \alpha_2 & \ddots & \\ & & \ddots & \ddots & \sqrt{\beta_{n-1}} \\ 0 & & & \sqrt{\beta_{n-1}} & \alpha_{n-1} \end{bmatrix} \in \mathbb{R}^{n\times n},$$

is called the Jacobi matrix. In particular, J contains the coefficients of the three term recurrence relation for the orthonormal polynomials, that is,

$$\sqrt{\beta_{k+1}}\phi^\star_{k+1}(x) = (x-\alpha_k)\phi^\star_k(x) - \sqrt{\beta_k}\phi^\star_{k-1}(x), \quad k \geq 0,$$

$$\phi^\star_{-1}(x) = 0, \quad \phi^\star_0(x) = \frac{1}{\sqrt{\beta_0}}.$$

In order to construct the Gauss quadrature rule, the central problem is to generate the coefficients α_k and β_k. In fact, the eigendecomposition of the matrix J provides the nodes x_i and the weights w_i, $i = 1, \ldots, n$, of the n-point Gaussian rule (see e.g. [10, Sect.2.7] and the reference therein). This step is efficiently implemented by the Golub and Welsch algorithm [28] which exploits the Q-R algorithm of Francis [18] for the computation of the eigenvalues and eigenvectors of a symmetric matrix. Some alternatives to this algorithm have been later developed and we refer to [42] for a general discussion and a rich bibliography. Then, the coefficients α_k and β_k can be derived by computing the associated power moments, defined as,

$$\mu_k = \int_0^\infty x^k w(x)dx, \quad k \geq 0, \tag{C.5}$$

and by using the Chebyshev algorithm (see [19, Sect.2.3] and [21]). Given the first $2n$ moments $\mu_0, \ldots, \mu_{2n-1}$, the algorithm uniquely determines the first n recurrence coefficients α_k and β_k, $k = 0, \ldots, n-1$, by using the mixed moments

$$\sigma_{kl} = \int_0^\infty \phi_k(x)x^l w(x)dx, \quad k, l \geq -1.$$

The Chebyshev algorithm is summarized in Algorithm 6.

Algorithm 6 *Initialization*

$$\alpha_0 = \frac{\mu_1}{\mu_0}, \ \beta_0 = \mu_0,$$
$$\sigma_{-1,l} = 0, \quad l = 1, 2, \ldots, 2n-2,$$
$$\sigma_{0,l} = \mu_l, \quad 0, 1, \ldots, 2n-1,$$

for $k = 1, 2, \ldots, n-1$

for $l = k, k+1, \ldots, 2n-k-1$

$$\sigma_{k,l} = \sigma_{k-1,l+1} - \alpha_{k-1}\sigma_{k-1,l} - \beta_{k-1}\sigma_{k-2,l},$$
$$\alpha_k = \frac{\sigma_{k,k+1}}{\sigma_{k,k}} - \frac{\sigma_{k-1,k}}{\sigma_{k-1,k-1}}, \quad \beta_k = \frac{\sigma_{k,k}}{\sigma_{k-1,k-1}}.$$

Nevertheless, it is well known (see e.g. [22]) that the computation of the recurrence coefficients can be inaccurate for growing k because the problem is severely ill conditioned when starting from the power moments (C.5). In order to overcome this difficulty, the so called modified Chebyshev algorithm (advanced by Gautschi in [19, Sect.2.4]) can be employed. It is based on the use of the modified moments

$$m_k = \int_0^\infty p_k(x)w(x)dx, \quad k \geq 0, \tag{C.6}$$

and on the mixed moments

$$\tilde{\sigma}_{kl} = \int_0^\infty \phi_k(x)p_l(x)w(x)dx, \quad k, l \geq -1, \tag{C.7}$$

where $\{p_k\}_{k\geq 0}$ is a given system of orthogonal polynomials, chosen to be close to the desired polynomials $\{\phi_k\}_{k\geq 0}$, which satisfies the three-term recurrence relation

$$p_{k+1}(x) = (x - a_k)p_k(x) - b_k p_{k-1}(x), \quad k \geq 0$$
$$p_{-1}(x) = 0, \quad p_0(x) = 1,$$

with coefficients $a_k \in \mathbb{R}$, $b_k \geq 0$ that are known. We remark that the idea of using modified moments was introduced by Sack and Donovan in [49], who developed an algorithm similar to the one of Gautschi. The same technique was independently obtained by Wheeler in [67]. The modified Chebyshev algorithm is summarized in Algorithm 7. We notice that the case $a_k = b_k = 0$ yields $p_k(x) = x^k$, and Algorithm 7 reduces to Algorithm 6.

Algorithm 7 *Initialization*

$$\alpha_0 = a_0 + \frac{m_1}{m_0}, \ \beta_0 = m_0,$$
$$\sigma_{-1,l} = 0, \quad l = 1, 2, \ldots, 2n-2,$$
$$\sigma_{0,l} = m_l, \quad 0, 1, \ldots, 2n-1,$$

for $k = 1, 2, \ldots, n-1$

for $l = k, k+1, \ldots, 2n-k-1$

$$\sigma_{k,l} = \sigma_{k-1,l+1} - (\alpha_{k-1} - a_l)\sigma_{k-1,l} - \beta_{k-1}\sigma_{k-2,l} + b_l\sigma_{k-1,l-1},$$
$$\alpha_k = a_k + \frac{\sigma_{k,k+1}}{\sigma_{k,k}} - \frac{\sigma_{k-1,k}}{\sigma_{k-1,k-1}}, \quad \beta_k = \frac{\sigma_{k,k}}{\sigma_{k-1,k-1}}.$$

We remark that this approach may be efficient in general but not always when working with unbounded intervals of integration (see [21] and [22]).

C.4 The Gauss-Kronrod quadrature formulae

In 1964 Kronrod [40] proposed to extend the n-point Gauss quadrature formula for the Legendre weight function to a $(2n+1)$-point formula by inserting $n+1$ additional nodes such that the new formula has maximum degree of exactness. The purpose was to estimate the error of the n-point Gauss-Legendre rule. In this section we give a brief description of integration rules of Gauss-Kronrod type.

Let $w(x)$ be a non negative weight function on $[a, b]$ and consider the corresponding Gauss quadrature formula

$$\int_a^b f(x)w(x)dx \cong \sum_{k=1}^{n} w_k f(x_k), \tag{C.8}$$

where $x_k = x_k^{(n)}$ are the zeros of the n-th degree (monic) orthogonal polynomial π_n relative to the weight function w on $[a, b]$. The Gauss-Kronrod quadrature formula, extending (C.8), has the form

$$\int_a^b f(x)w(x)dx \cong \sum_{k=1}^{n} \gamma_k f(x_k) + \sum_{j=1}^{n+1} \gamma_j^\star f(x_j^\star), \tag{C.9}$$

where x_k are the Gauss nodes, while the new nodes $x_j^\star = x_j^{\star(n)}$, called the Kronrod nodes, and all weights $\gamma_k = \gamma_k^{(n)}$, $\gamma_j^\star = \gamma_j^{\star(n)}$ are chosen such that formula (C.9) has maximum degree of exactness $3n+1$. In this setting, the nodes $x_j^\star$ are the zeros of a (monic) polynomial $\pi_{n+1}^\star$, orthogonal to all polynomials of lower degree with respect to the variable-sign weight function $w^\star(x) = \pi_n(x)w(x)$ on $[a, b]$, that is

$$\int_a^b \pi_{n+1}^\star(x)x^k\pi_n(x)w(x)dx = 0, \quad k = 0, 1, \ldots, n.$$

The polynomial $\pi^\star_{n+1}$ is referred to as the Stieltjes polynomial relative to the weight function w on $[a, b]$. The weights of formula (C.9) are given by

$$\gamma_k = w_k + \frac{\|\pi_n\|^2}{\pi'_n(x_k)\pi^\star_{n+1}(x_k)}, \quad k = 1, 2, \ldots, n,$$
$$\gamma^\star_j = \frac{\|\pi_n\|^2}{\pi_n(x^\star_j)(\pi^\star_{n+1})'(x^\star_j)}, \quad j = 1, 2, \ldots, n+1,$$

where $\|\cdot\|$ is the L_2-norm for the weight function w on $[a, b]$. Moreover, all $\gamma^\star_j$ are positive if and only if the nodes x_k and $x^\star_j$ interlace, that is,

$$x^\star_{n+1} < x_n < x^\star_n < \ldots < x^\star_2 < x_1 < x^\star_1. \tag{C.10}$$

We notice that, since the polynomial $\pi^\star_{n+1}$ is orthogonal with respect to a variable-sign weight function, it does not follow the usual theory for orthogonal polynomials. Therefore, all the known results have been derived for specific weight functions (see e.g. [46, 20] for complete and exhaustive surveys). In particular, for the Legendre weight function, in 1975 Szegő [58] was able to conclude that al nodes x_k, $x^\star_j$ are real, contained in $[-1, 1]$ and that property (C.10) holds. Moreover, in 1978, Monegato [45], relying on Szegő's work, proved that all weights γ_k, $\gamma^\star_j$ are positive, $\forall n \geq 1$.

Bibliography

[1] M. Abramowitz and I.A. Stegun, *Handbook of Mathematical Functions with Formulas, Graphs, and Mathematical Tables*, 7th ed., Dover Books on Intermediate and advanced Mathematics, Dover Publications, Inc., New York, 1970.

[2] W.L. Anderson, Computer Program. Numerical integration of related Hankel transforms of orders 0 and 1 by adaptive digital filtering, *Geophysics* **44(7)** (1979), 1287-1305.

[3] L. Armiijo, Minimization of functions having Lipschitz-continuous first partial derivatives, *Pacific J. Math.* **16** (1966), 1-3.

[4] R. Askey, *Orthogonal polynomials and special functions*, Regional Conference Series in Applied Mathematics, 21, Philadelphia, PA: SIAM, 59–60, 1975.

[5] W. Barrett, Convergence properties of Gaussian quadrature formulae, *Comput. J.* **3** (1960/1961), 272–277.

[6] C.G. Broyden, *The Convergence of a Class of Double-Rank Minimization Algorithms*, Journal Inst. Math. Applic., 1970.

[7] J.M. Carcione, *Wave fields in real media: Wave propagation in anisotropic, anelastic, porous and electromagnetic media*, Elsevier Science, Amsterdam, Handbook of Geophysical Exploration, 2014.

[8] J.M. Carcione, D. Gei, S. Picotti, A. Michelini, Cross-hole electromagnetic and seismic modeling for co2 detection and monitoring in a saline aquifer, *Journal of Petroleum Science and Engineering* **100** (2012), 162-172. doi: 10.1016/j.petrol.2012.03.018.

[9] N.B. Christensen, Optimized fast Hankel transform filters, *Geophysical Prospecting* **38** (1990), 545-568.

[10] P.J. Davis and P. Rabinowitz, *Methods of numerical integration*, Academic Press, Inc., New York. 1975.

[11] E. Denich and P. Novati, Gaussian rule for integrals involving Bessel functions, *arXiv:2110.05051v1* (2021), https://doi.org/10.48550/arXiv.2110.05051.

[12] E. Denich, Error estimates for a Gaussian rule involving Bessel functions, *preprint*.

[13] E. Denich, P. Novati and S. Picotti, A fast and accurate numerical approach for electromagnetic inversion, *Journal of Computational Physics* **475** (2023), 111846.

[14] J.E. Dennis, Jr. and R.B. Schnabel, *Numerical Methods for Unconstrained Optimization and Nonlinear Equations*, SIAM, Philadelphia, 1996.

[15] A. Erdelyi, Ed., *Tables of integral transforms*, McGraw-Hill Company, Inc., 1954.

[16] R. Fletcher, A New Approach to Variable Metric Algorithms, *Computer Journal*, (1970).

[17] R. Francese, G. Morelli, F. Santos, A. Bondesan, M. Giorgi and A. Tesarollo, An integrated geophysical approach to scan river embankments, *Fast Times*, **23(3)** (2018), 86–96.

[18] J.G.F. Francis, The QR Transformation: a Unitary Analogue to the LR Transformation. I,II, *Comput. J.*, **4** (1961/62), 265-271, 332-345.

[19] W. Gautschi, On generating orthogonal polynomials, *SIAM J. SCL. Stat. Comput.*, **3(3)** (1982), 289–317. doi: 10.1137/0903018

[20] W. Gautschi, *Gauss-Kronrod quadrature - a survey*, in Numerical Methods and Approximation Theory III, G.V. Milovanović, ed., Faculty of Electronic Engineering, University of Niš, Niš, 1988, 39-66.

[21] W. Gautschi, Algorithm 726: ORTHPOL–a package of routines for generating orthogonal polynomials and Gauss-type quadrature rules, *ACM Transactions on Mathematical Software*, **20(1)** (1994), 21–62. doi: 10.1145/174603.174605

[22] W. Gautschi, *Orthogonal polynomials: applications and computation*, Acta Numerica, Cambridge University Press, 1996, 45-119. doi: 10.1017/S0962492900002622

[23] Gautschi, W. (2005), *Computing polynomials orthogonal with respect to densely oscillating and exponentially decaying weight functions and related integrals*, Journal of Computational and Applied Mathematics, 184, 493-504. doi:10.1016/j.cam.2005.01.023

[24] W. Gautschi, *Orthogonal Polynomials, Quadrature, and Approximation: Computational Methods and Software (in Matlab)*, In: Marcellán F., Van Assche W. (eds) Orthogonal Polynomials and Special Functions, Lecture Notes in Mathematics, vol 1883, Springer, Berlin, Heidelberg, 2006. doi: $10.1007/978-3-540-36716-1\_1$

[25] D.P. Ghosh, The Application of Linear Filter Theory to the Direct Interpretation of Geoelectrical Resistivity Sounding Measurements, *Geophysical Prospecting* **19** (1971), 192-217.

[26] Goldfarb, D. , A Family of Variable Metric Updates Derived by Variational Means, *Mathematics of Computing*, **24** (1970).

[27] A. A. Goldstein, *Constructive Real Analysis*, Harper & Row. New York, 1967.

[28] G.H. Golub and J.H. Welsch, Calculation of Gauss Quadrature Rules, *Mathematics of Computation*, **23(106)** (1969), 221-230. doi: 10.1090/S0025-5718-69-99647-1

[29] I.S. Gradshteyn and I.M. Ryzhik, *Tables of Integrals, Series, and Products*, 4th ed., Academic Press, New York, 1980.

[30] D. Guptasarma, Optimization of short digital linear filters for increased accuracy, *Geophysical Prospecting* **30** (1982), 501-514.

[31] D. Guptasarma and B. Singh, New digital linear filters for Hankel J_0 and J_1 transforms, *Geophysical Prospecting* **45** (1997), 745-762.

[32] G.M. Hoversten, F. Cassassuce, E. Gasperikova, G.A. Newman, J. Chen, Y. Rubin, Z. Hou and D. Vasco, Direct reservoir parameter estimation using joint inversion of marine seismic AVA and CSEM data.i, *Geophysics*, **71(3)** (2006), C1-C13.

[33] T. Ingeman-Nielsen and F. Baumgartner , CR1Dmod: A Matlab program to model 1D complex resistivity effects in electrical and electromagnetic surveys, *Computer & Geosciences*, **32** (2006), 1411-1419.

[34] H.K. Johansen and K. Sorensen, Fast Hankel Transforms, *Geophysical Prospecting* **27** (1979), 876-901.

[35] D. Kahaner, C. Moler and S. Nash, *Numerical Methods and Software*, Prentice–Hall, 1989.

[36] J.H. Knight and A.P. Raiche, Transient electromagnetic calculations using the Gaver-Stehfest inverse Laplace transform method, *Geophysics* **47** (1982), 47-50.

[37] O. Koefoed and F.J. Dirks, Determination of resistivity sounding filters by the Wiener-Hopf least-squares method, *Geophysical Prospecting* **27** (1979), 245-250.

[38] O. Koefoed, D.P. Ghosh and G.J. Polman, Computation of type curves for electromagnetic depth sounding with a horizontal transmitting coil by means of a digital linear filter, *Geophysical Prospecting* **20** (1972), 406-420.

[39] F.N. Kong, Hankel transform filters for dipole antenna radiation in a conductive medium, *Geophysical Prospecting* **55** (2007), 83-89.

[40] A.S. Kronrod, Integration with control of accuracy (Russian), *Dokl. Acad. Nauk SSSR* **154** (1964), 283-286.

[41] D.P. Laurie, Computation of Gauss-type quadrature formulas, *Journal of Computational and Applied Mathematics*, **127** (2001), 201-217.

[42] D.P. Laurie, Anti-Gaussian quadrature formulas, *Math. Comp.*, **65** (1996), 739-747.

[43] J. Lund and K.L. Bowers, *Sinc Methods for Quadrature and Differential Equations*, SIAM, Philadelphia, 1992.

[44] J.D. McNeill, *Electromagnetic terrain conductivity measurements at low induction numbers*, Tech. Note TN-6. Geonics Ltd., Mississauga, ON, 1980.

[45] G. Monegato, Positivity of the weights of extended Gauss-Legendre quadrature rules, *Math. Comp.*, **32** (1978), 243-245.

[46] S.E. Notaris, Gauss-Kronrod quadrature formulae - a survey of fifty years of research, *Electronic Transactions on Numerical Analysis*, **45** (2016), 371-404.

[47] S.D. Pawar, P. Murugavel, D. M. Lal, Effect of relative humidity and sea level pressure on electrical conductivity of air over Indian ocean, *Journal of Geophysical Research*, **114 (D2)** (2009). doi:10.1029/2007JD009716.

[48] L. Reichel and M. M. Spalević, Averaged Gauss quadrature formulas: Properties and applications, *Journal of Computational and Applied Mathematics* **410** (2022), 114232.

[49] R.A. Sack and A.F. Donovan, An Algorithm for Gaussian Quadrature given Modified Moments, *Numer. Math.*, **18** (1972), 465-478. doi: 10.1007/BF01406683

[50] S.A. Schelkunoff, *Electromagnetic waves*, D. Van Nostrand Co., Inc., 1943.

[51] J.H. Schön, *Physical properties of rocks*, Pergamon Press, Handbook of Geophysical Exploration, 1996.

[52] L.F. Shampine, Vectorized Adaptive Quadrature in MATLAB, *Journal of Computational and Applied Mathematics*, **211** (2008), 131-140.

[53] D.F. Shanno, *Conditioning of Quasi-Newton Methods for Function Minimization*, Mathematics of Computing, 1970.

[54] N.P. Singh and T. Mogi, EMDPLER: A F77 program for modeling the EM response of dipolar sources over the non-magnetic layer earth models, *Computers & Geosciences* **36** (2010), 430-440.

[55] A. Sommerfeld, *Partial Differential Equations in Physics*, Academic Press, University of Michigan, 1964.

[56] M. M. Spalević, On generalized averaged Gaussian formulas, *Math. Comp.* **76** (2007), 1483-1492.

[57] J.A. Stratton, *Electromagnetic theory*, McGraw-Hill Book Company, New York and London, 1941.

[58] G. Szegö, *Orthogonal polynomials*, 4th edition, American Mathematical Society, Providence, Rhode Island, 1975.

[59] N. Trefethen, *Approximation Theory and Approximation Practice, Extended Edition*, SIAM, Philadelphia, 2019.

[60] J.R. Wait, Mutual electromagnetic coupling of loops over a homogeneous ground, *Geophysics* **20** (1955), 630-637.

[61] J.R. Wait, A note on the electromagnetic response of a stratified Earth, *Geophysics* **27** (1962), 382-385.

[62] J.R. Wait, *Geo-Electromagnetism*, Academic Press, Inc., New York, 1982.

[63] S.H. Ward and G.W. Hohmann, *Resistivity characteristics of geologic targets*, In: Nabighian, M.N., (ed.), Electromagnetic Methods in Applied Geophysics, Tulsa, Oklahoma, 53-129, 1987.

[64] S.H. Ward and G.W. Hohmann, *Electromagnetic theory for geophysical applications*, In: Nabighian, M.N., (ed.), Electromagnetic Methods in Applied Geophysics, Tulsa, Oklahoma, 131-311, 1988.

[65] G.N. Watson, *A treatise on the theory of Bessel functions*, Cambridge University press, 2nd. edition reprinted, 1966.

[66] D. Werthmüller, K. Key and E.C. Slob, A tool for designing digital filters for the Hankel and Fourier transforms in potential, diffusive, and wavefield modeling, *Geophysics* **84(2)** (2019).

[67] J.C. Wheeler, Modified Moments and Gaussian Quadratures, *Rocky Mountain Journal of Mathematics*, **4(2)** (1974), 287-296. doi: 10.1216/RMJ-1974-4-2-287

[68] A.A.R. Zohdy and D.B. Jackson, Application of deep electrical soundings for groundwater exploration in Hawaii, *Geophysics*, **34(4)** (1969), 584-600.